Stony Brook University

Natural Protective Features (NPFs) Along New York's Ocean Shoreline and Their Response to Extreme Events

A Dissertation Presented

by

Hanlu Huang

to

The Graduate School

in Partial Fulfillment of the

Requirements

for the Degree of

Doctor of Philosophy

in

Marine and Atmospheric Sciences

Stony Brook University

December 2016

Stony Brook University

The Graduate School

Hanlu Huang

We, the dissertation committee for the above candidate for the

Doctor of Philosophy degree, hereby recommend

acceptance of this dissertation.

Henry Bokuniewicz – Dissertation Advisor
Distinguished Service Professor, SoMAS

Robert Wilson – Chairperson of Defense
Associate Professor, SoMAS

Ali Farhadzadeh – Dissertation Committee
Assistant Professor, SoMAS

Gary Zarillo – Dissertation Committee
Professor, Florida Institute of Technology

Brian Batten – Dissertation Committee
Senior Coastal Scientist, Dewberry

This dissertation is accepted by the Graduate School

Charles Taber

Dean of the Graduate School

Abstract of the Dissertation

Natural Protective Features (NPFs) Along New York's Ocean Shoreline and its Response to Extreme Events

by

Hanlu Huang

Doctor of Philosophy

in

Marine and Atmospheric Sciences

Stony Brook University

2016

Features providing natural protection against erosion and flooding are defined in the laws of New York State to include dunes, bluffs, and beaches. In addition, structural hazard areas are defined to be stretches of the coast where the long-term recession rate is greater than one foot per year. LiDAR data was used to identify NPFs and examine shoreline recession rates at 750 transects along the south shore of eastern Long Island. Meaningful combinations of NPFs included dunes in front of bluffs, dunes formed on top of bluffs and multiple dunes. Single dunes were the NPFs along 27.1% of the shoreline; multiple dunes comprising 20.7%. Bluffs were the NPF along 26.6% of the shoreline. Dunes in front of a bluff comprised 12.1% and dune on top of a bluff crest made up 12.9%. (The remaining 0.6% of the shoreline was identified as the beach). Dunes provide the first line of defense against extreme events, but in the face of a long-term rise in sea level, the excavation of the bluff face is likely to be the factor controlling shoreline retreat. Combination of NPFs do not necessarily equate to high (or low) resilience.

Shoreline recession rates were calculated as a linear regression of high-water shorelines from 1983, 1999, 2003, 2010 and 2013. Calculated recession rates were biased by the occurrence of longshore sandwaves. These features were found to occur between 23% and 82% of the time. Spectra analysis shows a dominant wavelength of shoreline recession rate to be 1.5 km. The cause of sandwaves are debatable, but their presence can impact the calculation of recession rates.

A shore-process model (CSHORE) using wave and surge data for a 12-day period based on Superstorm Sandy were used predicted that the beach profile would have lost an average volume of 68 m^3/m but ranged up to 137 m^3/m. Model results were about twice those observed using LiDAR data after Hurricane Sandy, but neither that event or earlier historical events seemed to permanently alter the response of the shoreline to later conditions.

Table of Contents

List of Figures

List of Tables

List of Abbreviations

ECL	Environmental Conservation Law
NYCRR	New York Codes, Rules, and Regulations
NYSDEC	New York State Department of Environmental Conservation
NPF	Natural Protective Features
NPFA	Natural Protective Features Area
SHA	Structure Hazard Area
NYSERDA	New York State Energy Research and Development Authority
CEHA	Coastal Erosion Hazard Area
DEM	Digital Elevation Model
LIDAR	Light Detection and Ranging
FEMA	Federal Emergency Management Agency
NYSDOP	New York State Digital Ortho-imagery Program
NWI	National Wetlands Inventory
MLW	Mean Low Water
MHW	Mean High Water
NOAA	National Oceanic and Atmospheric Administration
NGVD	National Geodetic Vertical Datum

Acknowledgments

I had a great time during my Ph.D. period here in Stony Brook since October 2012. I thank for the world's most passionate and considerate advisor, Henry Bokuniewicz. His love of science and his energy encourage me through my research period. I feel lucky to have you as my advisor and guidance here. I also want to thank Eileen Doyle, for being the nicest secretary, handling all my forms and keep me in schedule.

Thanks for my committee members. Thanks to Ali Farhadzadeh for his tutorials on CSHORE, thanks to Gary Zarillo for his input from geomorphology point of view, thanks to Robert Wilsons for all the data analysis suggestions, thanks to Brain Batten for cooperated in the CEHA project. I also want to thank Joel Plummer for the R tool he wrote that help me identify those natural protective features.

Also, I want to thank my friend Hannah Clark, Amy Pritt, Cuiyu Wang and Xiayan Ye, with them I shared a great time. Also, thanks to Haikun Xu, who is a talented hard worker and considerate boyfriend. Although my parents are not in this country, they look after me all the time, I thank for their support and understanding.

Finally, I appreciate the support of the New York State Energy Research and Development Authority (Agreement No. 28256) and of the New York State Department of State, Office of Planning and Development, (MOU No. U1000563) in cooperation with the BOEM Marine Minerals Program (Cooperative Agreement No. M14AC00001)

Chapter 1: Coastal Erosion Hazard Area Delineate Program

1.1 Introduction

Many portions of New York State coastline are prone to significant erosion, include Lakes Erie and Ontario; the St. Lawrence and Niagara Rivers; the Hudson River south of the Federal Dam at Troy; The East River; the Harlem River; the Kill van Kull and Arthur Kill; Long Island Sound; and the Atlantic Ocean, as well as their connecting water bodies, bays, harbors, shallows, and marshes. To address erosion issues, New York Environmental Conservation Law, 3-0301, 34-0108, Article 34 Section 505.2 requires that areas of the coastline most prone to erosion be identified and any activities in these coastal erosion hazard areas are designed to minimize damage to property and natural protective features (NPFs) and other natural resources. Permanent development is limited to prevent the exacerbation of erosion hazards and protect human life. In 1983 the New York State Department of Environmental Conservation (NYSDEC) adopted New York Codes, Rules, and Regulations (NYCRR) Part 505, the Coastal Erosion Management Regulation. Under these regulations, land use and development are regulated based on mapped boundaries within erosion areas.

Part 505 prescribes how the NPFs along the coastline are to be mapped and how erosion recession rates are to be calculated to produce maps that identify coastal erosion areas. There are two types of Coastal Erosion Hazard Areas: The Natural Protective Feature Area and the Structural Hazard Area (SHA). NPFs include beaches, bluffs, and dunes that are defined by Coastal Erosion Hazard Area Act. The beach is defined as the zone of unconsolidated sediment that extends landward from the mean low water (MLW) line to the seaward toe of a dune or bluff, whichever is most seaward. (If there is no dune or bluff, it extends 100 feet landward from the place where there is a marked change in material or physiographic form or from the line of permanent vegetation, whichever is most seaward). Shorelines without dunes subject to seasonal or more frequent overwash or inundation are considered to be beaches. The bluff is a bank or cliff with a steeply sloped face at the shoreline. Bluffs are often composed of compacted sands, silts, and clay. The dune is defined as a ridge or hill of loose, windblown, or artificially placed sand. An SHA is defined as shoreline that recedes at a long-term average annual recession rate of one foot or more per year. Once prepared, maps (Figure 1.1) are presented to the local community through a public hearing process and are then certified by the Commissioner of the NYSDEC.

The original maps for the program were developed in 1983-1984. A set of aerial photographs were used to identify NPFs on eight-by-eight-inch stereo pairs to manually identify the landward toe of the dune and bluff crest. The original SHA line was based on earlier studies of parts of the shoreline on maps and aerial photography. Studies of the long-term trends in ocean shoreline position have been conducted by Taney (1961) for most of the south shore and by Leatherman and Allen (1985) for the area east of Fire Island Inlet. The earliest maps of the ocean shoreline in East Hampton dated from 1838. Taney compared the position of high-water shoreline for various time periods using several sets of Coast and Geodetic Survey charts and U.S. Army Corps of Engineers maps and ranges dating from 1838 to 1956. Leatherman and Allen (1985) developed maps of the shoreline at mean high tide based on Coast and Geodetic Survey T-sheets and aerial photographs and compared the shoreline position for four time periods (1838, 1891, 1933, 1962 and 1979) to

calculate the annual recession/accretion rates. T-sheets were used to retrieve the shoreline in 1838, 1891 and 1933. Aerial photographs were used for 1938, 1962 (after a major storm) and 1979.

Of course, further erosion has occurred on New York State coastlines in the last 30 years and mapping technologies have greatly advanced. As a result, New York initiated the Coastal Erosion Hazard Area Remap Program, to re-examine and revise the CEHA maps. Updated CEHA maps are intended to allow for more effective management of NY's coastal areas, especially because erosional trends might be expected to accelerate as a result of climate change and increased sea-level rise. Thirty-seven kilometers of shoreline were examined (Figure 1.2) along the south shore of Long Island for Coastal Erosion Hazard Area Remap Program in order to re-evaluate the Coastal Erosion Hazard Areas (CEHAs) along selected stretches of the coastline.

1.2 Study Area

Pleistocene glacial deposits (Williams 1976) including two moraines from Wisconsin Glaciation determined the topography of Long Island. The northern moraine, called the Harbor Hill Moraine, formed the North Fork of Long Island and southern, Ronkonkoma Moraine formed the South Fork of Long Island from the southeast tip of the island, Montauk Point. The entire ocean shore of Long Island has been divided into two physiographic provinces, the headlands' section in the east and the barrier beach section in the west (Taney 1961; Figure 1.3). The headlands' section extended 53 km westward from Montauk Point. The East Hampton ocean shoreline was, therefore, in the headlands' section where the ocean beach was cut directly into sands of the coastal glacial-outwash plain. High, unconsolidated bluffs provided the NPF along the easternmost 13 km of the headlands' section. Small stretches of shoreline in the easternmost 2 km of the study area, at Lake Montauk and Fort Pond, where the NPF had been classified as dunes, represented gaps in the moraine that had subsequently been bridged by a barrier beach as sea level rose after deglaciation.

The ocean shoreline of East Hampton is exposed to ocean waves, and extends 43 km from Montauk Point. Bluffs are replaced by a substantial primary dune system interrupted by coastal ponds at a distance of 43 km from Montauk Point. In particular, bluff recession tends to be catastrophic, fragmented and localized. The retreat is not gradual but rather occurs episodically by undercutting and collapse during extreme storms. Short sections of the bluff, mostly less than 500 m wide, recede in these events while intervening stretches of the coast may be unaffected. Bluff coastlines can only recede but beach shorelines can advance and recede over time. On the compartmentalized shoreline, substantial changes often represent a shift in sand from one end of the compartment to the other depending on local wind-wave conditions. On the ocean shoreline, however, short-term changes in beach width sometimes over 100's of feet are common and long-term trends may be difficult to resolve in the face of these large short-term variations. In addition, multi-year decadal oscillations of shoreline positions have been observed. Shoreline recession rates based on linear regressions will be most useful, but uncertainty in the designation of instantaneous, historical shorelines should be considered.

1.3 Methods

To remap NPFs and SHAs in East Hampton, NY, protocols and proceedings developed by Dewberry were used (Bokuniewicz et al. 2016). These had been extensively applied by Dewberry in other areas of the New York shoreline. The analysis included the use of Dewberry's proprietary software. New NPFs and SHAs have been remapped in the study area using a base topography of digital elevation models (DEMs). These had been derived from 2012 Light Detection and Ranging (LiDAR) with a horizontal accuracy requirement of 1 m and a vertical RMS error of 5.1 cm. Transects were produced from the LIDAR dataset using "GeoCoastal," an integrated GIS proprietary modeling system developed by Dewberry. Subaqueous topography for these areas had been added from the Federal Emergency Management Agency (FEMA) Region II Coastal Terrain Processing or from unpublished studies on Fire Island. Historical and modern digital aerial photography were also used. High-resolution ortho-imagery from 2010 was provided by the New York State Office of Cyber Security, New York State Digital Ortho-imagery Program (NYSDOP).

Photographs were scanned at a resolution of no less than 600 dpi with ten control points were sufficient for image georeferencing. Quality control of the DEMs used in NYS DEC mapping project, 2013, showed that they are of good quality and no additional modifications were required. The map layout was 11 X 17 inches at a 1" = 12400' scale as developed for the NYSDEC mapping project, 2013 in NAD 1983 State Plane coordinate for Long Island, New York. Consistency was most critical and rules were established to be generally applicable.

The total length of the study area was 37 km and 750 transects were delineated along the shoreline. They were created 50 meters (164 feet) apart perpendicular to a baseline and buffered 30.48 meters (100 feet) seaward from the Mean High Water (MHW) line. The platform was an integrated GIS modeling system developed by Dewberry called "GeoCoastal". MHW lines come from the NOAA's VDatum software (v3.1) and they were referenced to NAVD88 (Plummer et al. 2015). The profile of each transect had been delineated using Light Detection and Ranging (LiDAR) based data which had been collected in 2012 between November 2011 and April 2012 by NYSDEC and the National Oceanic and Atmospheric Administration (NOAA) and reviewed by Joel Plummer of Dewberry.

The identification of the NPFs was greatly facilitated by a proprietary code (the "R-tool", B. Batten and J. Plummer, Dewberry, personal communication 2014). A graphical user interface window had been designed to interpret the features in the topographic profiles (Figure 1.4). The "Guides" include three indicators to help identify NPFs and the mean high water mark. Those three indicators are the first derivative of the topographic profile, the second derivative and the curvature of the profile. Specifically:

$$Z' = \frac{\partial z}{\partial x} \qquad [1]$$

$$Z'' = \frac{\partial^2 z}{\partial x^2} \qquad [2]$$

$$|\kappa| = \frac{|Z''|}{(1+z'^2)^{3/2}} \qquad [3]$$

When Z'=0, code located the minimum and maximum value in the profile, that is, a crest or a valley. The second derivative Z''defined the rate of slope change at any location. The value of the curvature, |κ|, was positively correlated to the inflection of the profile with a higher the value indicating a sharper inflection (Figure 1.4). These indicators were tools to help me identify the NPF feature, i.e. the dune toe, dune heel, bluff toe, bluff crest etc. But these are just the program's suggestions, the user can choose to accept the suggestion or not.

After the NPFs had been identified by the LiDAR data, adjustments were made by visual comparison of NPFs points with modern high-resolution ortho-imageries. Site inspections were made on November 12, 2013.

Several informal rules were established to help discern between feature types and assist in the mapping process:

1. As a practical matter, it was found that in order to be classified as a bluff, the slope needs to be steeper than 1:4 and the elevation need to be higher than about 1.5 meters (5 feet).
2. Dunes are differentiated from bluffs because of the recognizable apex and back slope of the dune, as well as the differences in the material (e.g., sand versus rock) and vegetation.
3. The identified heel of the dune is the landward-most heel when more than one dune is present.
4. With no indication of bluff or dune features, the feature is classified as a vegetation line and its location placed at the point of significant change in persistent vegetation or geomorphologic structure.
5. A vegetation line is placed at a beachfront building with no protective NPF. The proper term "beach inland" became favored over "vegetation line."
6. Previous delineations considered NPFs landward of wetland areas. For this mapping effort, the NPF was designated at the protective feature seaward of wetland areas, as identified by the U.S. Fish and Wildlife Service National Wetlands Inventory (NWI).
7. In this study, the choice of beach location needs to be combined with the ortho-imageries, as where the vegetation changes or have a geomorphologic structure. The beach inland point had been put around the edge of the pond behind (Figure 1.5).

In the remapping program, the HWL was the shoreline indicator. For its ease of interpretation in the field and on aerial photography, it is the most commonly used shoreline indicator in the United States (Leatherman 2003). As described by Shalowitz (1964):

"From the standpoint of the surveyor, the high-water line is the only line of contact between land and water that is identifiable on the ground at all times and does not require the topographer being there at a specified time during the tidal cycle or the running of levels. The high-water line can

generally be closely approximated by noting the vegetation, driftwood, discoloration of rocks, or other visible signs of high tides. The mean high-water line must not be confused with the storm high-water line, which is usually marked by driftwood and the edge of considerable vegetation."

Both historical aerial photos and modern ortho-imagery were used to identify the high-water shoreline (HWL). Historical photos from April 2, 1983, had been converted to digital format by optical scanning. More than ten control points, such as buildings, parking lots and houses were chosen to georeferencing the historical photos. In total, there are 27 of historical pictures in the study area. Figure 1.6 is an example of an aerial photo near Montauk Point; here the offshore rock deposited during the glacial period had been a good control point. During the georeferencing, the 3rd order polynomial RMS error was lower than 10 m, the average RMS error is 1.99 m as showed in Table 1.1 (the average RMS error for 1st order and 2nd order is 12.54 m and 6.98 m). Modern, geo-rectified ortho-imagery (New York State Officer of Cyber Security, New York State Ortho-imagery Program) was available from 2004, 2010 and as well as in 2013 after Superstorm Sandy.

Orthoimagery was examined at a scale of 1:800. The HWL was identifiedd with respect to the wrack line (Figure 1.7). There are places where the wrack line was obscured, for example by truck marks, overwash or ridge-and-runnel features. By altering the color and contrast of the images (by changing the standard deviation value and using histogram stretching techniques), the wetted perimeter of HWL could be more easily to distinguish in some of these areas.

After identifying HWL from 1983, 2003, 2010 and 2013, long-term shoreline recession rate will be calculated. Here, two methods were used, the end point rate method and linear regression rate method. First, intersect points of the HWL and transects was identified by calculating the distance between the points, the long-term recession rate will be calculated (Figure 1.8).

1.4 Results

NPFs had been identified in each transect, the distribution of NPFs along the shoreline (Figure 1.9). The two sections of dune areas in the eastern part are found in front of Lake Montauk and Fort Pond, those are the connecting beach areas. Figure 1.10 shows the dune NPF at the western end. Those transects show clear dune-shaped profile with dune crest around 6.1m (20ft). The dune feature on Transect 602011 (Figure 1.11) showed as an isolated dune with a flat surface followed behind, that may due to the human structure which is a house built at that transect (Figure 1.10). At the western end, an area of bluff separates the dune fields and the reason for that gap as bluff may not only be the topography underline of that section of shoreline but also due to human structures, as in Figure 1.12-1.14, you can see, buildings are dense around this section. Such nearshore structures can be threatened where the long-term shoreline recession rate is high. In addition, the profiles have a steep slope. In the middle part of the shoreline, long section of shoreline was identified as dunes. Figure 1.15 shows the dune examples in this long stretch.

In many places more than one dune feature was be seen. Double dunes and multiple dunes could be found (Figure 1.15). These will be discussed in Chapter 2 as a new subclass, because a single

dune may be expected to react differently than a double dune or a multiple dune field to extreme events.

A transition from dunes to bluffs (Figure 1.16) occurred in the eastern part of the shoreline. The bluffs rose almost perpendicularly to a height ranging from 7.6-24.4 m (25-60 feet). Finally, examples from the two sections of duned shoreline separating bluffed shoreline on either side (Figure 1.17). The corresponding aerial photos (Figure 1.18) also showed a dense concentration of structures here. Both topography and human structure shaped these two connecting beaches.

Both end point rate and linear regression were used in this study to calculate the annual rate of shoreline retreat over a 30-year period from 1983-2013, that is after Superstorm Sandy. Use of the average-rate method and jack-knife method was not appropriate because of the limited dates for which shorelines were available. Prominent oscillations were seen in the recession rates attributed to longshore sandwaves (Figure 1.19). Upon inspection of the aerial photography many of these oscillation in the recession rate were attributed to ephemeral longshore sandwaves predominately in the 1983 shoreline. There were identified by inspection of the aerial photographs and checked using the vegetation. As such they were discounted in the identification of SHAs. The shoreline, however, could be characterized in four sections. At the extreme western end of the study area oscillation seemed to be superimposed on a linear trend in shoreline recession rate, decreasing to the east from about -0.4 m/yr; a central section where the spatial averaged rate was -0.06 m/yr followed by an eastern part where the rate again decreased linearly from about -0.5 m/yr (Figure 1.20). The extreme eastern section, dominated by the highest coastal bluffs was treated separately (Figure 1.21), with, again, a linear rate of shoreline recession for about -0.4 m/yr. The oscillations will be discussed in more detail in Chapter 3.

1.5 Discussion

During the process of delineating NPFs in the study area, combinations of NPFs could be identified. This leads Chapter 2 in the thesis: Dunes, bluffs, and peneplains on New York's Ocean Coast. In Chapter 2, combination from NPFs are used consider the response of the shoreline to extreme events in contrast to long-term sea level rise. In Chapter 3 Long-term Shoreline Changes and Storm Impacts at NY's Ocean Shoreline, variations in the calculated recession rates and the impact of Superstorm sandy are considered in the context of determining long-term shoreline recession, for the definition of SHAs. This involves the occurrence of transient shoreline undulations or longshore sandwaves. The fourth chapter considers evidence that extreme events can be "game-changers" by examining the response of the beach to earlier events in the context of Superstorm Sandy which occurred in 2012. With more details in each transect, better base topography can be put into beach profile model to predict the sand lost after a certain extreme event. This is done in Chapter 4: CSHORE, model beach profiles with different types of NPFs under extreme weather events.

1.6 Figures

Figure 1. 1. Example of NPFA and SHA in the study area.

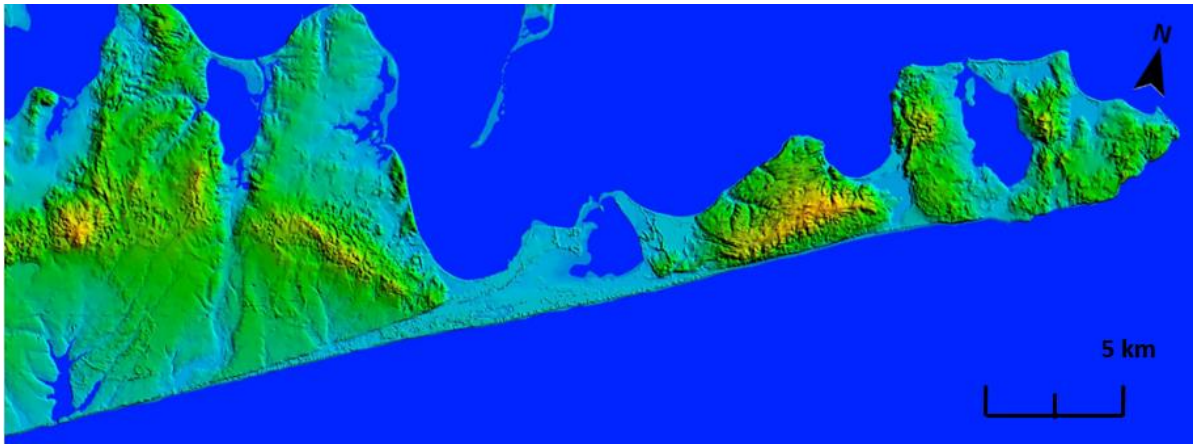

Figure 1. 2. Digital elevation image of the study area. The lighter colors represent higher elevations.

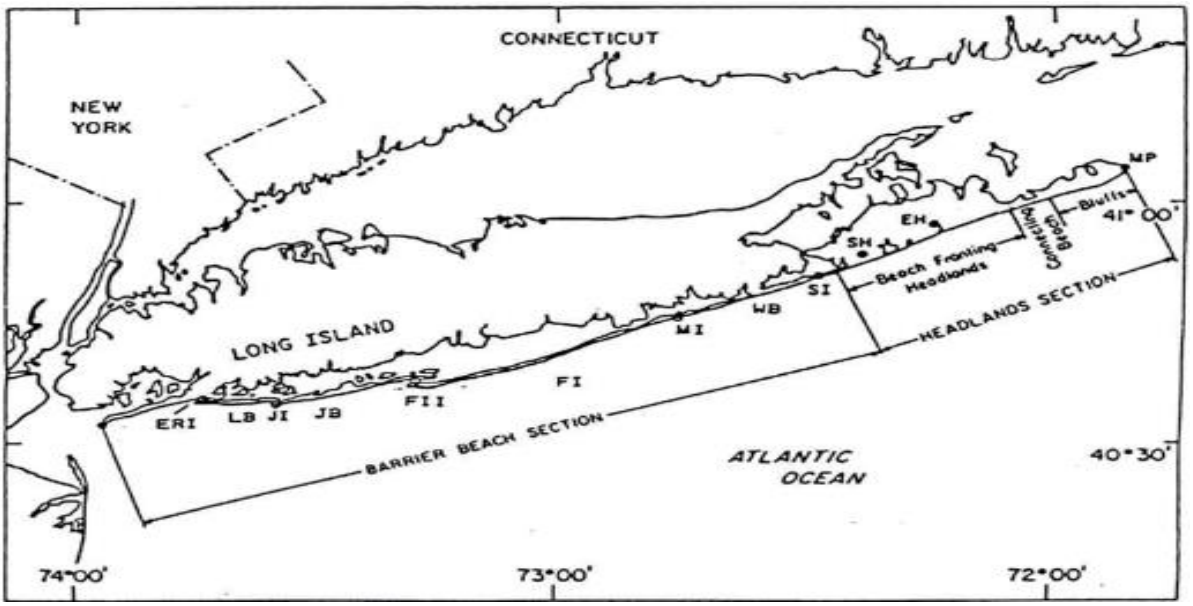

Figure 1. 3. Physiographic Provinces of New York's Ocean Shoreline (Taney 1961). "ERI" East Rockaway Inlet, "LB" Long Beach, "JI" Jones Inlet, "JB" Jones Beach, "FII" Fire Island Inlet, "FI" Fire Island, "MI" Moriches Inlet, "WB" Westhampton Beach, "SI" Shinnecock Inlet, "SH" Southampton Beach, "EH" East Hampton Beach, "MP" Montauk Point.

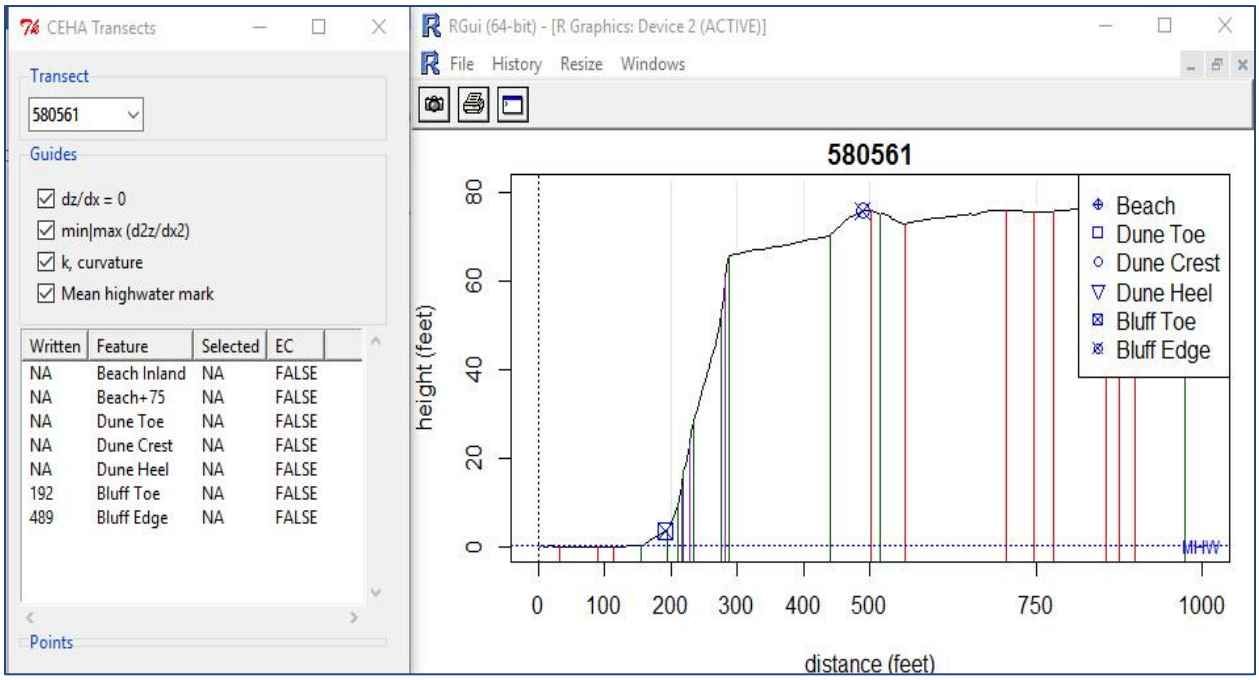

Figure 1. 4. The R-tool used to identify NPFs. Red line: first derivative of topography; purple line: second derivative of topography; green line: curvature of the profile.

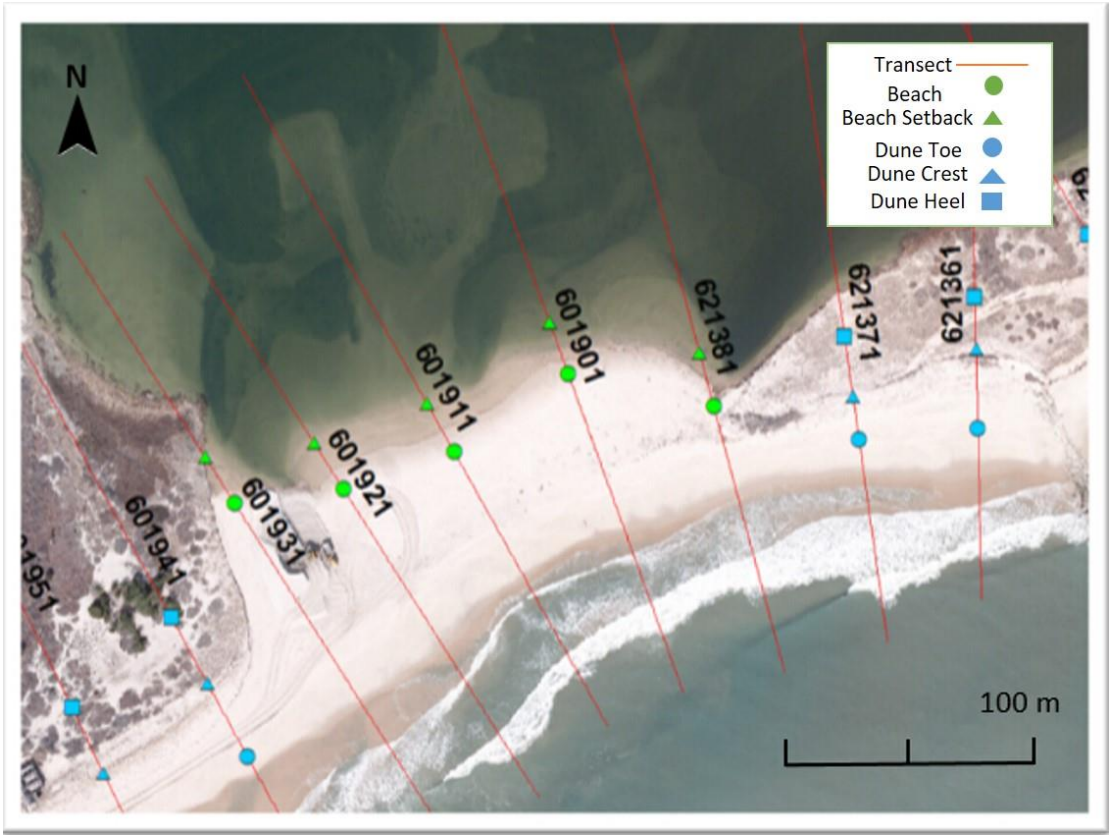

Figure 1. 5. Beach NPFs in the study area, no landward feature because of the Georgica Cove.

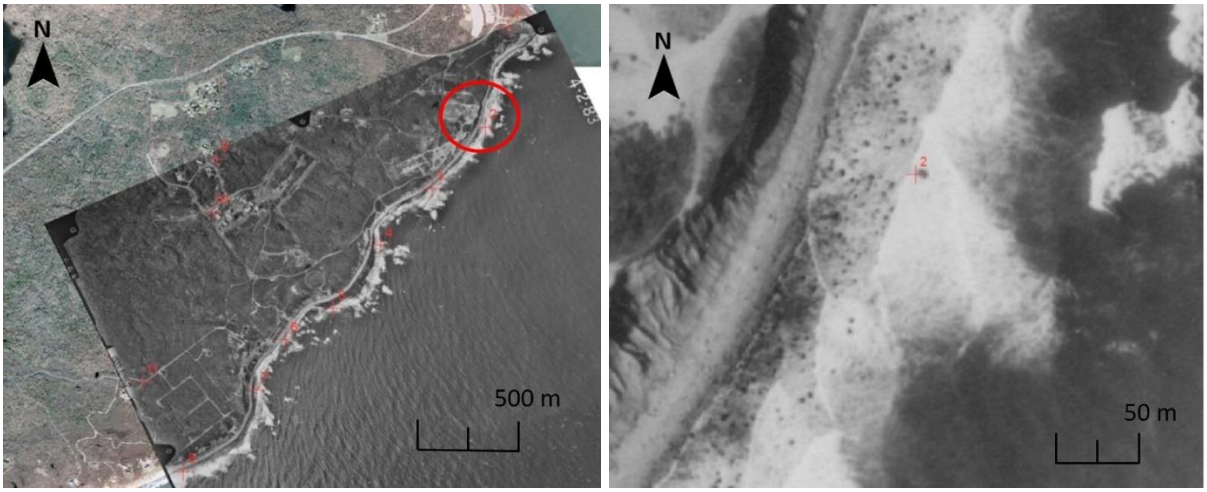

Figure 1. 6. Example of offshore rock as a control point for georeferencing, right picture is the enlarge picture for the area inside the red circle in the left picture.

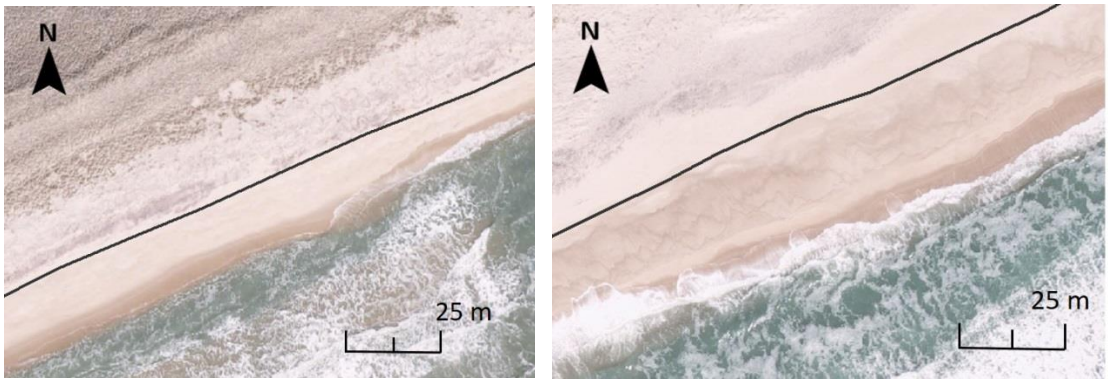

Figure 1. 7. Example of High Water Line.

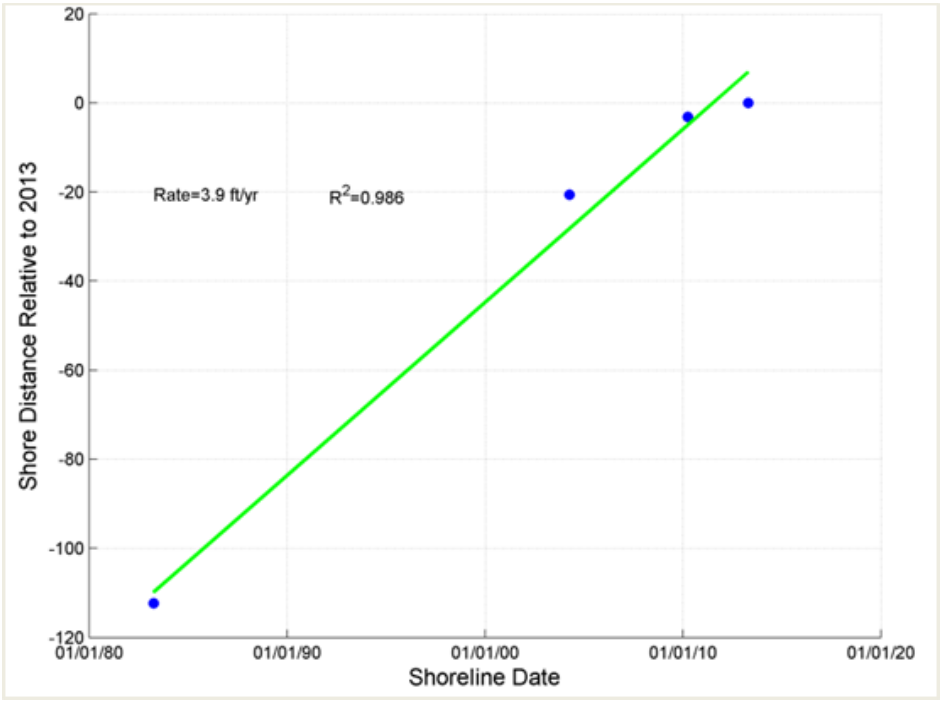

Figure 1. 8. An example of linear regression used to calculate recession rates.

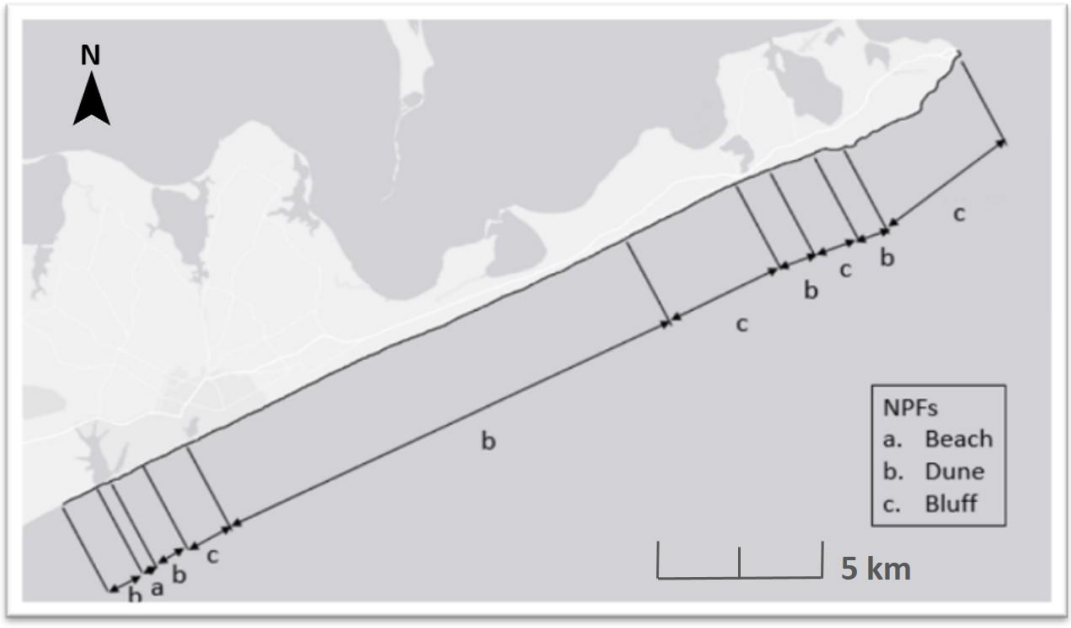

Figure 1. 9. NPFs' distribution.

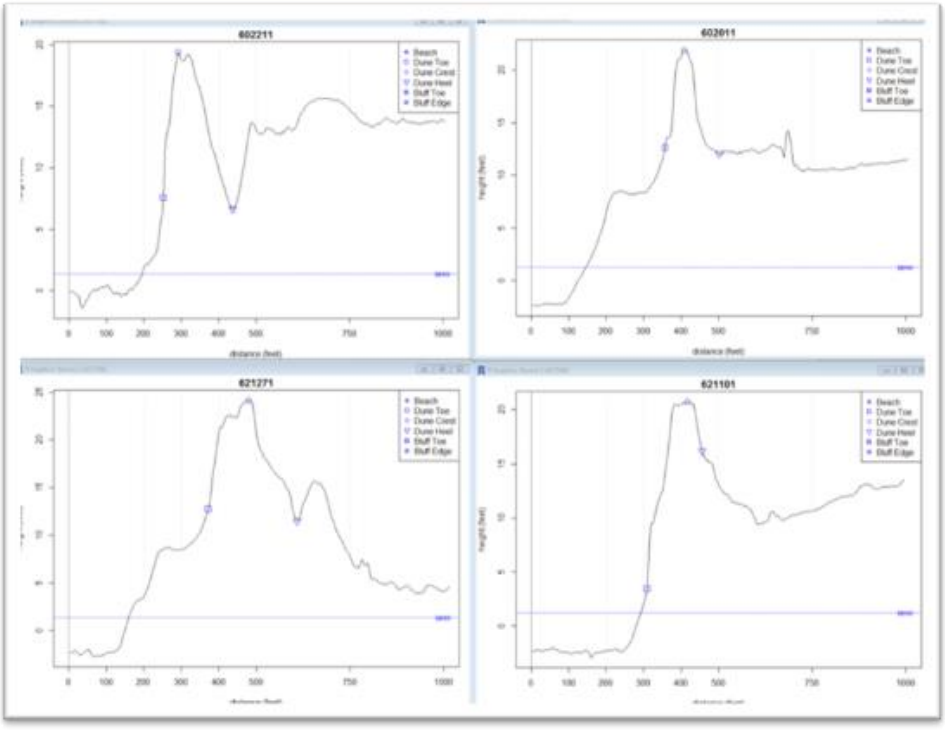

Figure 1. 10. Dune NPFs at the western end, the top right one's corresponding aerial photo is Figure 1.9.

Figure 1. 11. Transect 602011, an isolated dune followed with a flat surface.

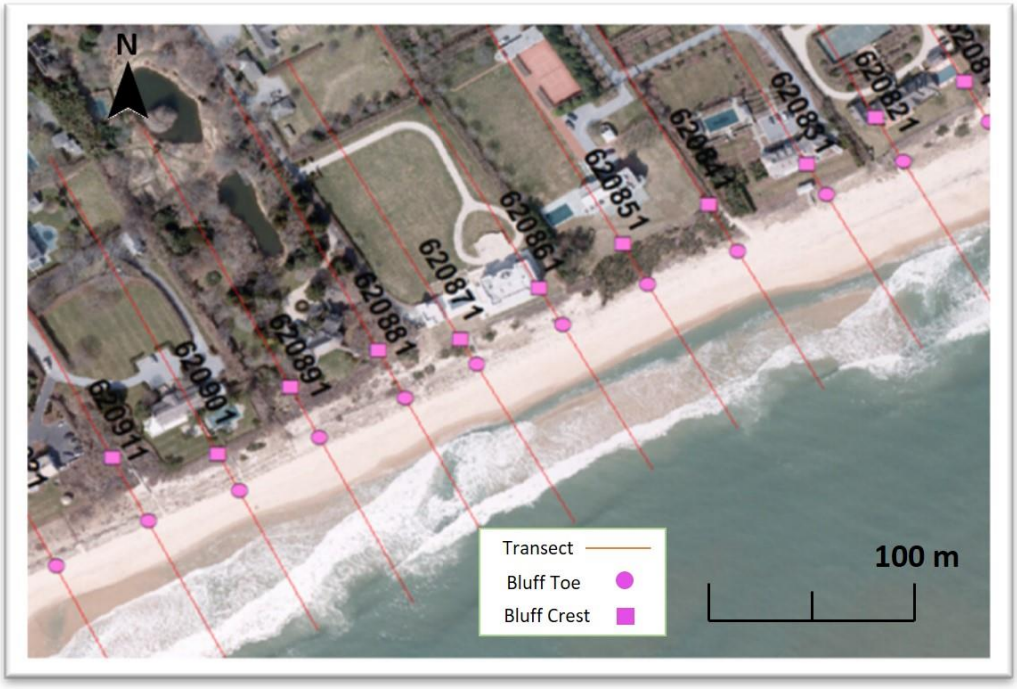

Figure 1. 12. The bluff section separates the western end dunes and middle part dunes.

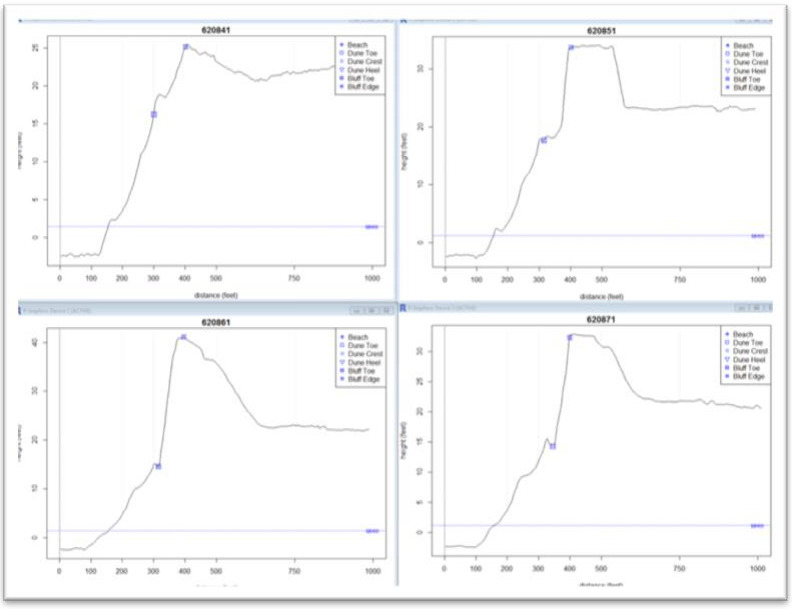

Figure 1. 13.The corresponding bluff transects in Figure 1.12, 620841-620871.

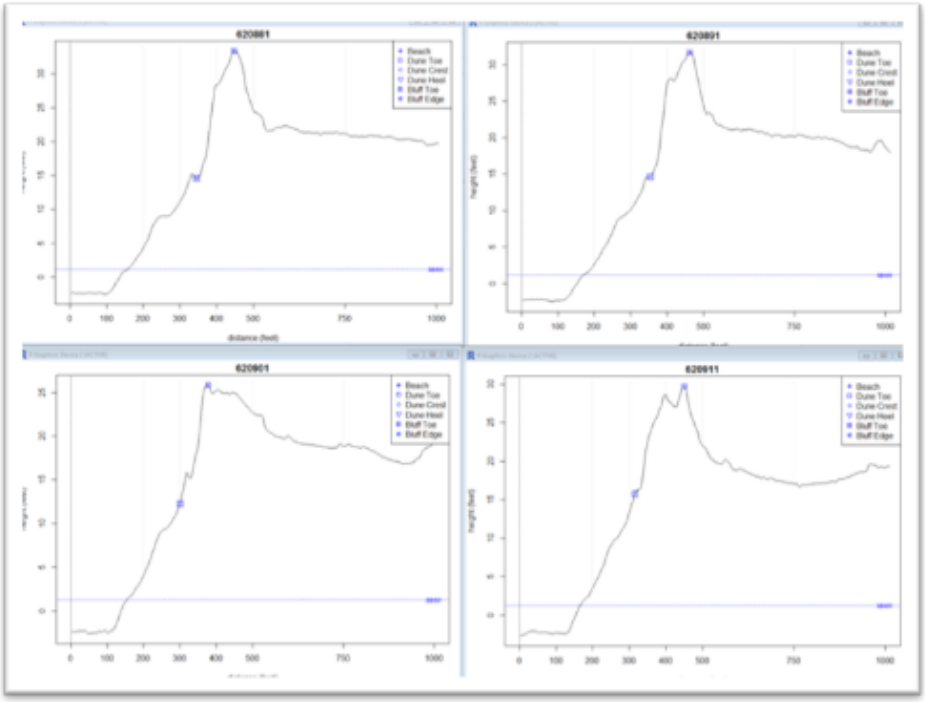

Figure 1. 14. The corresponding bluff transects in Figure 1.12, 620881-620911.

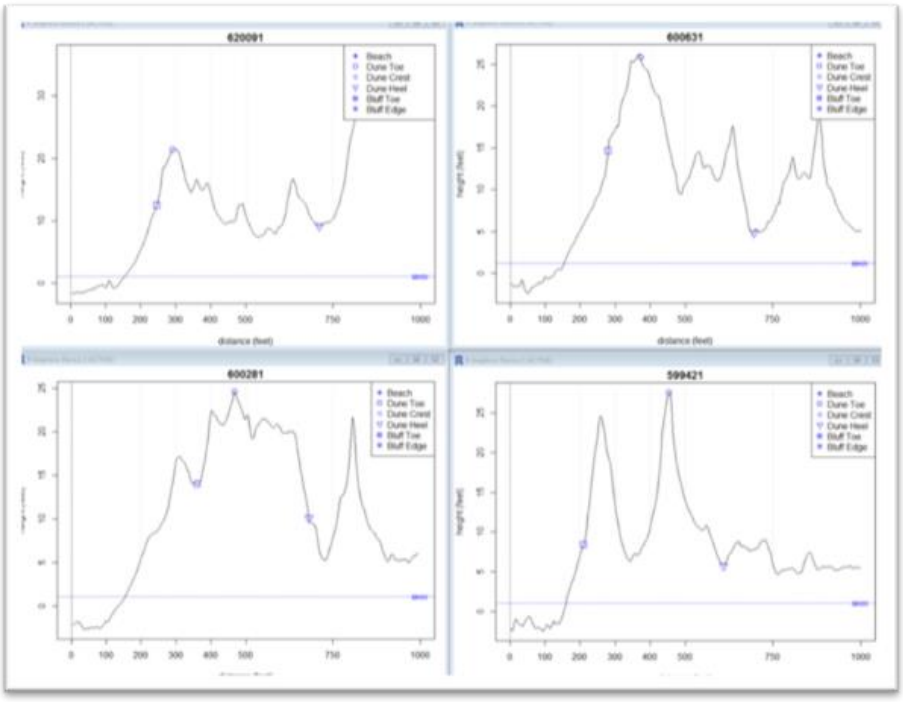

Figure 1. 15. Examples of multiple dune fields in the middle long stretch of shoreline.

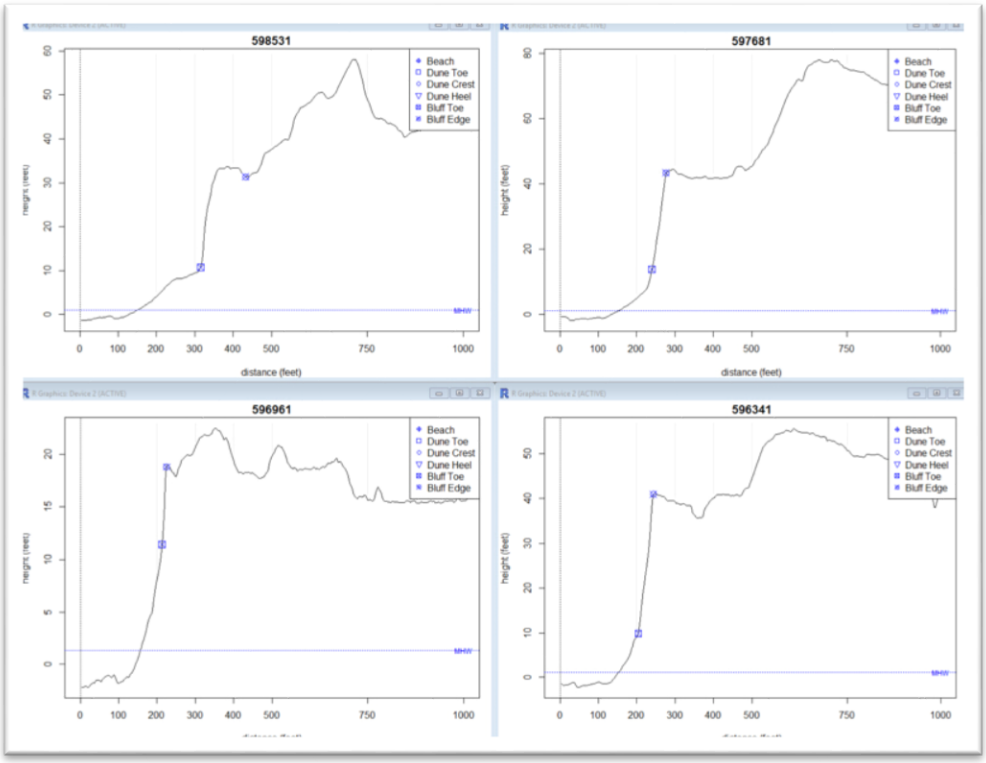

Figure 1. 16. Examples of bluff-transects at the eastern part.

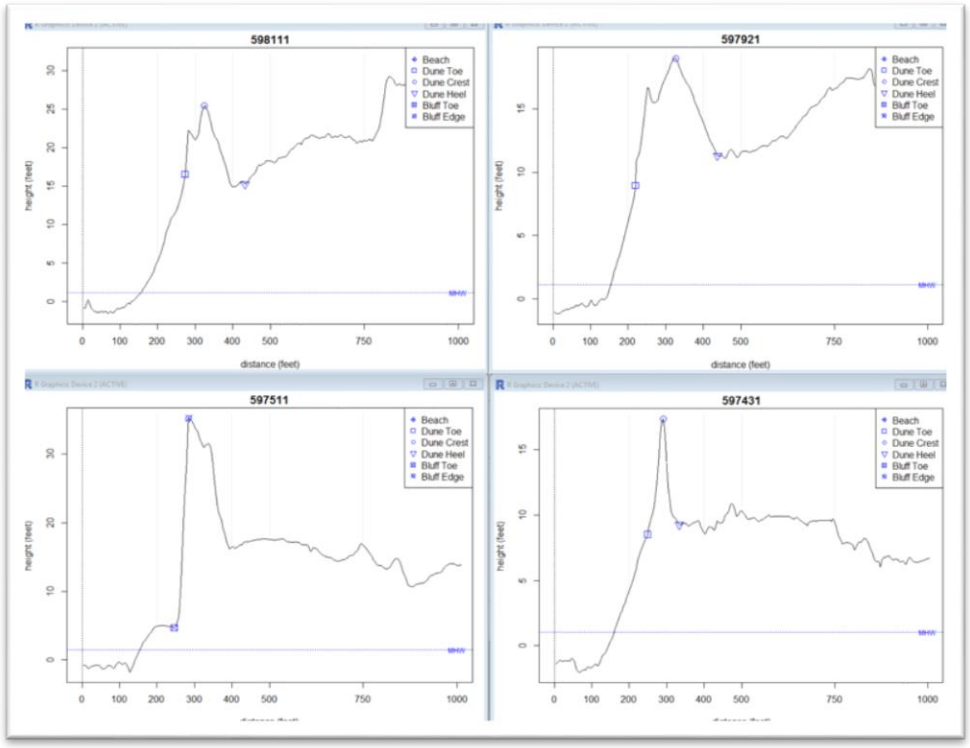

Figure 1. 17. Dune features at the eastern part in between bluff areas.

Figure 1. 18. Corresponding aerial photos for Figure 1.17.

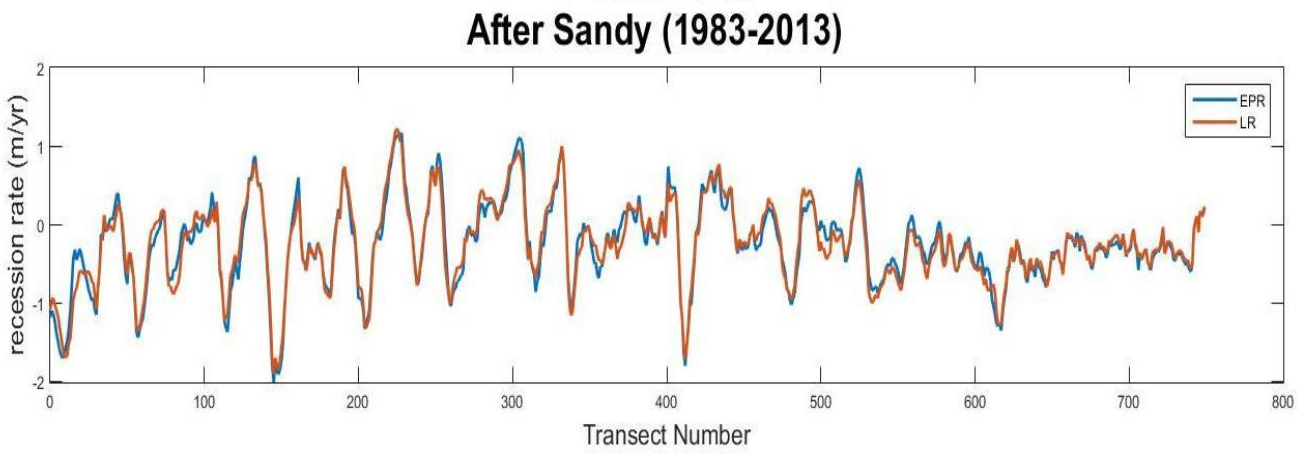

Figure 1. 19. Oscillations in recession rates that may attribute to longshore sandwaves using the end-point rate (EPR) and the linear regression (LR).

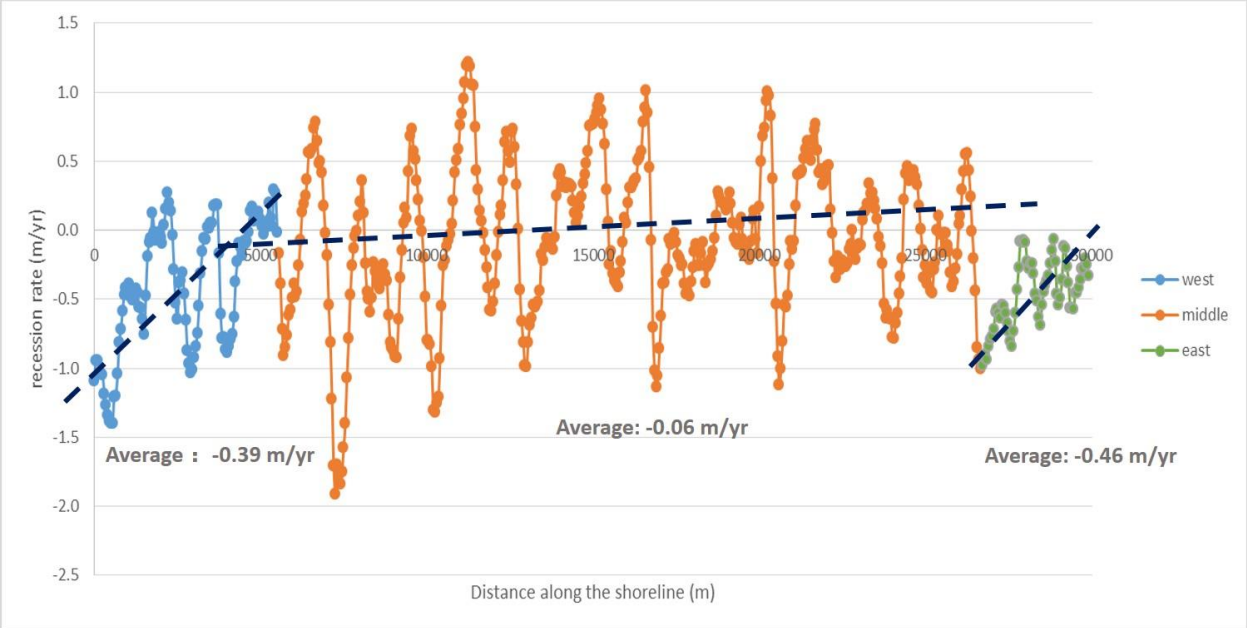

Figure 1. 20. Recession rates after Sandy in section 1.

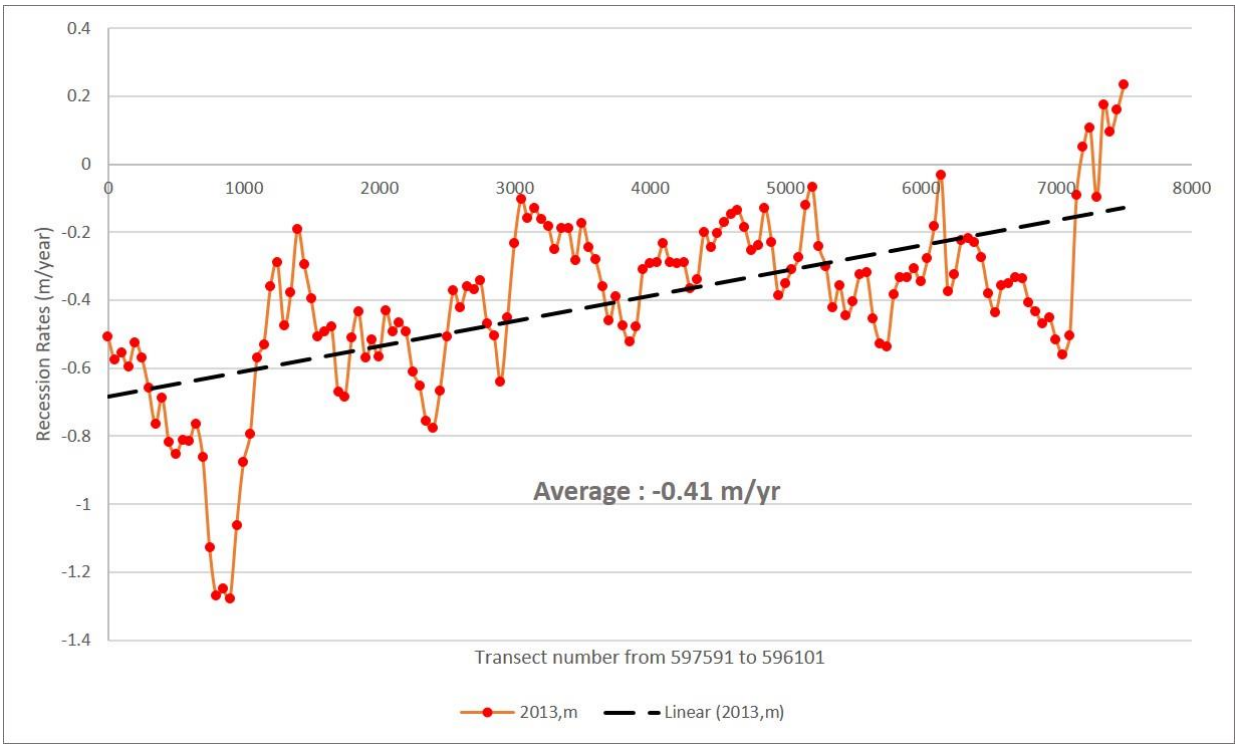

Figure 1. 21. Recession rates after Sandy in section 2.

1.7 Tables

Number	Image ID	1st Order Polynomial (m)	2nd Order Polynomial (m)	3rd Order Polynomial (m)
1	7-398	5.27	3.02	1.08
2	7-402	4.12	1.99	0.69
3	7-405	4.32	2.82	2.17
4	7-408	5.37	3.10	1.81
5	7-411	5.47	2.39	1.31
6	7-414	7.24	4.95	1.95
7	7-417	9.21	3.36	1.60
8	7-420	8.71	4.80	2.82
9	7-423	10.96	3.73	2.05
10	7-426	12.88	7.09	4.53
11	7-429	14.43	13.44	9.00
12	7-432	15.65	12.55	1.35
13	7-435	3.58	1.96	0.48
14	7-438	4.17	2.44	0.52
15	7-441	6.36	3.67	1.59
16	7-443	19.91	8.33	0.21
17	7-446	17.18	5.82	0.37
18	7-449	17.95	4.67	1.47
19	7-451	18.14	5.41	4.00
20	7-453	26.93	14.23	3.50
21	7-456	18.06	12.06	2.64
22	7-459	12.72	8.17	2.46
23	7-462	37.09	21.43	0.40
24	7-465	12.58	8.82	0.97
25	7-468	11.32	9.74	1.54
26	7-471	9.22	2.76	0.25
27	9-793	19.70	15.65	3.10
Average		12.54	6.98	1.99

Table 1.1. Georeferencing error for 27 sets of comparison between historical pictures from 1983 and modern image from 2010, unit is in meter.

Chapter 2: Dunes, Bluffs, and Peneplains on New York's Ocean Coast

New York State has a conservative policy that treats dune and bluff NPF's with the same intrinsic value. Recognizing the vulnerability of beaches without bluffs or dunes, a greater set-back was ascribed to there. As a practical matter, however, the characteristics of some features, or the combination of features, should provide different levels of protection to different erosional stresses. The characteristics of particular NPFs result in a degree of natural protection that should not only differ depending on the combination of NPFs superimposed, but also allow the shoreline to respond differently to extreme events than it does to long-term sea-level rise.

2.1 Introduction

Persistent problems of coastal erosion and flooding on NY's ocean shoreline were only accentuated by the impact of "Superstorm" Sandy on 29 October 2012. Superstorm Sandy had been viewed as a hybrid storm, with a distinctly warm tropical core transit to a cold-core, extratropical vortex (Halverson and Rabenhorst, 2013). From 24 October 2012, Sandy moved from the Caribbean to the East Coast of the United State. During 29-30 October 2012, the storm took its extratropical transition while the Atlantic's Gulf stream imply additional energy into its circulation. Sandy caused damages to many countries from the poorest Haiti to one of the richest countries, the US (Kunz et al. 2013). Below are different aspects of damages caused by Sandy (Halverson and Rabenhorst, 2013). High wind conditions followed the path of Sandy, the highest guest (90-100 mph) happened along the New Jersey's coastline and over New York City. With the wind, it raised big waves on the open sea. Also, during Sandy, two high tides imposed on the wind and wave. In NYC region, the storm tide reached 4.27 meter (14 feet). Hurricanes are known to come with heavy rainfall and so does this Superstorm Sandy, but another weather condition came with Sandy is the early season snowfall. Both the low temperatures due to the high elevation and the high moisturized tropical air mass contributed to the wet and heavy snow. Power outages and shortage of fuel is another aspect of this storm. Ten million people from Virginia to Maine (17 states) were under the influence of power outages, the time period lasted for weeks for some of them. In many of the gas stations, the fuel was being rationed according to odd and even days. It is the second-costliest hurricane (with an estimated value of 78-97 billion US$ for the US) in the history of the United States with the first one being Hurricane Katrina on 2005. Compared to Katrina, in the aspect of lives lost, the number decreased from 1800 and 125. But in terms of house damage, the total number of destructed building increased from 233,000 to 570,000. This was because of the high-density residence rate in the Northeast US including the south shore of Long Island. By any measure, Superstorm Sandy was a historic event and considered by some to be a "game-changer".

Long before Sandy, however, NY, like other coastal states, managed its shoreline with long-standing policy and regulations. As documented in the first chapter, one of the mainstays of NY's program has been the preservation of NPFs. Alterations of NPF's might reduce the protection against erosion and coastal flooding, or they may lower the reserves of sand available to replenish storm losses through natural processes.

Classically, the cross-sectional geometry of the coast has been used to examine how the shoreline responds to erosional stress. This type of study, in particular, seeks to evaluate the mode of the shore's response to rising sea level by examination of the coast's cross-sectional geometry. The technique is not new. As early as 1919, D.W. Johnson examined the development of the barrier island by looking at the altitude of the offshore slope with respect to the slope of the coastal peneplain (Johnson 1919) concluding that, if the landward extrapolation of the shelf slope intersected the sea level datum at or seaward of the marginal bays, barrier island formed as spits in response to longshore action, under the assumption that sea level was stable. If the intersection occurred landward of the bay, barrier formation occurred by increasing deposition offshore, in addition to longshore deposition. Since Johnson's seminal research, other investigators have conducted similar studies along the shoreline of the United States over the years (e.g. Bruun 1962; Schwartz 1967; Dubois 1977; Hands 1980; Rosen 1978; Fisher 1982; Weggel 1979; and Maurmeyer and Dean 1982). Although superseded by other quantitative methods, profile geometry is still useful in interpreting features along the ocean coast and characteristics of the shoreline response to rising sea level.

For this study, the cross-sectional geometry of the eastern ocean shore of Long Island was re-examined using modern surveying techniques in order to redefine the NPFs. As discussed in Chapter 1, LiDAR datasets from November 2011 and April 2012 had been used to identify NPFs. The character of NPFs is now better resolved especially where features overlap.

In the study area, dunes crest typically at elevations about 7 m although the crests of some dunes are above 12 m. The late geomorphologist, Rhodes Fairbridge, suggested that, because of their size, the largest dunes along Long Island's ocean shoreline were relict features built at a time of lower sea level when a greater expanse of beach sand was available (H. Bokuniewicz, Stony Brook University, personal communication, 2013). As early as 1914, Myron L. Fuller identified many of the large ridges on Long Island as dune sand resting on terraces. Some were "conspicuous hills from 50 to 100 feet high" and "of relatively recent origin" (Fuller 1914).

As part of the research, it was shown that the elevation of dune crests along the headland section can be attributed to the growth of dune structure upon a pre-existing terrace. The East Hampton terrace, at an elevation of about 7 m grows to become the dominant bluffs at Montauk Point. Where dunes are present they are likely to provide the first line of protecting for storm events. However, in the face of a long-term rise in sea level, the excavation of the underlying bluff may be the controlling factor.

2.2 Methods

The original classification of the NPFs are the beach, dune, and bluff, but in some transects, more than one NPF were found. Each transect had been reexamined and newly classified by reviewing the LiDAR topography. These subclasses were characterized using the methods described in Chapter 1 and added to form a new classification. The updated classification includes three new classes: dunes formed on top of a bluff, dunes formed in front of a bluff and multiple dunes.

2.3 Results

The distribution of NPFs including the new subclasses is shown in Figure 2.1. The NPFs change from dunes to bluffs from west to east. NPFs captured the most landward feature so that the beach itself as an NPF only consisted 0.6% of the study area. In the new classification, the eastern section was identified as either dune on top of a bluff or as dune in front of a bluff. Different types of dunes were found in two connecting beaches at the east end as well as combinations of dunes and bluffs (Figure 2.2).

The revised classification of NPFs (Table 2.1; Figure 2.2) had single dunes being the NPFs along 27.1% of the shoreline; multiple dunes comprising 20.7%. Bluffs were the NPF along 26.6% of the shoreline. Dunes in front of a bluff comprised 12.1% and dune on top of a bluff crest made up 12.9%. The remaining 0.6% of the shoreline was identified as the beach. The coast at Montauk Point remained a well-defined bluff (Figure 2.2 and 2.3). The peneplain is capped by the Ronkonkoma Moraine. The beaches in front of the bluff are coarse sediment, cobbles in some places, with little or no source of sand suitable for building dunes. During major storms, the storm-tides can submerge the beach and allow waves to undercut the toe of the bluff. An undercut bluff face may collapse, removing protective vegetation and carrying sediment to the beach along a stretch of the shoreline usually only a few hundred meters in extent. Bluffs on the north shore of Long Island exhibited collapsed features mostly less than 100 m in longshore extent (Bokuniewicz and Tanski, 1980). Over the long term, the bluff crest migrates landward by the various and random occurrence and coalescence of individual collapsed sections.

Among the bluffed section, short stretches of shoreline begin to appear where dunes have formed on top of the bluff crest (Figure 2.2 and 2.4). The elevation of the bluff crest decreases below about 7.1 m between segments on the moraine. These segments were those that had been connected by short stretches of barrier beach as sea level rose after the last deglaciation at Lake Montauk and Fort Pond. The beaches, apparently, provided a source of sand needed to grow dunes because the dune crests have been constructed above the elevation the bluff face. Bluff crests here have been buried by dune sand. At the margins of the connecting beach in front of Fort Pond, the source of sand seemed to be inadequate to cover the bluff crest, but still sufficient to create a dune in front of the bluff face (Figure 2.2 and 2.5).

Further, west, the line of bluffs is interrupted by what are known as the Walking Dunes east of Napeague Harbor where the outwash peneplain is absent for a short stretch of the shoreline, Napeague Beach (Figure 2.2 and 2.6). The shoreline spanned a gap in the moraine that had been bridged by marine sands to form a connecting beach. It would seem that this section formed as a barrier beach connecting a headland island at Montauk and the then-terminal headland of the moraine segment further west. Dune fields crest at about 9 m in front of low-lying sandy terrain. It seems likely that the connecting beach was formed by the elongation of sand spit from the east. This process would have created a series of curving beach ridges prograding across the gap. The abundance of sand in the subaerial connecting beach and the low relief allowed prevailing winds to create multiple, secondary dunes. If eroded in extreme weather events, these could reform as long as the source of wind-driven sand remains adequate. Any multiple dunes formed as relic ridges, however, would be irretrievably lost as NPFs. Continuing west, the bluff crest gradually approached the shoreline. Dunes that dominate the NPFs eventually were found first in front of the bluff face and then on top of the bluff crest (Figure 2.2).

Bluff crests without dunes ranged in elevation from 4.1 m to 33.5 m (Figure 2.7). The average dune crest elevations along entire the study area average 7.1 m, but the distribution was not uniform. The highest dune crests were found along the connecting beaches in front of Lake Montauk, Fort Pond, and Napeague Harbor. In the absence of bluffs, dune crests ranged in elevation from 3.7 m to 10.5 m. Slightly higher dune-crest elevations, ranging from 5 m to 15.4 m, could be found in front of bluffs where the bluff crests were from 6.2 m to 22.9 m high (Figure 2.7). Bluff crests with elevations lower than 7.1 m tended to be found covered by dune sand. The highest dune-crest elevations, ranging from 3.7 m to 21.1 m, could be found on top of bluff crests from 2.3 m to 16.4 m in height. Above that elevation, whether or not the bluff crest was covered seemed to depend on having an adequate source of dune sand. Where they existed on top of the bluff crests, dunes tended to crest about 2.5 m above the bluff crest ranging from 1.0 to 5.5 m. It seems possible that the dunes on the highest bluffs were not formed by climbing directly from the beach, but rather from the redistribution of sand inland. No dunes have formed in front of bluffs with crest elevations above about 12 m.

Where the dune crest elevation was below the bluff crest, the dune provides the first line of defense against extreme events. The eroded dune may be expected to recover after an extreme event, as long as the sand source area was sufficient. However, if the dune was compromised, the bluff itself provided protection against flooding and resistance to landward migration of the shoreline. In the face of a long-term rise in sea-level, the dune may be less important as an NPF. Rather, the bluff provides protection and controls the shoreline response. Bluffs and relic dunes will not recover as NPFs if compromised by erosion.

2.4 Discussion

2.4.1 The role of dune NPF

The primary NPF for extreme events is identified as dune. FEMA sets an empirical minimum cross-sectional area for a dune expected to survive the 100-year storm. The frontal dune reserve, that is, area of the dune profile from the dune crest to the 100-year storm surge elevation, must be greater than 540 square feet (Hallermeier and Rhodes, 1986)[1]. This is equivalent to 540 ft^3/ft of shoreline, or 165 m^3/m. In the study area, the 100-year storm surges's elevation ranged from 8.7 to 9.7 feet National Geodetic Vertical Datum (NGVD) and between 1995 and 2002, 24% of the dunes in the study area exceeded these criteria (Batten 2003). The resiliency of dune protection would then rely on the ability of the dune to rebuild or to be rebuilt by people, before the next event and this, of course, could depend on the volume of sand lost. Multiple dune lines provide extra protection, but if they are eroded they would require an adequate source of wind-driven sand to recover. Reforming multiple dunes naturally requires not only a source of sand but also a long period of time for the winds to act. If the dune is truly a relic feature, say for example, a beach ridge now isolated from the former growth of a spit, no natural recovery would be expected; the feature would not be resilient regardless of the erosional loss. The dunes would play a smaller role in determining the shoreline response to the long-term rise in sea level. Rather, the underlying bluff face and terrace would control the retreat rate of the shoreline in the long-term. The geometry of the submerged equilibrium beach and ramp might be assumed to be invariant if the wave climate and source sediment grain-size distributions are relatively constant. The long-term retreat of the shoreline in the face of rising sea level would require not only the recession of the subaerial bluff face but also by the excavation of the bluff sediment buried below the submerged equilibrium beach to form the ramp.

2.4.2 Three scenarios of sea level rise

Recognizing the control exerted by the bluffs on the response of the shoreline to long-term sea level rise, three scenarios might be distinguished. The special case where the slope of the coastal peneplain was approximately equal to the slope of the ramp had been examined by Zimmerman (1983). To maintain the coastal morphology as sea level rises at a rate of 3 mm/year, it had been estimated that a wedge of sediment with a volume of 14 m^3/m of shoreline must be excavated and displaced from the bluff sediment under the dune (Zimmerman 1983). The fine fraction of this sediment would be suspended, dispersed and likely end up in estuaries and salt marshes in the region. The coarse fraction would probably be left in place as a lag pavement blanketed by the

[1] FEMA rules have undergone revisions. A value of 1080 square feet may be used.

mobile sand fraction. The sand fraction would add to the active sand reservoir feeding the longshore transport, maintaining the equilibrium beach and serving as a source of dune sand. In this case, the position of the dune, whether in front of the bluff or on top of the bluff crest remains in place as the shoreline moves landward under a rising sea level (Figure 2.8 A), but the bluff, whether exposed or buried under (transient) dune sand, must be excavated for the shoreline to retreat. The shoreline recession is the rise in sea level divided by the slope of the ramp (or coastal peneplain).

If the slope of the coastal peneplain is less than that of the ramp, the elevation of the bluff crest decreases as sea-level rises and dunes in front of the bluff would eventually migrate over the bluff crest (Figure 2.8 B). Secondary dunes behind the primary dune could be reformed if they are active aeolian features, as long as the sand source remained sufficient. The secondary dunes maybe relic features. Napeague Beach, for example, is blanketed by dune sand over older beach ridges. If these are lost in a severe storm, it seems unlikely that the current arrangements of NPFs would reform because the existing dune structure is a relict morphology. In the case where the slope of the coastal peneplain is greater than the slope of the ramp, the recession is controlled by undercutting and collapse of the bluff face which depends on the shear strength of the bluff soils. The dunes were expected to be "squeezed out" in front of a steeply sloping, subaerial bluff face.

2.4.3 Dune on top and dune in front.

For dunes formed in front of the bluff, the source of the sand will be from the underlying beach with the wind blowing sand to pile up in front of the bluff. For dune on top of the bluff, the source of the sand has a different explanation. Three possible sources were discussed by Jennings 1967 about the cliff-top dunes along the shoreline of Australia. The sand may come from a beach source with the unusual direction of sand drifting; the source laid seaward and disappeared after coastal recession or inundation; the sand was emplaced during a time period of high sea level (Jennings 1967).

In this case, the barrier beach formed further west, so there is no seaward source. It is possible the sand is fed from the underlying beach for bluff with lower elevation, but the bluffs around the east end of the study area are with elevation up to 33.5 meters. For those high bluffs, it is unlikely the source of sand is from the underlying beach. So the bluffs can be a result of sand piling during the high sea level time period. If the bluff coast is higher than 18 m (Figure 2.7), dune seemed unable to form from the beach on top of the bluff crest.

2.4.5 Human structures

In the study area, human structures include buildings, parking lots, roads, revetment and groins. At the westernmost section of the study area there are three groins (Bokuniewicz 2003), the corresponding NPFs are dunes (Figure 2.9). The density of building in the study area is dense (Figure 2.10), expect in the western part of Napeague Harbor and around the Montauk Point. A detailed land-use Map is available at:

http://www.Suffolkcountyny.gov/Departments/Planning/Divisions/CartographyandGIS.aspx.

The western section is dominated by low density residential development, medium density residential land-use is found in places on the ocean beach by Napeague Harbor and low to medium density in the Village of Montauk.

2.5 Conclusion

The southeastern ocean shoreline of Long Island is characterized by six types of NPFs: beaches, bluffs, single dunes, multiple dunes, dunes fronting bluffs and dunes formed on top of a bluff crest. Where dunes are present they provide the first line of protecting for storm events. However, in the face of a long-term rise in sea level, the excavation of the underlying bluff is likely to be the controlling factor. Assuming an invariant cross-sectional geometry, the retreat of shoreline requires the excavation of the material on a bluffed coast down to the depth of wave-base, where the ramp is formed.

2.6 Figures

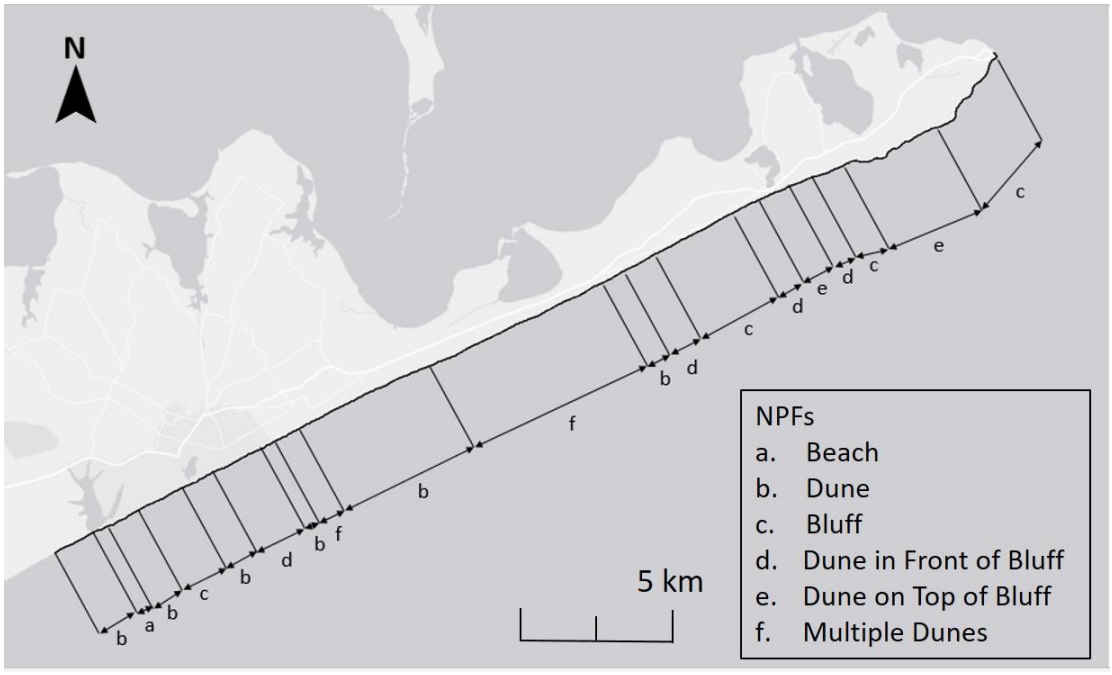

Figure 2. 1. NPFs' distribution after subclasses.

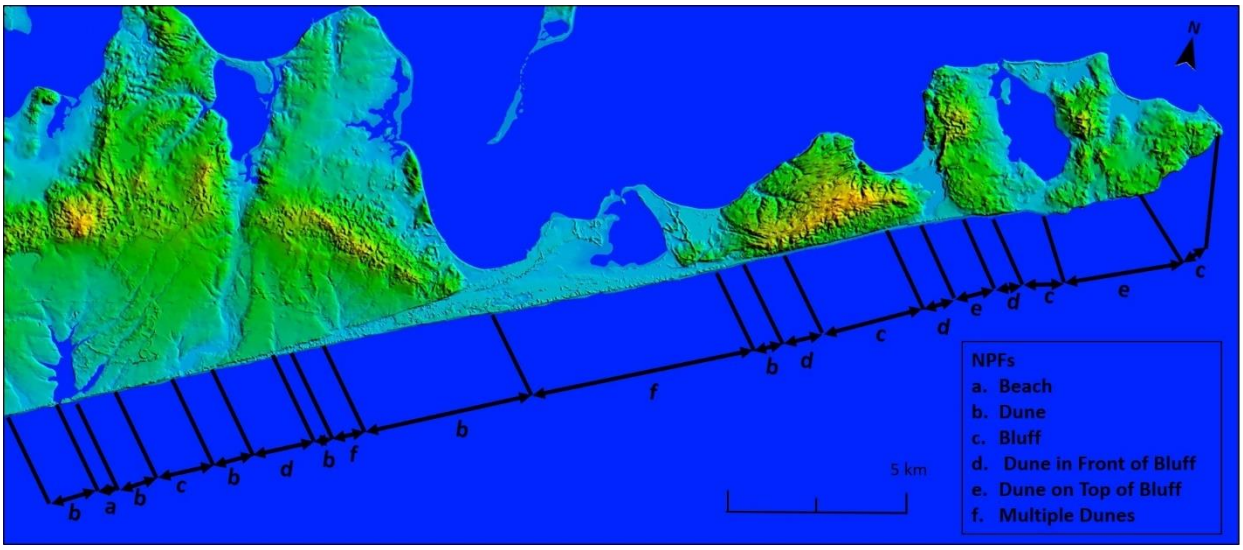

Figure 2. 2. The Study Area with the revised designation of NPFs. The new NPFs are dune in front of the bluff (labeled "d"); dune on top of the bluff (labeled "e"); and multiple dunes (labeled "f").

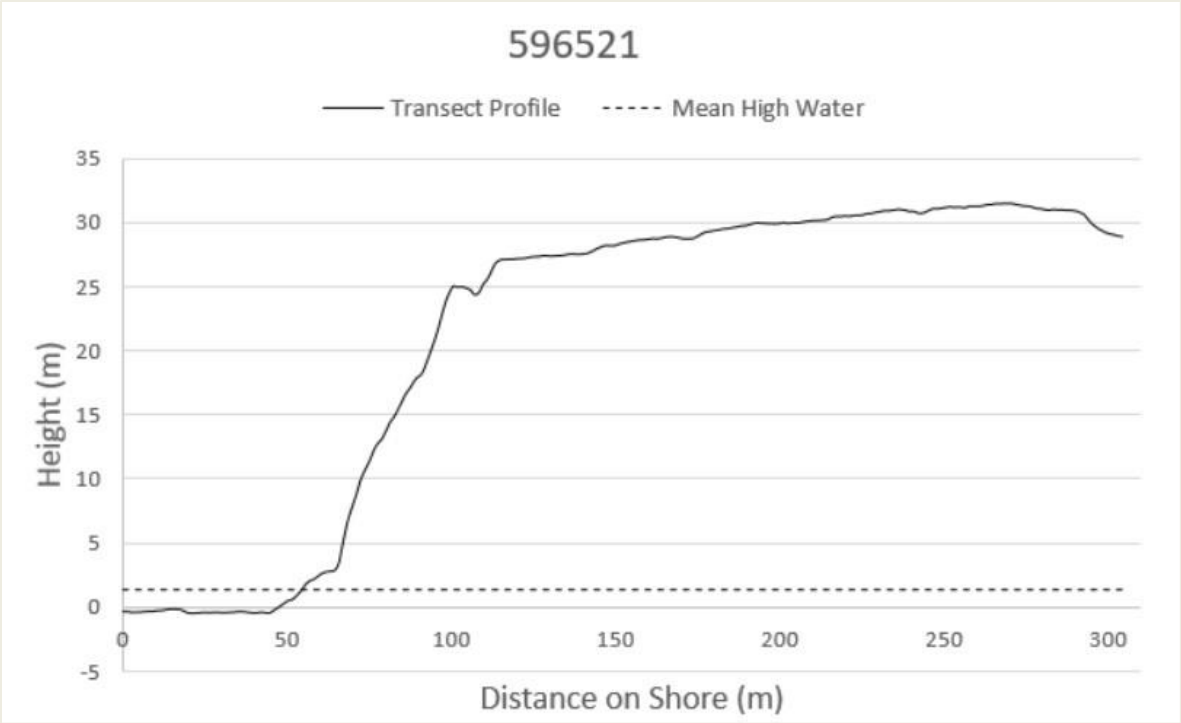

Figure 2. 3. Profile across the bluffed coast at Montauk.

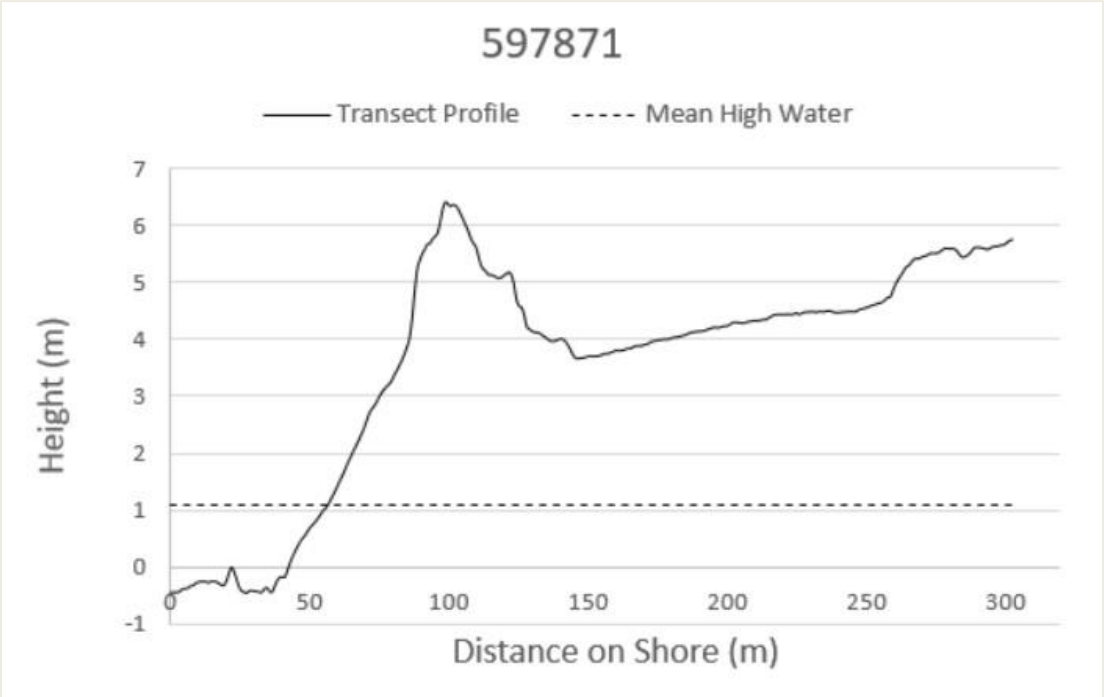

Figure 2. 4. Profile of a dune burying the bluff crest.

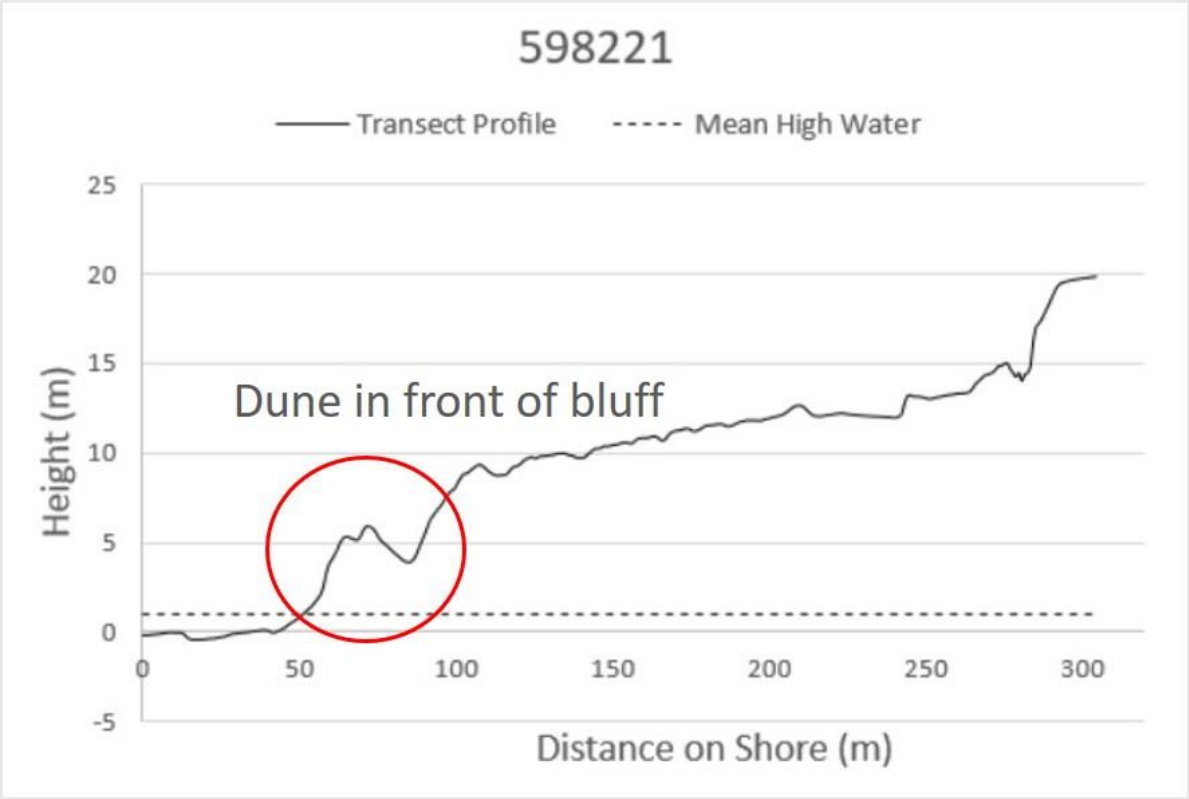

Figure 2. 5. Profile showing a dune in front of a bluff.

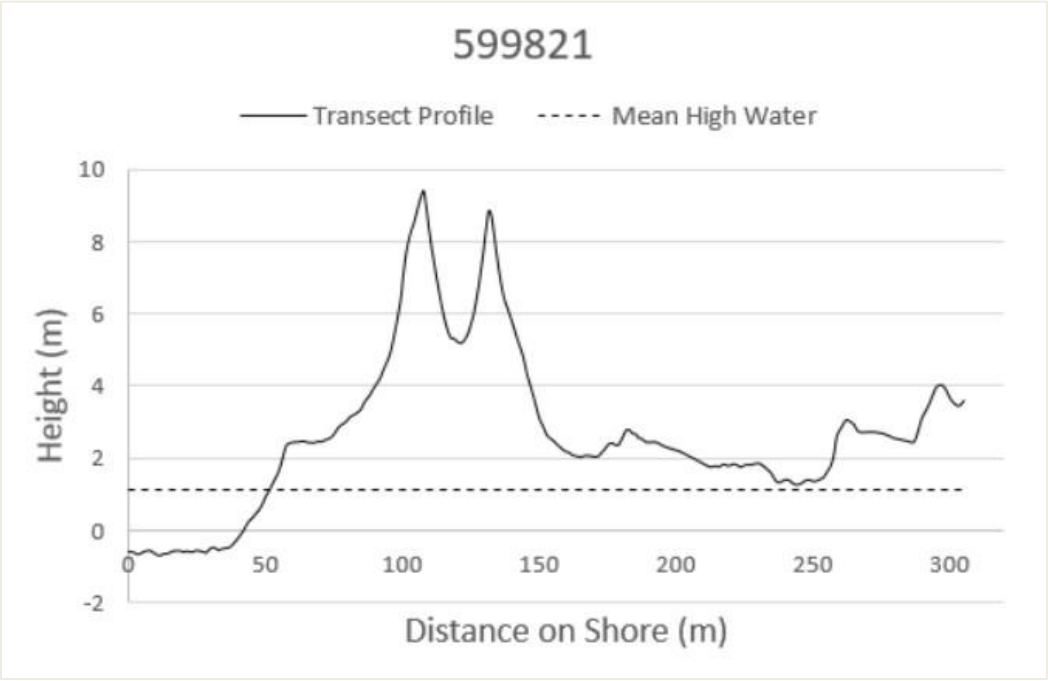

Figure 2. 6. Transect across a double-dune field.

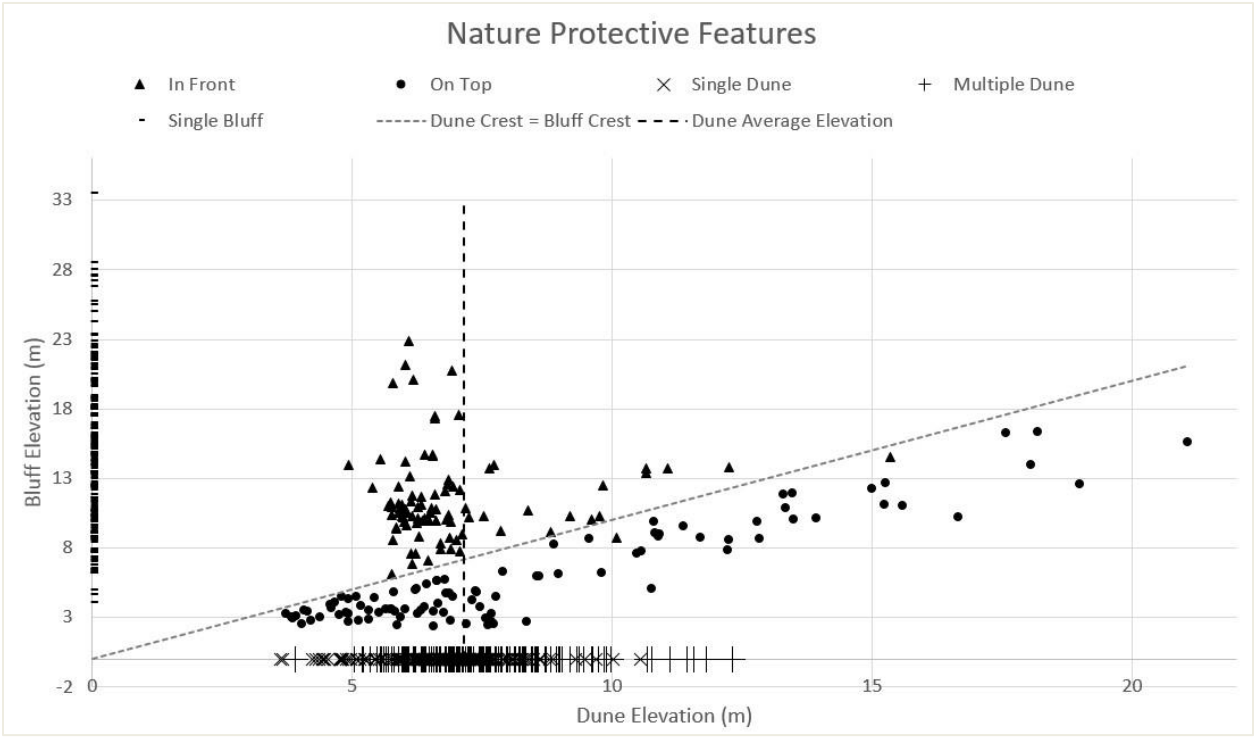

Figure 2. 7. Elevations of NPFs in the study area.

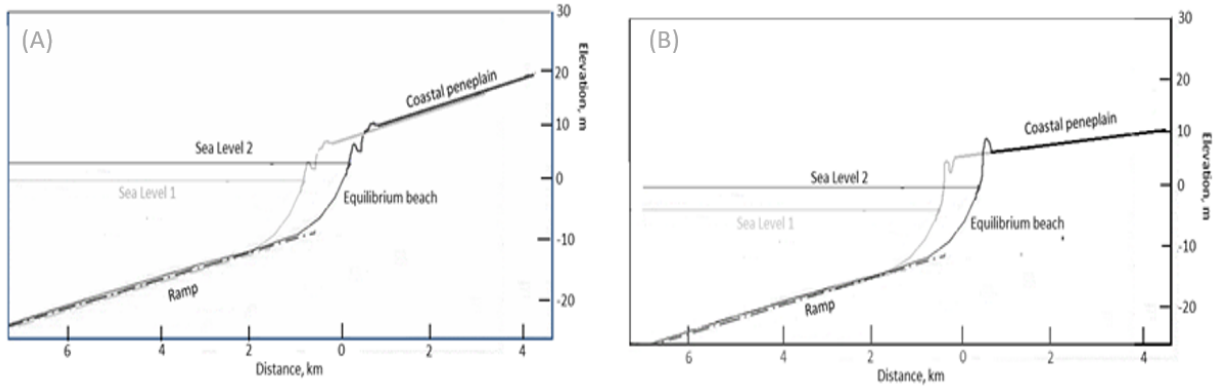

Figure 2. 8. (A) Bluff, with a dune in front, at the edge of a coastal peneplain which has the same slope as the ramp. As sea level rises from position 1 to position 2, the geometry remains invariant; (B) Bluff, with a dune in front, at the edge of a coastal peneplain which has a slope lower than that of the ramp. As sea level rises from position 1 to position 2, the submerged profile remains invariant but the dune migrates over the bluff crest.

Figure 2. 9. Three groins on the westernmost part of study area (Georgica Pond).

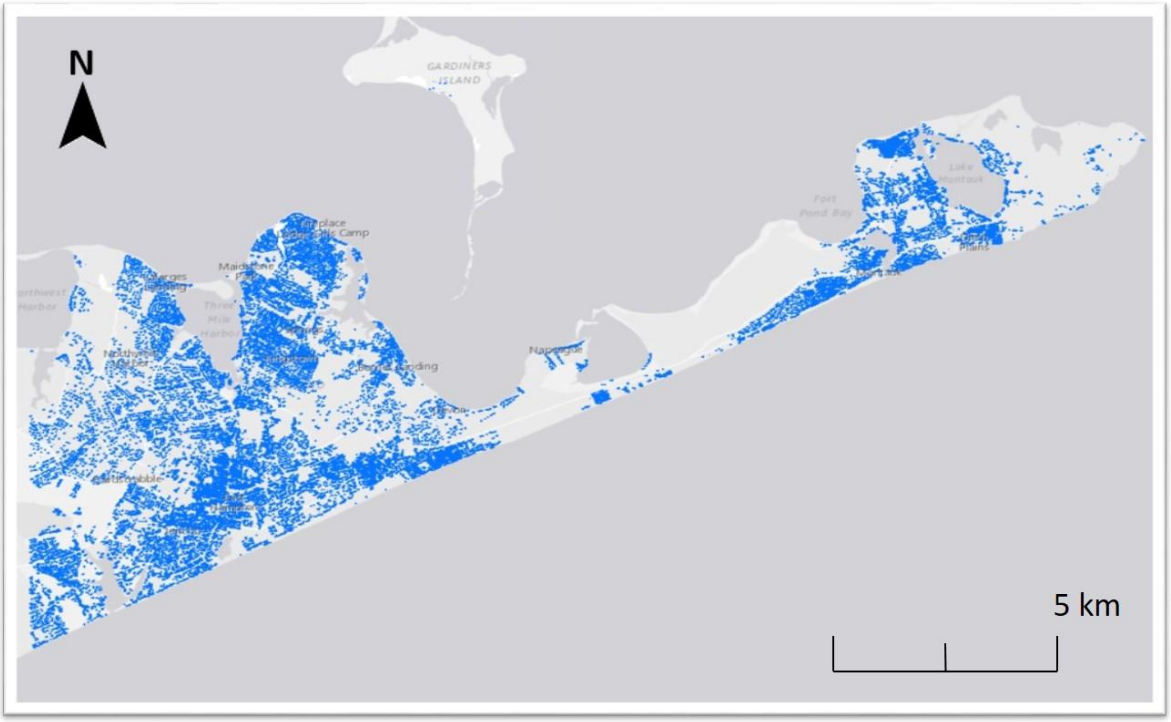

Figure 2. 10. The building footprints in the study area, blue stands for the buildings.

2.7 Tables

Original percentages	
Dune	448 (59.73%)
Bluff	297 (39.6%)
Beach	5 (0.6%)
New classification	
Single dune	203 (27.1%)
Multiple dune	155 (20.7%)
Single bluff	199 (26.6%)
On top	97(12.9%)
In front	91 (12.1%)
Beach	5 (0.6%)

Table 2. 1. The composition of the coastal geomorphology in the study area.

CHAPTER 3: Long-term Shoreline Changes, and Storm Impacts at NY's Ocean shoreline

3.1 Introduction

3.1.1 Structure Hazard Areas (SHAs)

The NPF areas and the Structural Hazard Areas (SHAs) were two designations of CEHAs (Figure 3.1). Chapter 2 discussed NPFs which include beaches, bluffs, dunes, and added three new classifications, dunes on top of bluffs, dunes in front of bluffs and multiple dunes. The SHA is defined in law to be "Those shorelands [sic] located landward of natural protective features, and having shorelines receding at a long-term average annual recession rate of one foot or more per year". The inland boundary of an SHA is delineated 40 times of the long-term average annual recession rate landward of the NPF area boundary.

The determination of long-term recession rates is an engaging task. Almost all methods are based on comparisons of maps, survey T-sheets, and aerial photographs. Often the rate is calculated as a linear regression (LR) against less than dozens of historical shorelines, sometimes only two, the so-called end-point regression (EPR). The disadvantage of EPR is that a spurious data can influence the result in a great level. Usually, we can choose from four methods, other than LR and EPR, the other two methods are average of rates (AOR) and Jack-knife (JK). By using AOR, the data used were survived over a time criteria and short-term variability was filtered out. LR method is using the method of Least Squares to get the best fit line. JK is similar to LR method, while JK method is all the possible combinations of LRs by omitting one point in each iteration. Robert et al. (1991) compared four methods to calculate shoreline recession and accretion in a 65km long shoreline from Cape Hatteras to Oregon Inlet. To estimate the true long-term trend, more than 10 years of data need to be included. There is no best method when calculating the recession rates.

As a practical matter as was done in the CEHA remapping project (Chapter 1), the ephemeral shoreline undulations must be taken into account when delineating SHA. If the features along the shoreline have a regular spacing or approximate wavelength, they can count as shoreline rhythmic features. In the other hand, longshore undulations are alternating, but irregular, landward and seaward displacements of the shoreline. Compared to the rhythmic pattern, a shoreline undulation is more irregular and have a longer wavelength. Longshore sand waves, beach cusps and rhythmic bars, as well as isolated erosional hot spots, created ephemeral shoreline patterns.

3.1.2 Major Storms

Another issue is the occurrence of a major storm in the time period being considered as "long-term". Some rare events are thought of as "game changers" substantially shifting the long-term

trends by a single, unrelated occurrence. This area routinely is impacted by major storms (Table 3.1). Superstorm Sandy was considered by some to be a "game changer" but other memorable storms have frequently impacted the shoreline here. Prior to 1994, the region had been impacted by a memorable northeaster in 22 and 23 January, 1980; the northeaster of 28 to 30 March, 1984; Hurricane Gloria on 27 September, 1985; Hurricane Bob on 19 August, 1991; the northeaster known as the "Halloween Storm" or "The Perfect Storm" of 30 October, 1991; the northeaster known as the "Storm from Hell" of 11 and 12 December, 1992 and the northeaster of 13 March, 1993; The recent events since 1994 are briefly described as follows:

- *1994 to 2003 storm events.* Substantial erosion events occurred during the northeaster of 23 December, 1994; the northeasters of 27, 28 January and 3, 4 February 1998 known as the "Back-to-Back Storms" ; Tropical Storm Floyd on 16 September, 1999; and Hurricane Gert on 19-24 September, 1999;
- *2004 storm events.* 2004 saw the effects of Hurricanes Jeanne (13-28 September) and Ivan (12-24 September). Neither of these hurricanes crossed Long Island but they had each gave an indirect "one-two" punch. While they were still in the Caribbean, they each sent hurricane swells to the East Hampton coast. Subsequently, when they reached the northern latitudes inland, rainfall raised the water table in East Hampton; such events are thought to increase beach erosion. Hurricane Ivan reached its closest approach to East Hampton on 19 September and Jeanne on 29 September 2004. Although the impact of storm swells is understandable, the impact of heavy rain is a topic of current research. It has been implicated as a cause of substantial beach erosion in other areas. Heavy rains saturate the beach so that waves cannot percolate into the dry sand and disappear, but rather, swash back out to sea carrying beach sand seaward.
- *2005 storm events.* There were 15 hurricanes in 2005 which exceeded the previous record of 12 set in 1969. Beach erosion on Long Island, however, was little impacted by hurricanes in 2005. Hurricane Irene passed far offshore around 10 August. Maria also passed far offshore 2 September, Ophelia passed offshore as a tropical storm around 7 September and Hurricane Wilma on 25 October. In terms of erosion along the Village Beach, however, "extratropical" storms and nor'easters were more important.

  Coastal storms in the northeast can be classified, similar to hurricanes, on a scale from 1 to 5 with a Level 5 storm being most severe. The severe nor'easter we had in December 1992 was a category 5 storm. In 2005 there was one Level 5 storm, two Level 4 storms and twenty-six Level 3 storms. The most significant storm occurred between 9 and 16 October 2005, but important storms also occurred between 2 and 8 February and between 25 and 26 October 2005. Other noteworthy events occurred on or around 23 January, 1 March, 24 March, 3 April and 16 December 2005. All of these storms caused losses of sand from the Village Beach.
- *2006 storm events.* We had five hurricanes in 2006, but the stronger ones did not make landfall. An El Nino developed in the Pacific in July 2006 and tended to steer away from the US east coast over cooler waters. There were no category 5 storms in 2006. Category 4 storms occurred on January 3, 2006, and on November 22, 2006. There were twenty-three category 3 storms scattered through 2006 and sixty-six ranked storms in all this year.

- *2007 storm events.* Three major storms affected the East Hampton shoreline in 2007. A strong, spring nor'easter blew in between 14 and 17, April 2007. Early in November when former Hurricane Noel passed Long Island about 300 miles offshore of Montauk Point. The third important storm of 2007 was Tropical Storm Barry which passed over the Hamptons on 2 June 2007.
- *2008 storm events.* Two tropical storms and one hurricane moved close enough to be expected to impact the Long Island coast in 2008. Tropical Storm Cristobal passed some 200 nautical miles out in the Atlantic on 22 July 2008 and Tropical Storm Hanna ran up along the coast in September 2008. The only hurricane, Hurricane Kyle, in the region passed about 220 nautical miles offshore of Long Island to the east on September 28, 2008.
- *2009 storm events.* Six tropical storms and three hurricanes occurred in 2009. For Long Island, the most important event was Hurricane Bill which swept by at a distance of about 250 miles from Long Island on 22 August 2009. Beaches were closed and ten to twelve foot waves were reported.
- *2010 storm events.* Only two storms, Tropical Storm Colin and Hurricane Earl, came near Long Island in 2010. Colin passed about 125 miles to the southwest of East Hampton on 7 and 8 August 2010. In a typical response, the Village beaches lost some sand but became wider and flatter. Earl passed about 150 miles east of Long Island as a Category 1 hurricane on 2 September 2010. There were, however, other notable storms, nor'easters, as well as important winter storms on 11 and 25 February; 15 and 29 March. The spring of 2011 brought another serious storm on 16 April.
- *2011 storm events.* Hurricane Irene crossed Long Island on 28 August 2011. It was a minimal hurricane, with wind speeds of 75 mph, and made landfall 75 miles from East Hampton. However, it was an important rain event. Hurricane Irene made landfall near Atlantic City, NJ as a Category 1 (85 mph) storm. She passed just east of New York City as a minimal hurricane (75 mph) during the morning hours of 28 August. It had been 25 years since our last hurricane, Hurricane Gloria, made a direct landfall on Long Island in 1985. Irene produced periods of strong winds and flooding. The track of Irene from the tropics to New England was similar to Hurricane Floyd which gave us similar rainfall in 1999, but because Floyd occurred in a dry season, there was less flooding.

  Irene weakened to a tropical storm (60 mph) producing a storm surge of 3 to 4 feet in the vicinity of East Hampton. This was superimposed on high tide which occurred at 7 AM. Offshore waves up to 20 feet high around Irene could have accounted for a large part of the storm surge.
- *2012 storm events.* On 27 October, Hurricane Sandy was transitioning from a hurricane to an extratropical cyclone or "nor'easter". Winds dropped below 50 knots but this storm was worse than Irene for Long Island. Sandy produced sustained winds of (45-60 mph, gusts to 80 mph, while gust only reached had wind gusts to 60 mph during Irene). By the afternoon of 29 October, Sandy had increased her forward motion and made landfall on the southern New Jersey coast with sustained winds of 35kts and gusts to 55kts (60 mph). Peak winds were 94 mph at Eaton's Neck 70-80 mph at many other locations. The storm surge reached record levels of 3 meters at the Battery.

3.2 Previous Work

When choosing the method, the purpose of the investigation should be clear and the temporal variability of the system need to be evaluated. In this study, we calculated the long term recession rate by both the end-point regression and the linear regression method over 30 years from between 1983 to 2013. Except for errors that are inherited in each calculating method, other sources of error exist. Data sources (T-sheets or aerial photos), long-term, short-term variability and storm influences and spatial data collections also can be a source of inaccuracy.

The quality of the map that was been used can be an important source of error (Crowell et al., 1991). For the early National Ocean Service (NOS) T-sheets, the obsolete latitude-longitude coordinate system needs to be updated; distortion factors need to be calculated for uneven map shrinkage. And other map defects like tears, folds and creases also need to be addressed. For aerial photos that become the substitutes of T-sheets now, problems like tilting map, relief displacement, and radial lens distortion can also cause inaccuracy in identify the shoreline indicator and lead to errors when calculating recession or accretion rates.

Although we use aerial photos more often nowadays because of the advancing technique, but another question for aerial photography is that we assumed the pictures used in shoreline position studies recorded some typical position and configuration, but actually, the aerial photographs can only reflect the instantaneous shoreline condition at the time of photography. That snapshot is not necessarily representative of the seasonal mean shoreline position. One method to compensate that is the use of a combination of aerial photographs and beach profiling (short-term changes). Smith and Zarillo (1990) did such a combination study in a 1.2km barrier beach fronting Mecox Bay, typical of a micro-tidal and wave-dominated shoreline, on the south shore of Long Island. They found that the short-term shoreline changes derived from beach profiling can be up to 20m over a year while the average long-term change rate is about 1.0 m/year to 1.2 m/year. The short-term shoreline position changes were one large source of error when calculating long-term trends. For accurate long-term recession rates, short-term shoreline changes need to be evaluated and understand. In rare cases, a sequence of beach profiles is available, usually done twice a year but, in the case, we will discuss here, more frequently. The shoreline monitoring program along the East Hampton Village shoreline has been in operation for over 35 years with measurements being taken about every six weeks. These include measurements of width and volume of the subaerial beach.

To interpret recession rates, the time of year and the influence of major storm events should also take into consideration. Beaches typically exhibit seasonal cycles in width and volume related to increased storminess in winter months. However, Long Island is a storm dominated coast and the seasonal cycle has relatively small amplitude compared to changes due to episodic events. The

seasonal cycle was calculated to account for 15% of the total variation of the beach profile (Johnston and Bokuniewicz 2001). The seasonal change in beach width was found to be 39.01 to 25.91 meters and, in beach volume between 20.07 and 30.10 cubic meters per meter of beach. Between 1979 and 1997 seasonal changes at East Hampton were estimated to be 6.10 meter and 20.07 cubic meter per meter, and, for the period between 1997 and 1999; 15.24 meter and 75.25 cubic meters per meter. With this longer record, the seasonal changes were near the minimum values estimated earlier. Depending on the timing of storm events and other processes, seasonal extremes were observed to occur independently of yearly maxima and minima (Johnston and Bokuniewicz 2001).

Another aspect of the shoreline is the undulation and rhythmic features. Walton (1999) used many data analysis methods (autocorrelation, spatial frequency plot, spatial cross covariance plot and cross covariance plot) to study the rhythmic pattern along a 40km shoreline along Brevard County, Florida. The result showed a low-frequency shoreline oscillation is inherent the shoreline. But whether that's typical to that portion of shoreline or other similar wave climate shorelines requires more data to determine.

The shoreline on Fire Island has been mapped several times using sub-meter GPS (Allen and LaBash 1996). Erosion hot spots were examined along on the shoreline and also the spectra were analysis and compared with other studies. One hot spot at Smith Point was documented to first migrate west and then to the east at 2.1m/day and 4.2m/day. In November 2005, dominant wavelengths appeared at 4800, 3200, 2800, 2300 and 1700 meters (Seaver et al. 2006), while in December 2005, dominant wavelengths appeared at 6000, 3200, 2500, 1900 and 1500 meters. Meanwhile, dominant wavelengths of 1830 m and 1045 m had been previously found by Gravens (1999).

Longshore sand waves are relatively large features; long-wavelength semi-rhythmic shoreline undulations are inherent in sandy shorelines (e.g. Todd 1999) including New York's ocean shoreline. Longshore sand waves have been documented over a century, other names can be found in early documents, like "cusp-type sand waves", "migrating sand bumps" and "accretion and erosion waves" etc. They are relatively large features than beach cusps. Thevenot et al. (1995) studied 11 longshore sand waves at Southampton beach, Long Island, New York. The average length and amplitude of the longshore sand wave is 0.75km and 40m. Thevenot et al. (1995) combined movement of sand particles and movement of large sand bodies as a 2-D model to simulate the movement, but still, detailed field survey data were required to improve the model prediction. Neither shoreline undulations nor sandwaves have been previously documented in the East Hampton study area.

In the study area over twenty major storm events occurred since 1980, including northeasters, tropical storms, and hurricanes (Table 3.1). With all these storm events, the storm-induced data may be regarded as either a noise or a signal? Fenster et al. (2001) use 134 years of data in Hatteras Island, North Carolina to evaluate the role of storm-influenced data. Statistically, these data cannot

be treated as outliers. For stable beaches with fewer storms, storm-induced data may be noise, but in other coastal situation we need to retain the shoreline positions follow the storm events, because they represent as a signal and can be useful in predicting long-term shoreline change trend. As discussed this seems to be the case in the study.

The last error source, spatial data collection means the way we collect the shoreline position data or the distance between each transect. Long distance will lead to inconclusive results while short distance will cause oversampling data. Dolan et al. (1991) compared two methods to determine the optimal sample size, they are classical approach and geostatistics method. But two methods gave out two different results while classical approach suggested more transects while geostatistics showed that fewer transects need to be evaluated. We still need to come out with a more practical way to determine the transect distance, however, the errors due to spatial data collection are less than the temporal collection. In this study, a fixed distance of 50 m between transects were used to collect data. To get accurate long-term recession rates and interpret them correctly, many aspects need to understood and evaluated.

Studies of the long-term trends in shoreline position have been conducted by Taney (1961) for most of the south shore and by Leatherman and Allen (1985) including this eastern shoreline. Taney (1961) compared the position of high-water shorelines using several sets of Coast and Geodetic Survey charts and U.S. Army Corps of Engineers maps dating from 1834 to 1956. Leatherman and Allen (1985) developed maps of the shoreline at mean high tide based on Coast and Geodetic Survey charts and aerial photographs and compared the shoreline position for four time periods (1834/1838, 1873/1892, 1933, and 1979) to calculate annual recession/accretion rates. Earlier, Rich (1975) had examined the same area using ten sets of aerial photographs taken between 1938 and 1972 documenting changes not only in the HWL but also in the limits of vegetation line and in the dune base.

In the study area, rates of shoreline change since 1873 (to 1979) were found mostly to be between + 0.3 m/yr (accretion) and -0.3 m/yr (erosion); since 1933, shoreline changes were between +0.2 m/yr and -0.6 m/yr (Leatherman and Allen 1985). In both time periods, larger recession rates, on the order of 0.8 to 0.6 m/yr, were found immediately to the west of our study area (Leatherman and Allen 1985).

In the 2010-1118 Natural Assessment of Shoreline Changes, the USGS studied 3518 transects, covering 176 km of coastline in Long Island region (Hapke et al., 2011). The variations in the rate change correspond to the level of structures or beach nourishment along the coast. The short-term (EPR method) net shoreline change rates were 0.8 m/yr (accretional) while the long-term net shoreline change rates are -0.08 m/year (erosional). In long-term shoreline change rates, 60 percent of the Long Island coast is undergoing erosion and 9 percent of the erosion rates were greater than -1.0 m/yr. A shoreline with permanent but ephemeral undulation can bias the calculation of shoreline recession rates, such undulation is believed to occur dune to a modulation of the longshore transport of sand at very high angles of wave attack. The proper wave conditions should

be expected to be episodic and must persist long enough for the longshore transport of sand to construct substantial longshore features.

3.3 Methods

3.3.1 Recession Rates

The Recession rates had been calculated from the high-water line (HWL) using the methods described in Chapter 1. To fill in the gap of 1983 and 2004, a new HWL from spring 1999 using aerial photographs obtained from the Atlantic Coast of New York Monitoring Program was added in. After examining a range of options of varying quality (Table B1) 1999 spring aerial photographs from the spring, 1999, were chosen as the best representative. Twenty-five new aerial photographs were georeferenced. These new photographs did not have the high resolution of the orthoimages from 2004, 2010 and 2013, so they were examined scale of 1:1500 instead of 1:800. The average 3rd order polynomial RMS error is 1.71 m; for 1st order and 2nd order, the value is 13.34 m and 6.18 m (Table B2). Table 3.2 compares the recession rates. The standard deviation value after added the new HWL did not change, was 0.55 m/yr before Sandy and 0.50 m/yr after Sandy If ignore the 1983 aerial photograph, the standard deviation changed to 1.07 before Sandy and 0.82 after Sandy (Figure 3.2). If the regression were started at 1999 instead of 1983, the undulation still appeared, not all are in the same location, and, in some cases, the amplitudes are larger due perhaps to the compression of the time frame. From this, it seems that the sandwaves present in 1983 significantly impacted the calculated recession rates. The FFT analysis was also carried out for the new dataset (Figure 3.3). The dominant wavelength, the value of the peak and the shape of the spectra remain the same, but, if the 1983 aerial photographs were not included, the peak wavelength changed. Again, 1983 aerial photographs had an important influence on the results of both recession rates and the undulation wavelength.

Recession rates of the bluff crest were calculated separately in the same way. The area chosen to calculate the bluff edge recession rates covered 176 transects, and the length is 8.75 km (Figure 3.4). To learn the recession rates of bluff crests, instead of identifying the HWL bluff edges were identified in 1983 historical images and 2013 modern ortho-images (Figure 3.5).

Recession rates influenced by the shoreline undulations might be exposed by associated periodicities. The longshore distribution of recession rates was subjected to spectral analysis to look for dominant frequencies and changes of phase, which would indicate migration. The shoreline recession rates from 1983-2010 (LR method) were subjected to a Fast Fourier Transform (FFT) in Matlab. Linear trend was moved to get the power spectra. The x-axis is the frequency (m^{-1}) while the y-axis is the absolute value after the FFT transform. Then the results were being compared to the wavelengths of shoreline undulations determined by earlier investigators (Gravens

1999; Seaver 2006). In order to investigate possible impacts of Superstorm Sandy, the analysis was then repeated without the 2013 HWL shoreline.

3.3.2 Beach Profiles

Since shoreline changes are variable, it is necessary to monitor the condition of the beach in order to put observed changes into perspective and to recognize looming problems. In addition, the site-specific nature of shoreline processes usually does not allow for the application of data from one beach to another. Monitoring of each specific location is required in order to determine accurately those processes occurring at the site. The shoreline monitoring program along the East Hampton Village shoreline has been in operation for over 35 years (since 1978) with measurements being taken about every six weeks. These include measurements of width and volume of the subaerial beach. They have been very successful in discovering long terms trends within the beaches from the data collected.

Twenty locations were initially established and surveys were started with volunteers using simple stadia staffs. After a few years, standard surveys were done with a surveyor's level. More recently, beach profile survey data was collected using a Nikon digital total station. The latest surveys were done with a GPS. Elevation data was imported into the Beach Morphology Analysis Package (U.S. Army Corps of Engineers, BMAP) to calculate profile volume and shoreline position from the reference monument to the National Geodetic Vertical Datum (NGVD). NGVD is 0.2m above local sea level and is the standard vertical reference for U.S. Army Corps of Engineers/New York State monitoring program.

Records at Georgica Beach and Main Beach are the longest and most continuous; they will be used as examples here (Figure 3.6). Main Beach station is located at the southwest corner of the facility parking lot. Georgica Beach station is a permanent benchmark set by USACE and is on the western side of the Georgica Beach parking lot. This station is at the top of an unprotected dune. The stations' examinations also varied over the years. Stations were reset, relocated or lost, especially in the period between 1981 and 1994 at Main Beach and between 1981 and 1997 at Georgica Beach. Widths were adjusted to be comparable to the current stations by the landward shifts in position and correlation to each nearby, overlapping station. These data provide an unprecedented, statistical characterization of the beach there. In particular, an occasional reversal in the longshore drift from west to east, especially after storms, has been shown to impact Georgica Beach. The response of the East Hampton beaches to these particular events is documented in the context of its historical behavior.

3.3.3 Shoreline undulations

In the CEHA Remapping Project, ephemeral shoreline undulations were present predominantly in one set of aerial photographs, used as a starting point in the calculation of recession rates, in East Hampton, seemed to modulate calculated recession rates into alternating stretches of shoreline retreat and advance. In order to determine the frequency of occurrence of shoreline undulations here, the shoreline was divided into 10 sections (Table 3.3), historical photos covering a period of 30 years between 1983 to 2013 were examined to identify sandwaves (Table B3). In addition to the 1983, 2004, 2010, 2013 aerial photographs used in the remapping project, other photographs were examined from the Atlantic Coast of New York Monitoring Program (ACNYMP), a cooperative effort of the New York State Department of State, U.S. Army Corps of Engineers' New York District and New York Sea Grant. Sandwave occurrence was documented along with wave direction.

3.4 Results

3.4.1 Impact of Sandy on long-term recession rates

Because of the limited number of shoreline dates, average of rate method and jack-knife method is not appropriate. Both end point rate and linear regression were used in this study to calculate the results. To assess the impacts of Superstorm Sandy, EPR and LR answers were over a 30-year period from 1983-2010 (before Sandy) and compared to those calculated from 1983 to 2013 (after Sandy, Table 3.4). During the study period, the difference of EPR and LR can be seen in the box-plot (Figure 3.7) and by direct comparison of the value of recession rates (Figure 3.8). The two methods gave similar results in the study area, however, because the end-point-rate method ignores information at intervening dates, the linear-rate-regression results were used here for further analysis.

Along the East Hampton ocean shoreline, 750 transects were evaluated before and after Sandy. The distribution of recession rates along the shoreline showed an influence of shoreline undulations (Figure 3.9). As we will discuss, the oscillatory longshore pattern seemed to have been produced predominantly by sandwaves in the 1983 imagery that were not seen in the later images (Figure 3.10). Of these, 45% (340 locations) had regression rates (calculated by linear regression) greater than or equal to 0.3 m/yr before Sandy. After Sandy, recession rates of that magnitude were found as 41% (311 locations). The maximum recession rate was 1.93 m/yr before Sandy and 1.91 m/yr after Sandy. The maximum accretion rate was 1.35 m/yr before Sandy and 1.22 m/yr after

Sandy. Average recession rate before Sandy in -0.22 m/yr and -0.21 m/yr after Sandy. Before Sandy, 237 locations or 32.8% had an accretion rate greater than zero; after Sandy accretion was seen at 219 locations or 29.2% of the shoreline. But Superstorm Sandy was an accretion event in many places. For example, in Figure 3.11, locations 1, 2 and 3 showed accretion. In location 1 (Figure 3.12), the vegetation area was covered with sand after Sandy, even extending to near the pond. In location 2 (Figure 3.13), the beach widened substantially. Location 3 (Figure 3.14) was similar to location 2, obvious accretion can be seen in a southwest direction (lower left part of the picture).

The shoreline can be divided into two sections, as in the first section from east to west, the shoreline is relatively straight (Figure 3.15). The second section that goes to Montauk Point is much more crenulated. In the straight section, the recession rates showed a strong periodicity apparently influenced by shoreline undulations (Figure 3.16). This section of shoreline could itself be divided into three portions and the dominant wavelengths of periodic variations in the recession rates were determined (Figure 3.17). The portion to the west showed a (linear) trend, with an average recession rate of -0.44 m/yr before Sandy and -0.39m/yr after Sandy. Shoreline undulations superimposed on this trend had a dominant wavelength of 1110m before Sandy and 1388m after Sandy. The middle portion had a regular pattern apparently produced by predominant sandwaves in the 1983 imagery. A spectrum of this portion showed a dominant wavelength of 1511m both before and after Sandy. The average recession rate here was -0.05 m/yr before Sandy and -0.06 m/yr after Sandy (Table 3.5). The value is relatively small and we can view this portion of shoreline unchanged in total. In the part to the east, the average recession rate was -0.54 m/yr before Sandy and -0.46 m/yr after Sandy. A spectrum of this eastern portion showed a dominant wavelength of about 1083m before Sandy and 3250m after Sandy also superimposed on a linear trend of recession rates. The size of undulations seen here seemed the same as the size of shoreline undulations and longshore sandwaves found further west along New York's ocean shoreline.

Wavelet analysis was performed on the spatial data set of recession rates (1983 to 2013; Figure 3.18) with the help of Dr. Wilson (Stony Brook University 2016, personal communication). This technique identifies the dominant scales of variability, in this case of the calculated recession rates distributed along the shore. The wavelet analysis (Figure 3.18) showed power in a strong, dominant scale with a wavelength of about 1.5 km. An abrupt transition occurred at a distance of about 29 km from the western boundary of the study area, corresponding approximately to the boundary between Section 1 and Section 2. The shoreline changes character here and the wavelet analysis suggests a smaller dominant wavelength of about 28 km which may represent the control of shoreline shape by bluff erosion. There is little structure of coherence to periodic variations at smaller scales. Wavelet analysis might be used to filter small scale spatial variation ("noise") out of the distribution. Future research might explore the use of wavelet analysis to remove the influence of ephemeral shoreline oscillations in the calculation of long-term recession rates.

For the second section (Figure 3.19), the shoreline was not smooth as in section 1, but instead, the shoreline had more curves and turns. Also, the NPFs in this section were all bluffs, and the

shoreline changes here are all erosional rather than showing an alternating pattern of erosion and accretion except a small portion of the east tip (Figure 3.20). The standard deviation before Sandy is 0.27 m/yr, after Sandy is 0.26 m/yr. The average recession rate was -0.37 m/yr before Sandy and -0.41 m/yr after Sandy (Table 3.6).

Spectral analysis of section 2 shows a dominant wavelength of 1510m both before and after Sandy (Figure 3.21). This number is almost the same with the dominant wavelength in the middle portion of section 2. A spectrum of the whole study area was also conducted and showed in Figure 3.22; the peak dominant wavelength remained around 1500m, but an additional wavelength appeared at 38 km both before and after Sandy. From these numbers of dominant wavelength, the separation of the shoreline in the study area is reasonable and the peak periodicity of shoreline undulation is about 1500m.

The bluff edge recession rates are showed in Figure 3.23. The maximum recession rate is 1.06 m/yr, the minimum recession rate is near zero and the average recession rate is 0.33 m/yr, which is near but slightly less than the average HWL shoreline recession rate in the same area. Bluff erosion is episodic and occurs over limited extents so it was not surprising that recession did not occur in the study period at some places and that the crest recession rate tended to be larger than the recession of the HWL in general. The spectra have also been calculated with the peak wavelength showed around 2200m (Figure 3.24). This was slightly larger than the dominant undulation in the shoreline recession rates. The two features are controlled by different processes with the pattern of bluff recession being determined by the geotechnical strength of the earth material. (The maximum bluff recession rate was located on a pond where the transect intersected the waterline at a high angle; Figure 3.25).

3.4.2 Long-term changes in beach width, volume and elevation.

Shoreline changes due to Superstorm Sandy did not seem to unduly alter the long-term recession rates, but to explore how other storms could have been manifest in changes in the beach profile, the frequent ground surveys at Georgica Beach and Main Beach in East Hampton were further examined.

Over the entire record, both Georgica and Main beaches showed a small linear decrease in width, the main beach showed a stronger decrease with a slope value of -0.2964 (m/yr, Figure 3.26-3.27, linear regression). The average beach width for Main Beach is 66.80 m for Georgica Beach is 82.25 m. Standard deviation for Main Beach width is 24.52 m and 33.34 for Georgica Beach (Table 3.7). The Main beach lost about 0.30 meter per year and Georgica about 0.04 meter per year. From the polynomial fit (Figure 3.28), a multiyear trend inside the beach width data was found, both Georgica and Main beach widened since 1979 until 1989, then decreased in width until about 1999. Beach widths increase again until 2007-2009, narrowed again, then since 2014, both beaches started to increase in width again.

Beach surveys were made at East Hampton on Thursday, 1 September 2011, 4 days after Irene passed. Dunes were scarped all along the coast. Main Beach and Georgica Beach were the most severely hit (Figure 3.29-3.30). Georgica Beach lowered in elevation by around 2.13 m.

Surveys had been done at both the Main Beach and Georgica Beach on done October 11 and November 5, 2012 (a few days after Sandy). Immediately after Sandy the beaches generally lost volume but gained 17 to 25 m in width. "Superstorm" Sandy eroded sand up high on the dune, ten feet or more. When the storm subsided the beach was wide, but very low in elevation. Both decreased in berm elevation by 0.5 m (where the elevation was calculated as the volume divided by the width). Almost every high tide could reach the dune. Sand mobilized by Sandy returned to the beach, but not immediately to the dune. This left the beach vulnerable to the nor'easters that followed when some of the most serious beach erosion occurred.

The beach widths were subject to harmonic analysis for the period between October 1979 to June 2016. The beach volume time-series was also subject to harmonic analyses, but for a different time interval, that is, between August 1994 to June 2016 at Main Beach but between August 1997 to June 2016 at Georgica Beach. The periodogram is shown in Figure 3.31 to Figure 3.34. In both the width and volume spectra, the seasonal signal was dominant at 1 year, 0.99 years, 1.01 year, 0.99 years, respectively.

Beach volume record for Main Beach is from August 24, 1994, to June 6, 2016; for Georgica Beach is from August 20, 1997, to June 6, 2016 (Figure 3.35-3.36). Both volume trends showed volume decrease, with a -2.1862 (m/yr) slope value for Main Beach and -2.8187 (m/yr) slope value for Georgica Beach. From the polynomial fit, same multiyear trend stands out for Main Beach and Georgica Beach, but with an apparent, and unexplained, lag about two years (Figure 3.37). The average beach volume for Main Beach was 144.65 m^3/m compared to 274.61 m^3/m for Georgica Beach. The standard deviation for Main Beach volume is 36.89 m^3/m and for Georgica Beach volume is 60.35 m^3/m (Table 3.7).

Dividing the beach volume by the beach width provided an estimate of the average beach elevation (Figure 3.38-3.39). This parameter may be characteristic of the major storm events and was also be examined. The average Main Beach elevation was 2.21 m, with a standard deviation of 0.6 m. During Irene, the elevation dropped 0.04 m (2.17 m) and, during Sandy, 0.51 m (1.70 m). The average Georgica Beach elevation was 3.21 m, with a standard deviation of 0.89 m. During Irene, the elevation dropped by 0.27 m to 2.94 m and, during Sandy, by1.02 m to 2.19 m. A peak elevation was found at 7/17/2013 in Main Beach and 3/30/2006 in Georgica Beach. The reasons were unclear for these multiannual trends in beach erosion or accretion persisting over many years. The most important fluxes of sand occur during short periods of heavy weather, so, in general, the long-term trends reflect the "storminess" of the era. This will be explored further, specifically looking for aggregate parameters of storminess that may be correlated with the data.

3.4.3 Sandwave and wave direction

The occurrence of sandwaves seemed that it could be an important influence on the determination of long-term recession rates. Sandwaves were visually identified on aerial photographs from 22 different dates, in order to estimate the frequency of occurrences. In total there are 220 records, ten on each date (11 of them were uncertain, Table 3.8). The wave direction was from the southeast in 141 records and from the southwest in 71 of the records. The results show no clear relationship between sandwave existence and the direction of sandwave. Sandwaves could be found regardless of the wave direction. However, when waves were from the southeast, no sandwaves or a lower occurrence of sandwaves were seen. For each section, the chance of appearance of sandwave is different (Table 3.9). No sandwaves were found near Montauk Sections 9 and 10), but rather were concentrated on the middle part of the study area which had the highest frequency of occurrence, sandwaves being formed 81.9% of the time.

3.5 Discussion

Because there are various alternative methods of determining rates of shoreline change (e.g. Dolan et al. 1991), consistency is a major strength of any assessment. Nevertheless, the result must be interpreted in terms of the particular characteristics of the data. In this case, the distribution of HWL in time tended to emphasize the importance of the initial 1983 shoreline in determining the trend and the influence of ephemeral sandwave occurring in the segment of photographs used. A time interval of 11 years separated the 1983 shoreline from the next HWL used whereas the remaining HWLs were separated by intervals of six and three years. This made the final regression sensitive to the initial coverage in 1983, although the presence of sandwaves in any of the sequence could bias the results.

Weather or wave conditions that led to the 1983 shoreline morphology is unclear, although a tropical cyclone seems to have come within 270 km of the coast on March 13, 1983, and a second system also came nearby on March 25, 1983. Undulations in the distribution of recession rates could be matched for the most part one-for-one with alongshore sandwaves present in the 1983 imagery.

Longshore sandwaves have been found to occur fairly frequently in the study area, but also vary in characteristics along the shore. In general, sandwaves were classified into four types by Sonu (1968), who also discussed the possible causes. Recognizing the transition from a barred shoreline to a bar-less one may be one way to anticipate sandwave occurrence (Sonu 1968). Offshore wave steepness (wave height/wave period) has long been used as a parameter to predict beach morphology with higher wave steepness resulting in lower beach slopes (e.g. Komar 1998). The conventional wisdom first put forward by Johnson (1949, as cited in Komar, 1998) is that if the

wave steepness was greater than 0.03 an offshore bar forms. A barless profile, called a berm beach, forms when wave steepness drops below about 0.012 (Rector 1954 and Watts, 1954 as cited in Komar 1998).

Alternatively, or additionally, wave convergences/divergences modify longshore sediment transport in time and space, particularly in the vicinity of offshore topography Offshore bathymetry, particularly the occurrence of oblique shoreface ridges, have been implicated (Inman 1987). Models of longshore transport have shown that high-angle (~45^{o}) wave attack is capable of producing rhythmic shorelines (Aston and Murray 2006). The Wave Information Studies of the US Army Corps of Engineers (USACE) provides a database of hindcast, nearshore wave conditions< http://wis.usace.army.mil/wis.shtml >. Annual wave roses at approximately every ten degrees of Longitude along the study area. In the study area, the wave attack in 1983, when prominent sandwaves were found, were consistently at a higher angle than those in 2010 when sandwaves were largely absent (Figure 3.40). Although not definitive, the trend may suggest that the direction of wave attack may have been an important determinant.

Seafloor bathymetry < https://pubs.usgs.gov/of/2000/of00-243/report.htm > shows an offshore ridge of sand offshore of Section 2 angled south east to northwest toward Section 1 and a corresponding trough approaching Part 3 of Section 2 along the same trend. A third trough lies offshore of the Napeague Harbor connecting beach (Part 2 of Section 1), Although beyond the scope of this research, such features would cause wave convergences and divergences that could possibly be playing a role in the shoreline variations.

Regionally, New York's ocean shoreline is seen as relatively straight and smooth without prominent headlands or seaside embayment; there is no inherent reason for the long-term recession to be high in one place and low in the adjacent places as would be expected on embayed shorelines. In the long term, the ocean shoreline here might be expected to be seen at any time as relatively straight and smooth. So, if the 20-year recession rate is high in one place, we might expect that, in the future, it will go down, or accrete, while the neighboring shoreline catches up. If we add a constraint that the regional shoreline remains fairly straight, then a wide spatial average of short-term recession rates, including both high and low values, may be more representative of the longer-term shoreline change, perhaps over 50 to 100 years.

3.6 Conclusion

Aerial photographs for use in calculating shoreline recession is usually chosen to having been taken in the same season. This is a prudent strategy because a seasonal difference of a dozen meters or so would result in a change in recession rate over 30 years of 0.4m/yr. There seemed to be no consistent accounting for the storm events that occur near the date of the aerial photography. Although the records at East Hampton suggest that beaches tend to be found narrower a few weeks of an important storm, even changes of the Superstorm Sandy did not substantially alter the recession rates calculated here.

Shoreline undulations are another that matter. There might be expected to be found up to 81.9% of the time in the study area and as demonstrated, can introduce in the calculated recession rate, especially if they occur near the beginning on the end of the sequence. Ephemeral shoreline morphology must be taken into account when interpreting rates of shoreline change. This requires documentation of shoreline undulations and the occurrence of alongshore sandwaves in the fundamental imagery. In this case, oscillatory patterns of recession rates along shore yielded local recession rates that were up to over 30-times the regional average. The morphological condition of the earliest shoreline in the analysis had a greater influence on the calculated recession rates than the occurrence of the storm of the record before the last recorded shoreline.

Future research might consider using the dominant wavelength of longshore oscillations, as revealed in the periodogram, as filters to mitigate the influence of ephemeral sandwaves, in the calculation of long-term recession rates.

3.7 Figures

Figure 3. 1. Two type of (Coastal Erosion Hazard Area) CEHA, Natural Protective Feature Area (NPFA) line and Structural Hazard Area (SHA) line.

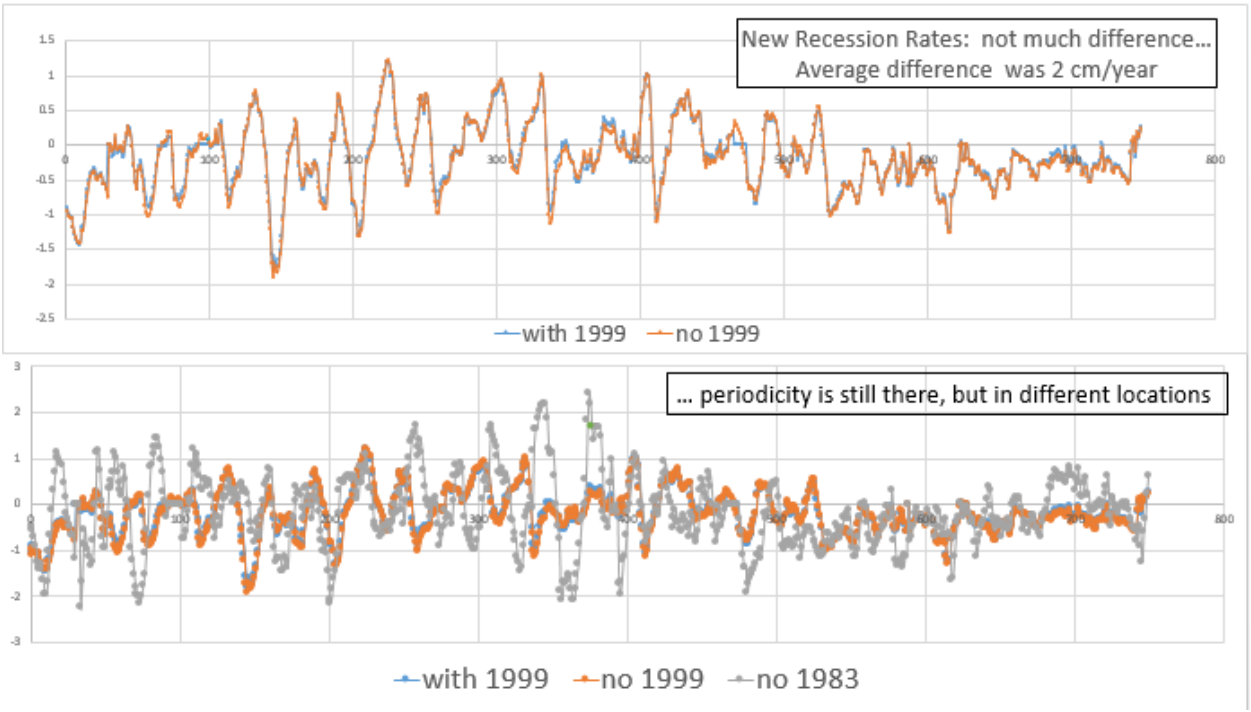

Figure 3. 2. Recession rate with and without 1999 HWL and recession rate without 1983 HWL.

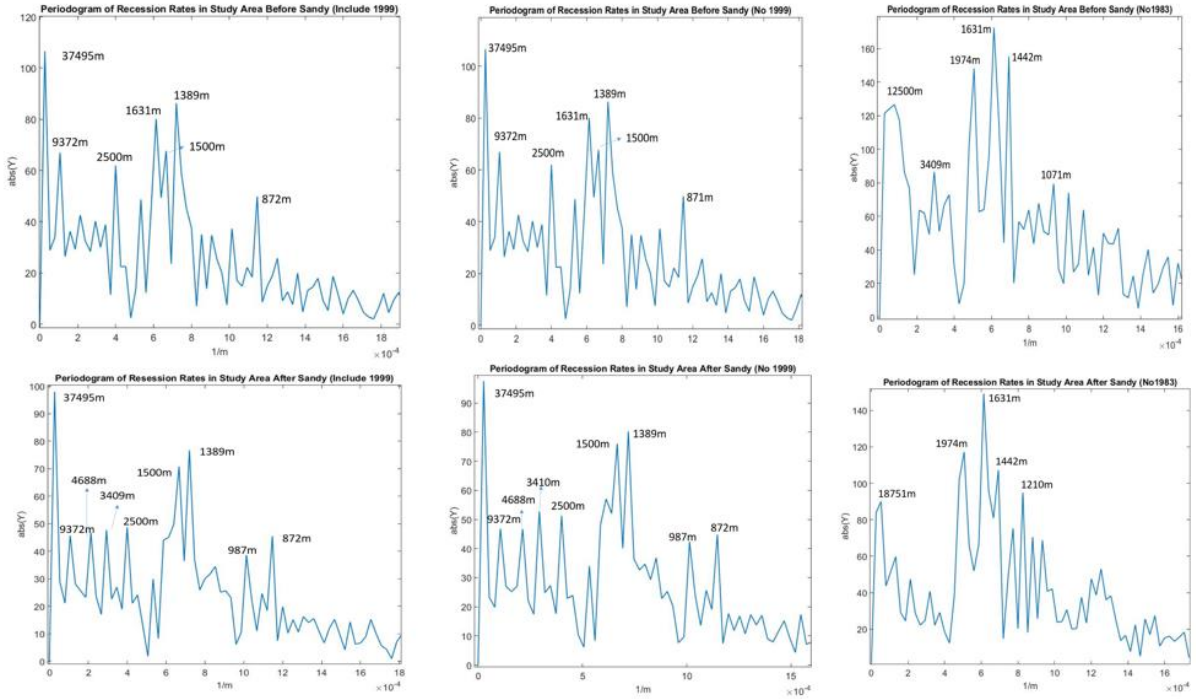

Figure 3. 3. Spectra with and without 1999 HWL.

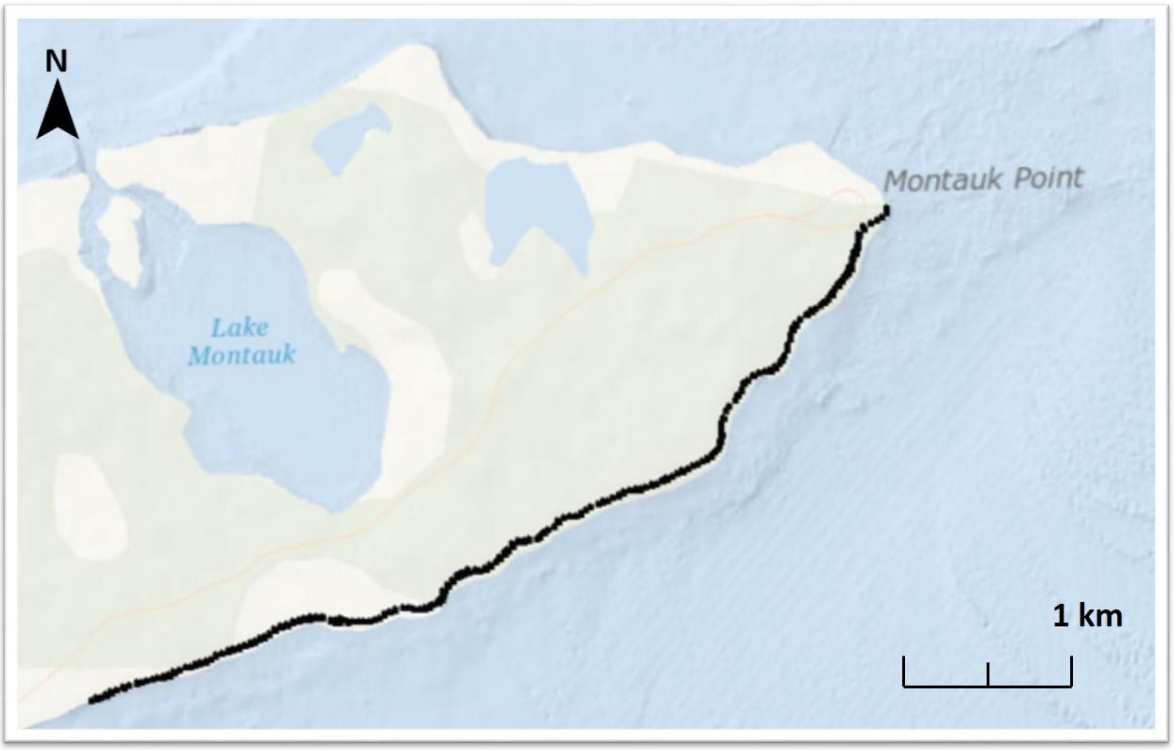

Figure 3. 4. Bluff section (black dots) for calculation of bluff edge recession rates.

Figure 3. 5. Bluff edge points (red points) along the bluff on 2013 modern ortho-images.

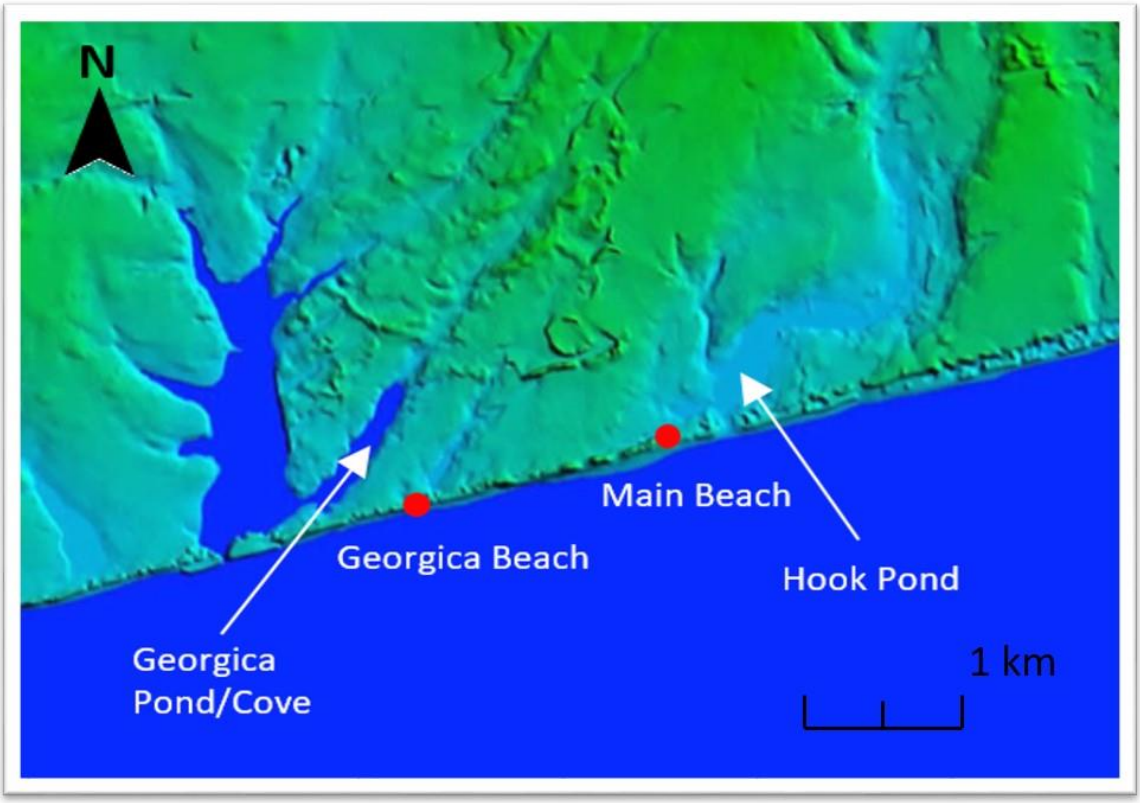

Figure 3. 6. Beach profile stations in this study, Main beach, and Georgica beach.

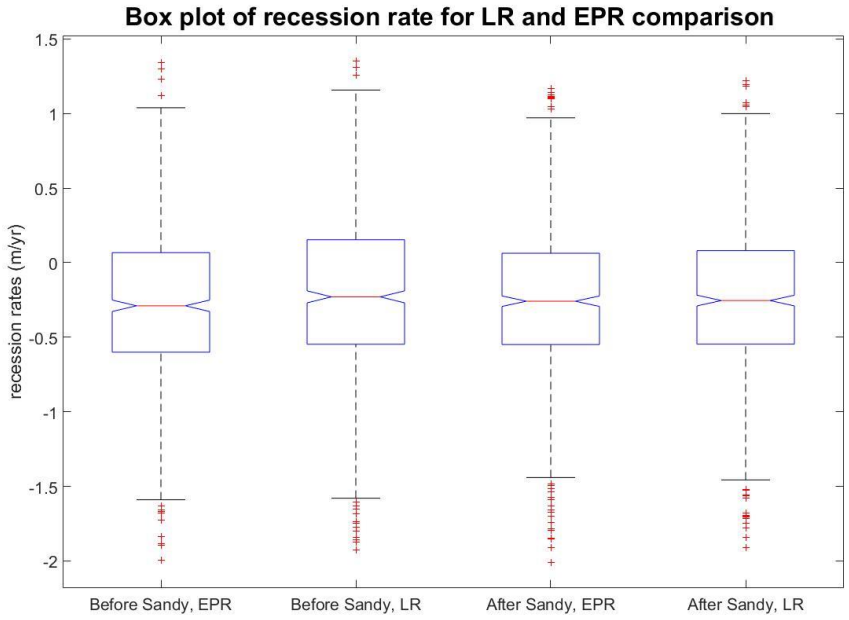

Figure 3. 7. linear regression and end point regression comparison by box plot.

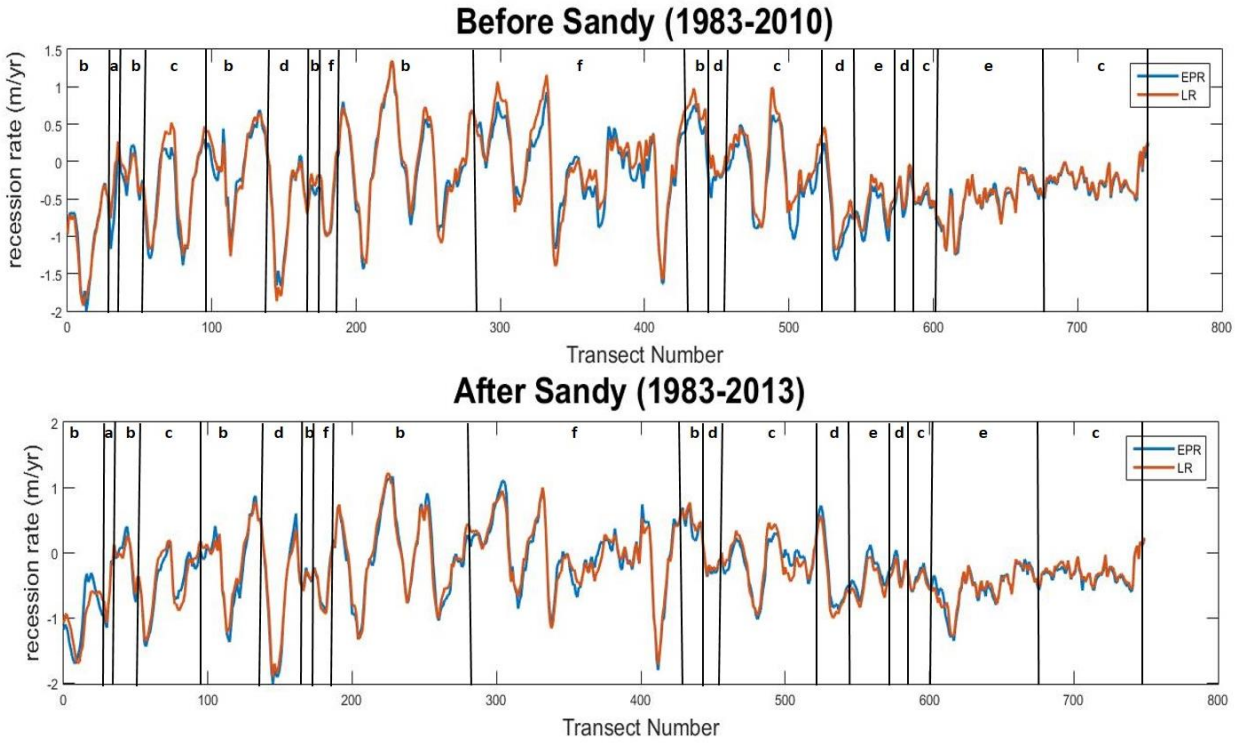

Figure 3. 8. Before and after Sandy comparison of linear regression and end point regression. Overlay with this figure is the new NPF classification with the same notation as in Figure 2.1.

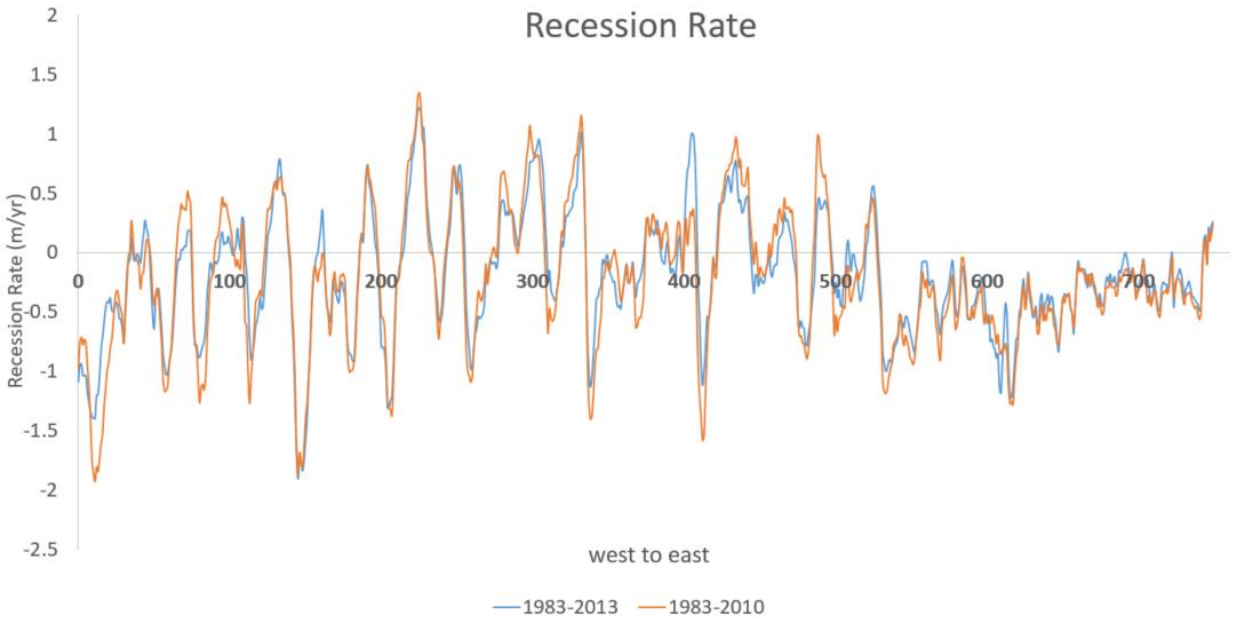

Figure 3. 9. Shoreline recession rates along the ocean shoreline in East Hampton, NY.

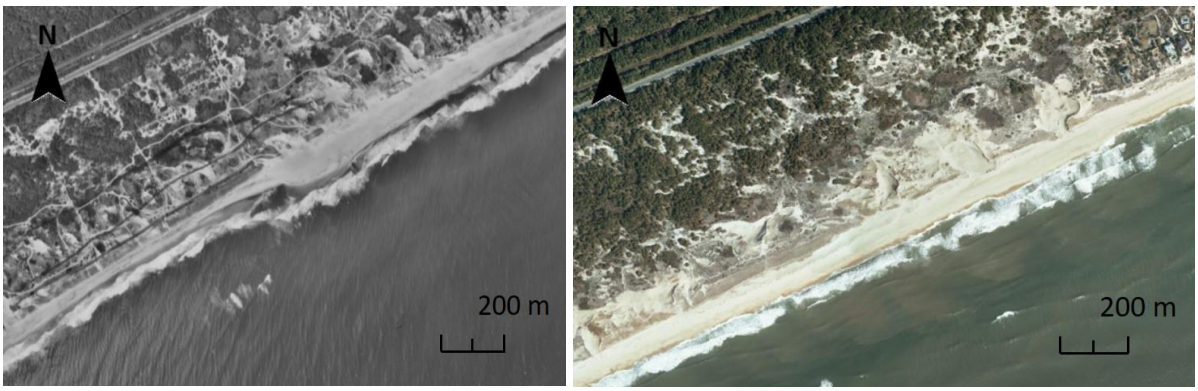

Figure 3. 10. An example of an alongshore sandwave in the 1983 imagery (top) compared with the 2013 post-Sandy imagery of the same area (bottom).

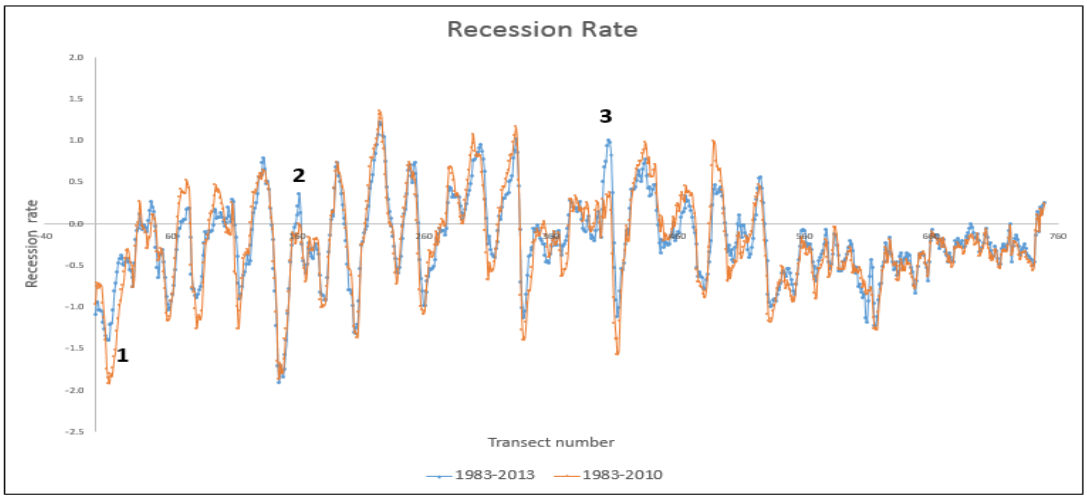

Figure 3. 11. Recession rate before and after Sandy with example accretional place 1, 2 and 3.

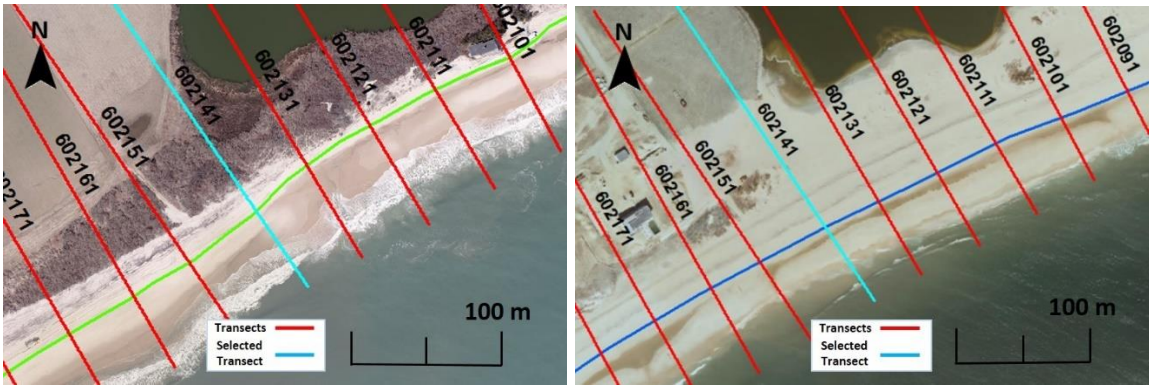

Figure 3. 12. Location 1, transect 602141.

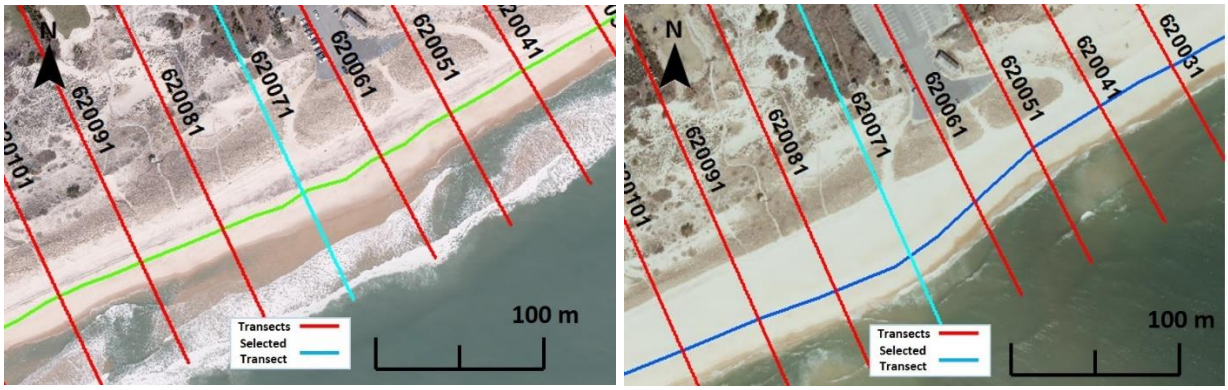

Figure 3. 13. Location 2, transect 620071.

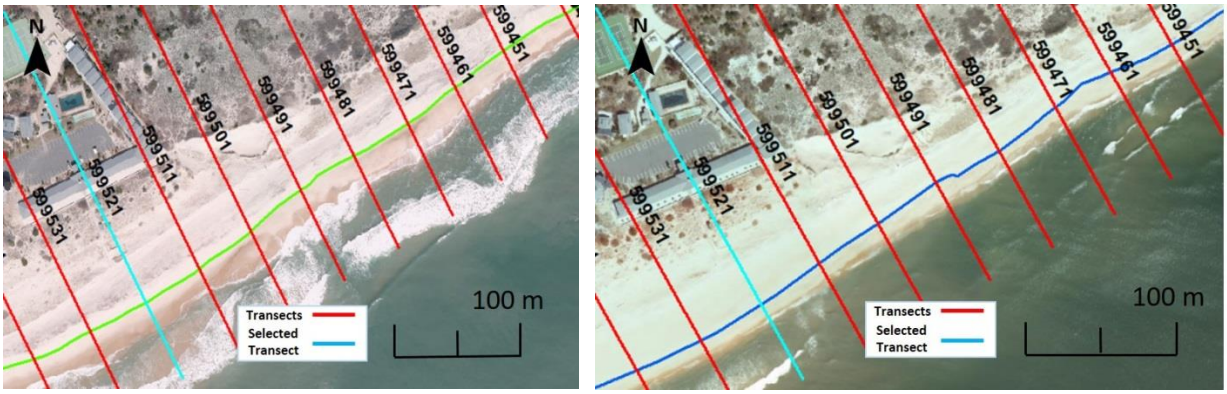

Figure 3. 14. Location 3, transect 599521.

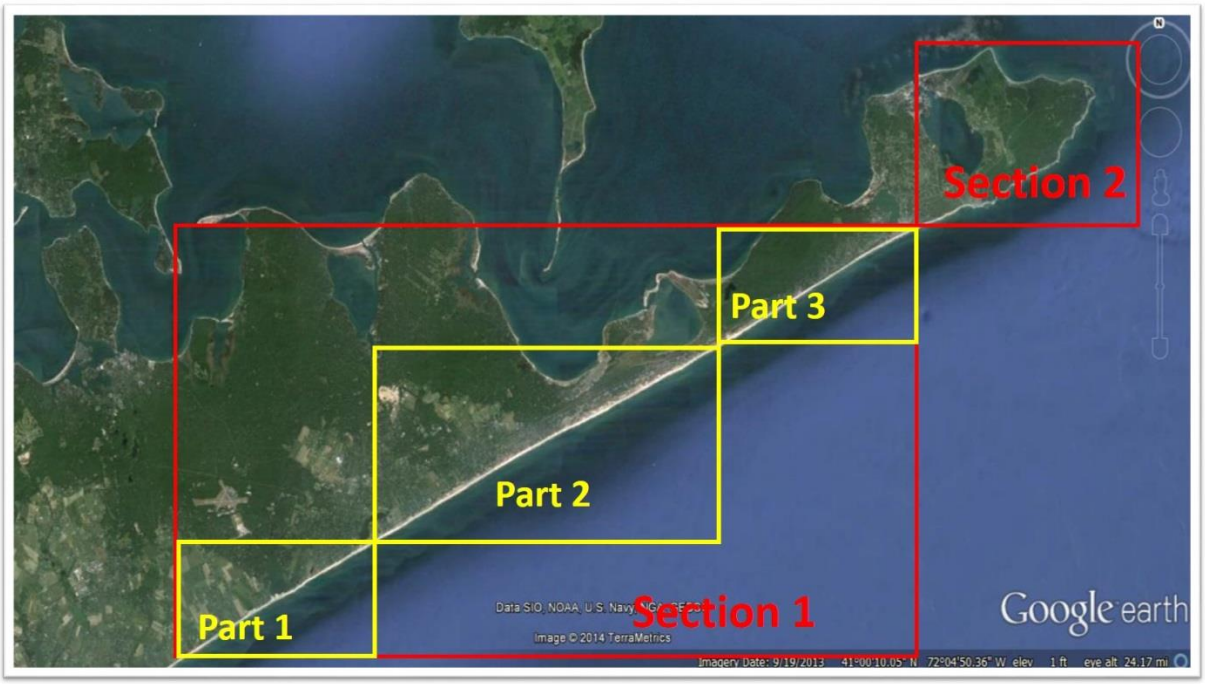

Figure 3. 15. The two sections of shoreline in the study area; left, section 1, right, section2. Section 1 had been divided into 3 parts. The boundary between sections and parts correspond (west to east) to transect number: 620581, 598251, 597601.

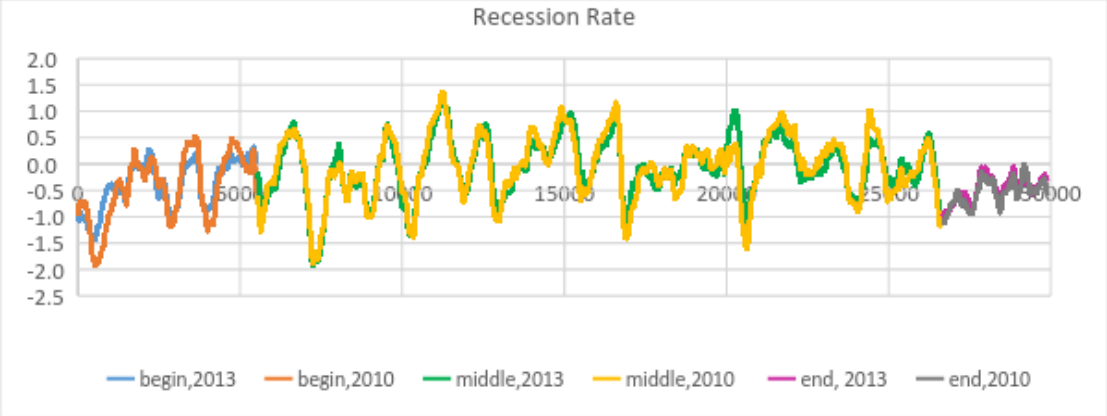

Figure 3. 16. Three portions of the study area (section 1).

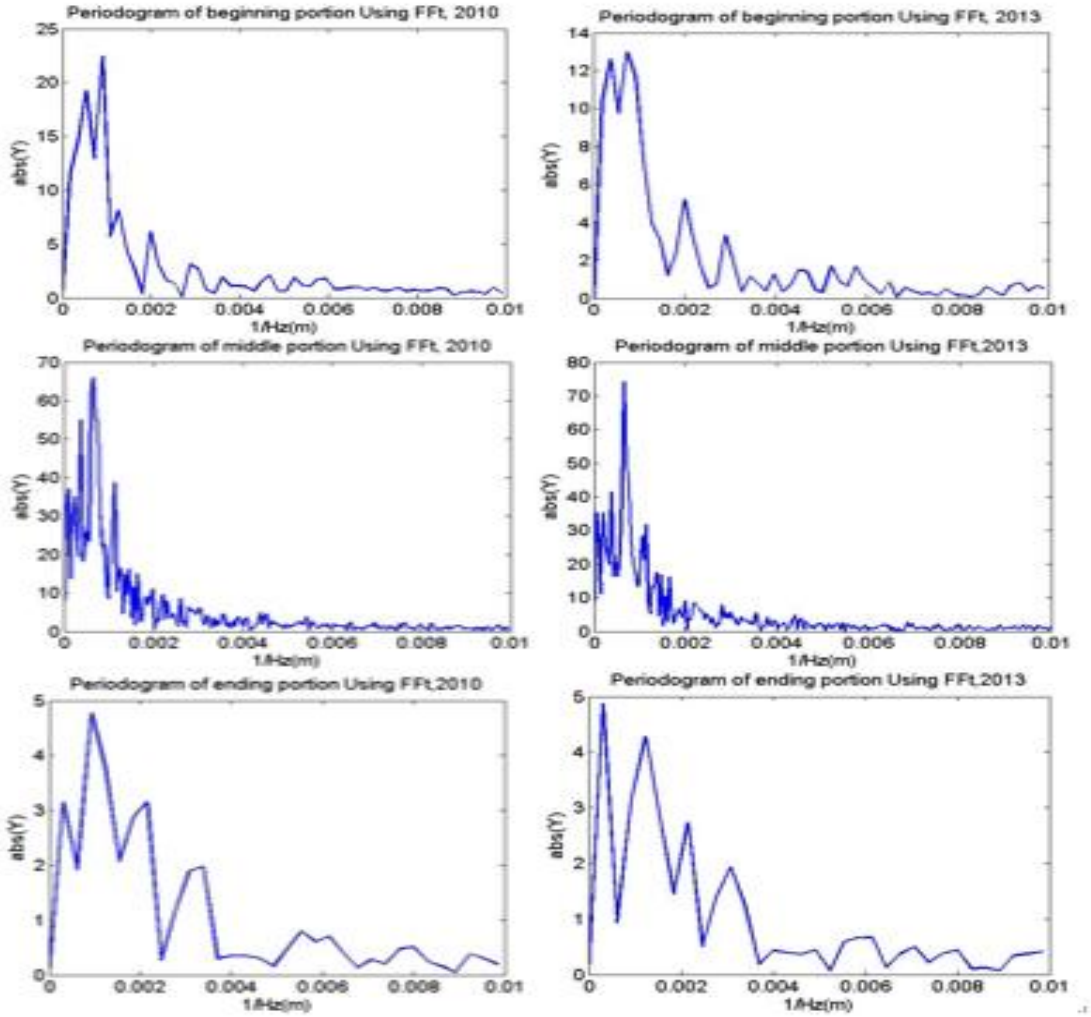

Figure 3. 17. Dominant wavelength comparison before and after Sandy in three portions of coastline in section 1.

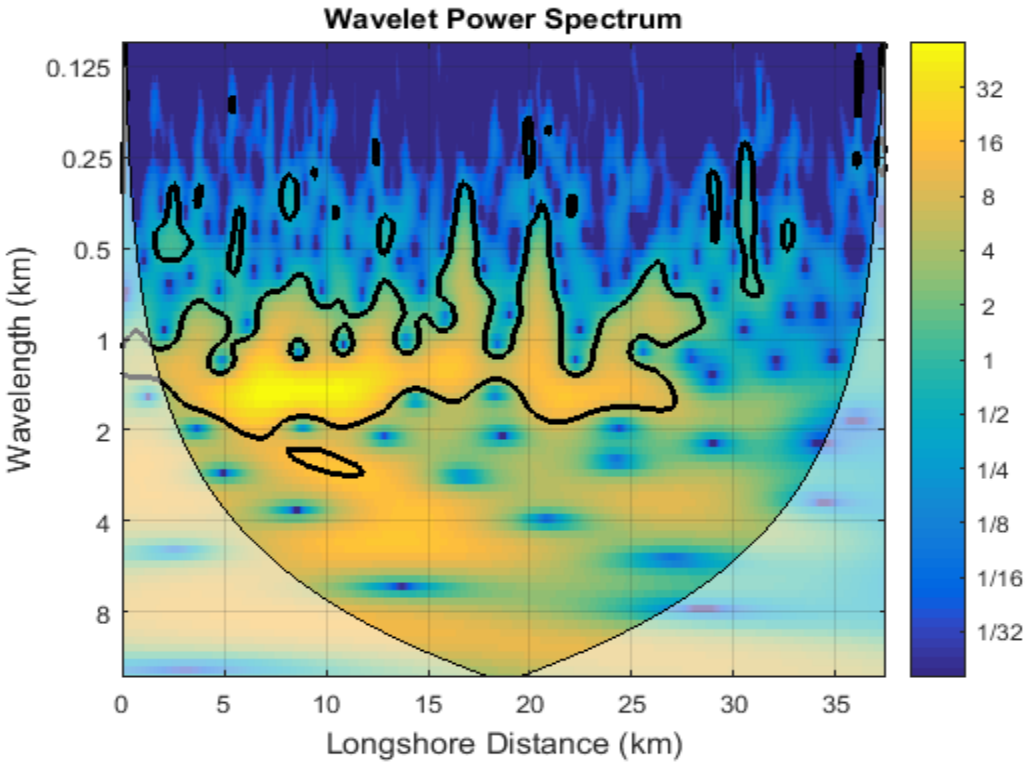

Figure 3. 18. Wavelet analysis of the longshore variations in recession rates from the western boundary of the study area to Montauk Point.

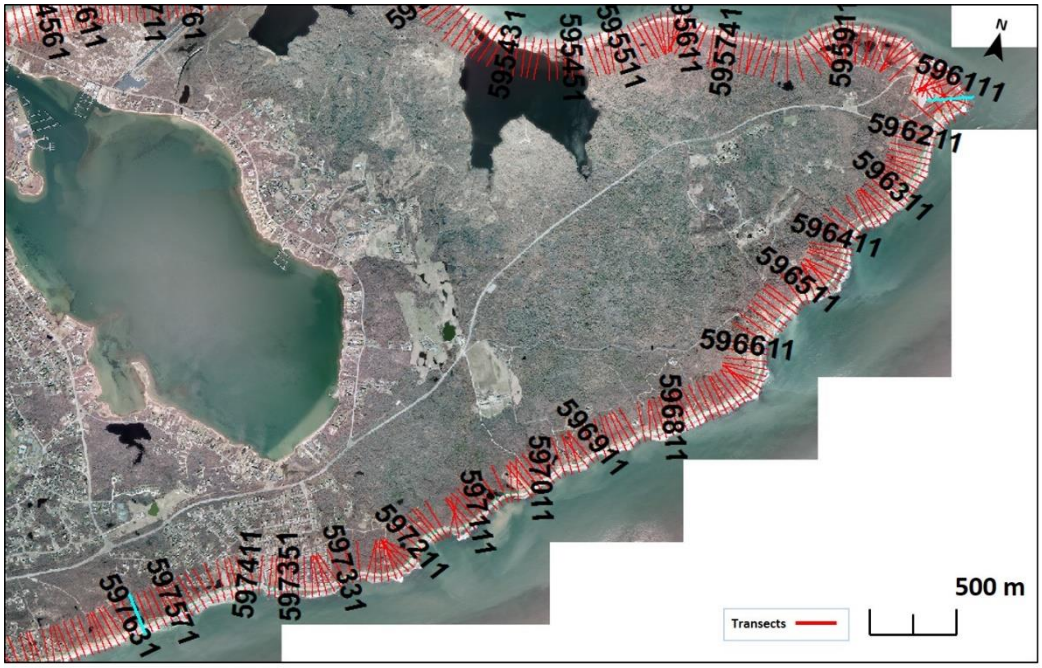

Figure 3. 19. The corresponding shoreline for section 2. The begin and end transect are showed by the blue highlight color.

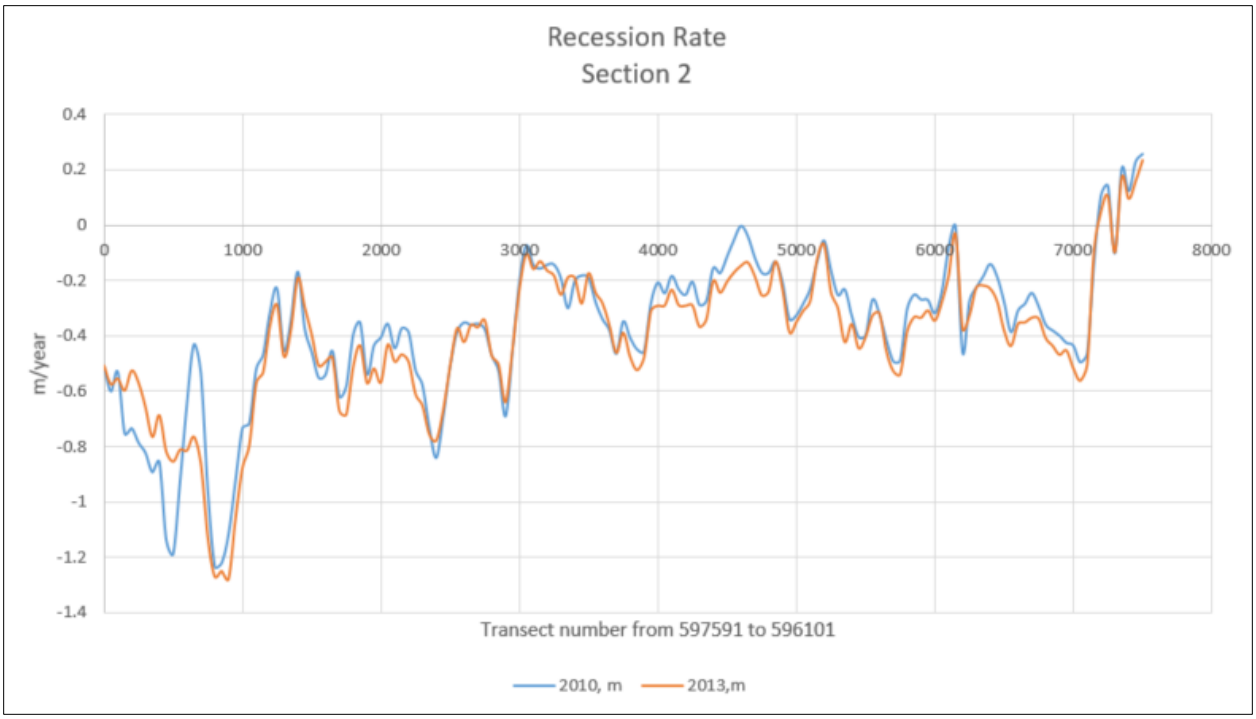

Figure 3. 20. Recession rates in section 2 of shoreline.

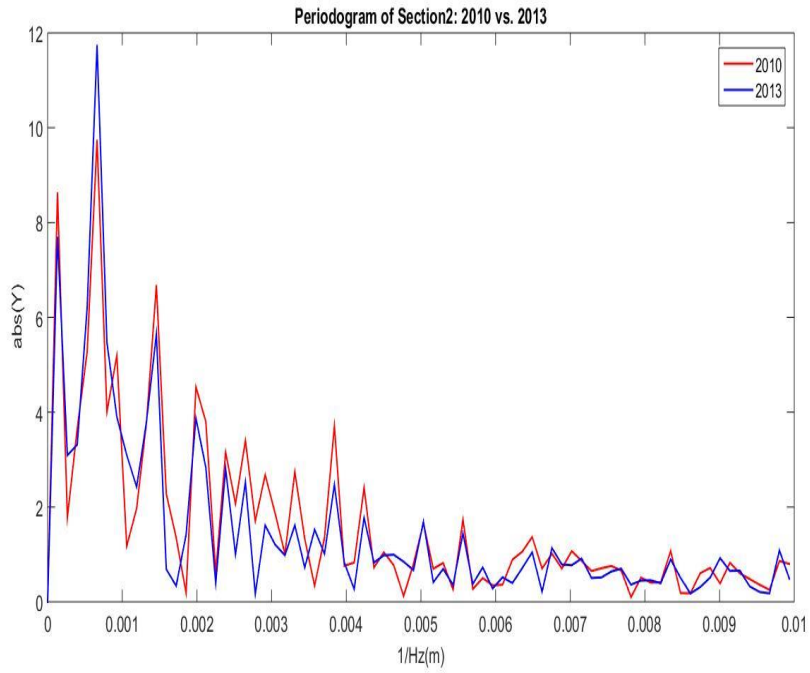

Figure 3. 21. Spectra of section 2 of shoreline, peak wavelength is 1510 m.

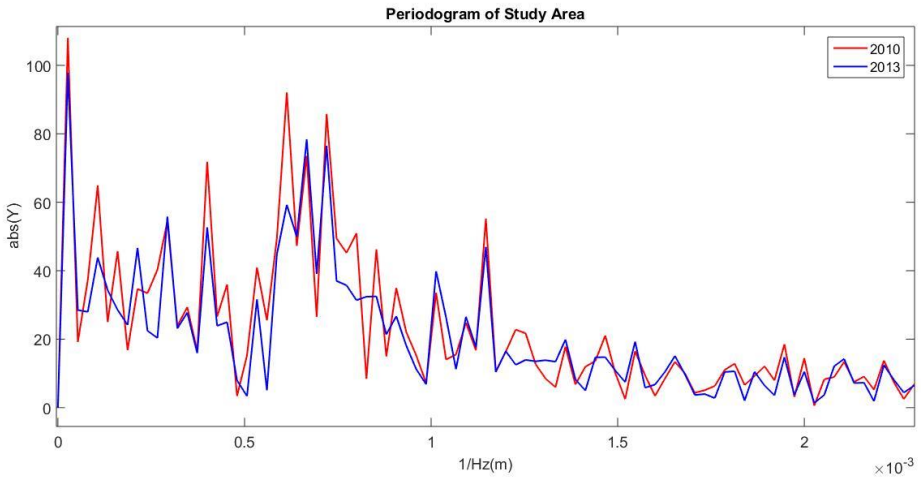

Figure 3. 22. Spectra of the whole study area, no separation, peak wavelength before Sandy is 1631 m and 1500m after Sandy, a much longer wavelength also showed up as in 37495 m.

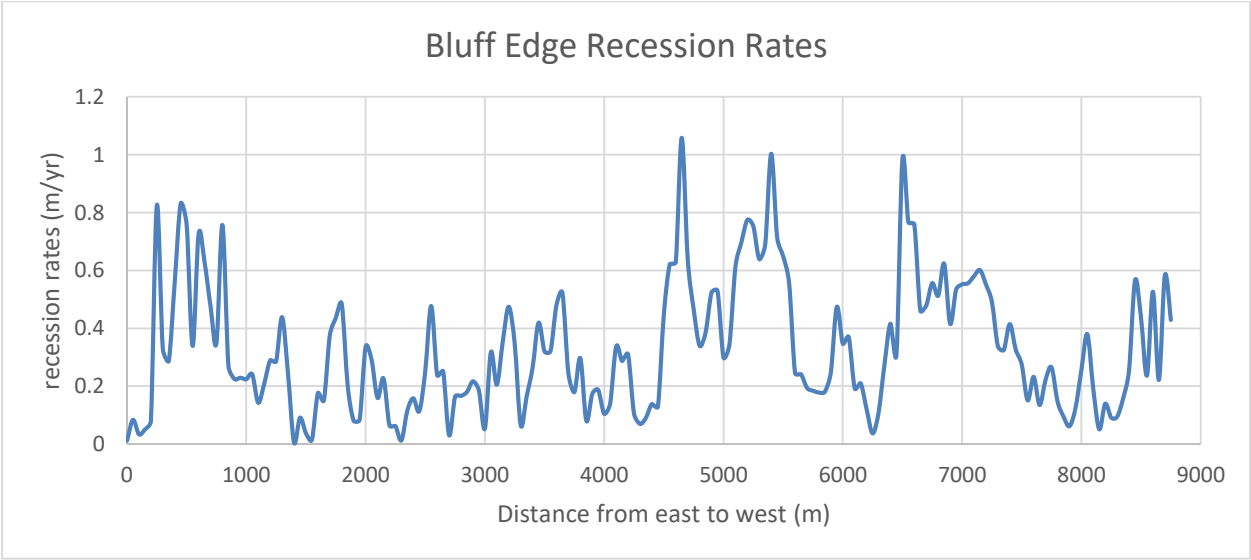

Figure 3. 23. Bluff edge recession rates from east to west.

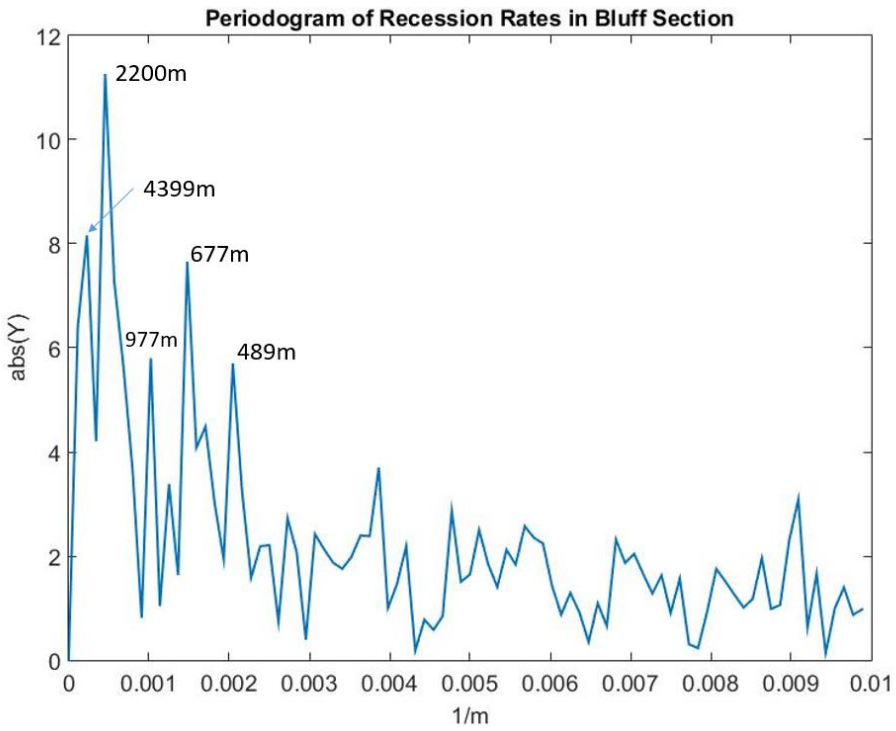

Figure 3. 24. Spectra of bluff edge recession rates.

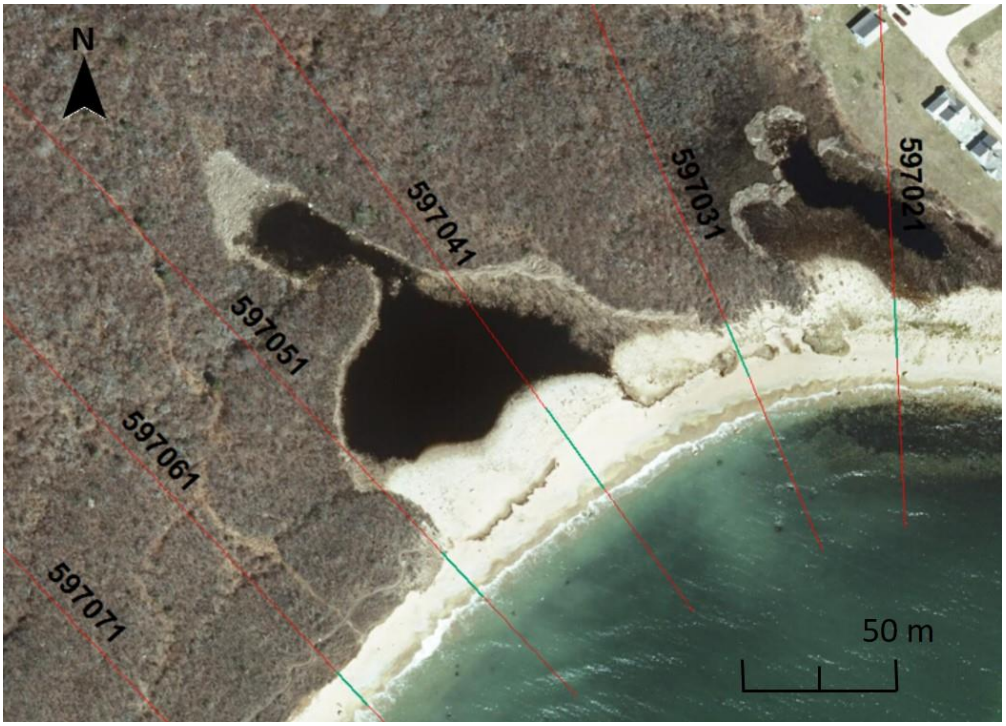

Figure 3. 25. Transect 597041 has the maximum bluff recession rate, the value is control by the topography here. There was no bluff actually, but a pond behind.

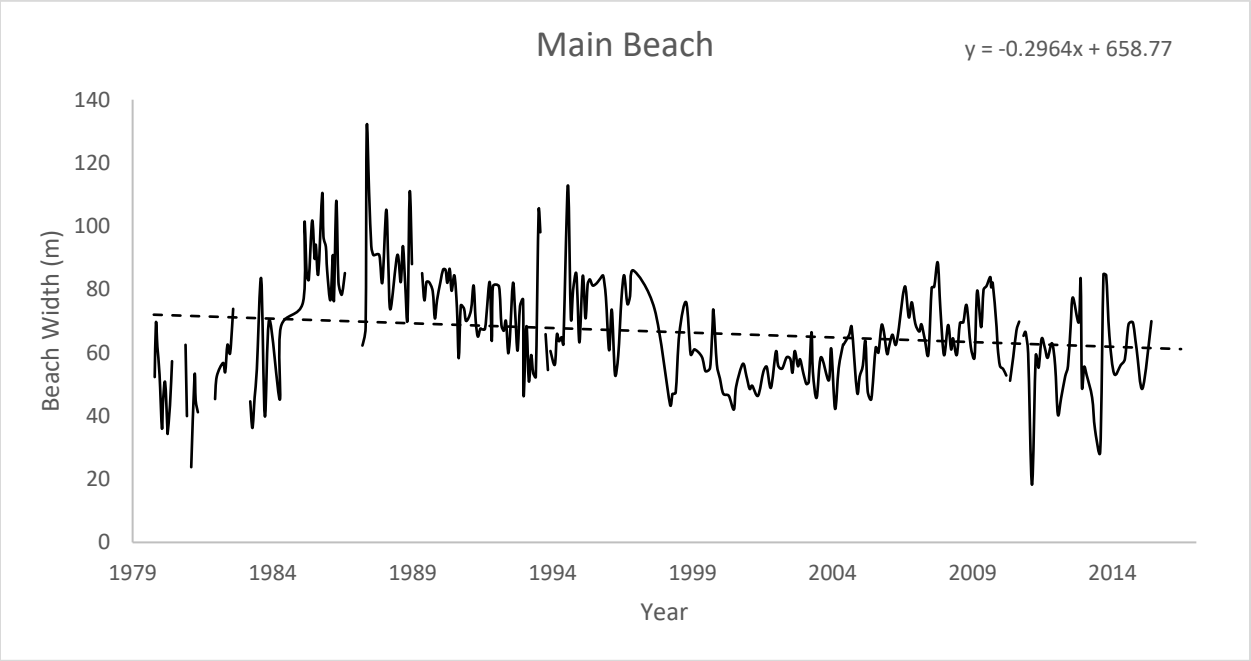

Figure 3. 26. Main beach width changes since 1979 with linear regression trend.

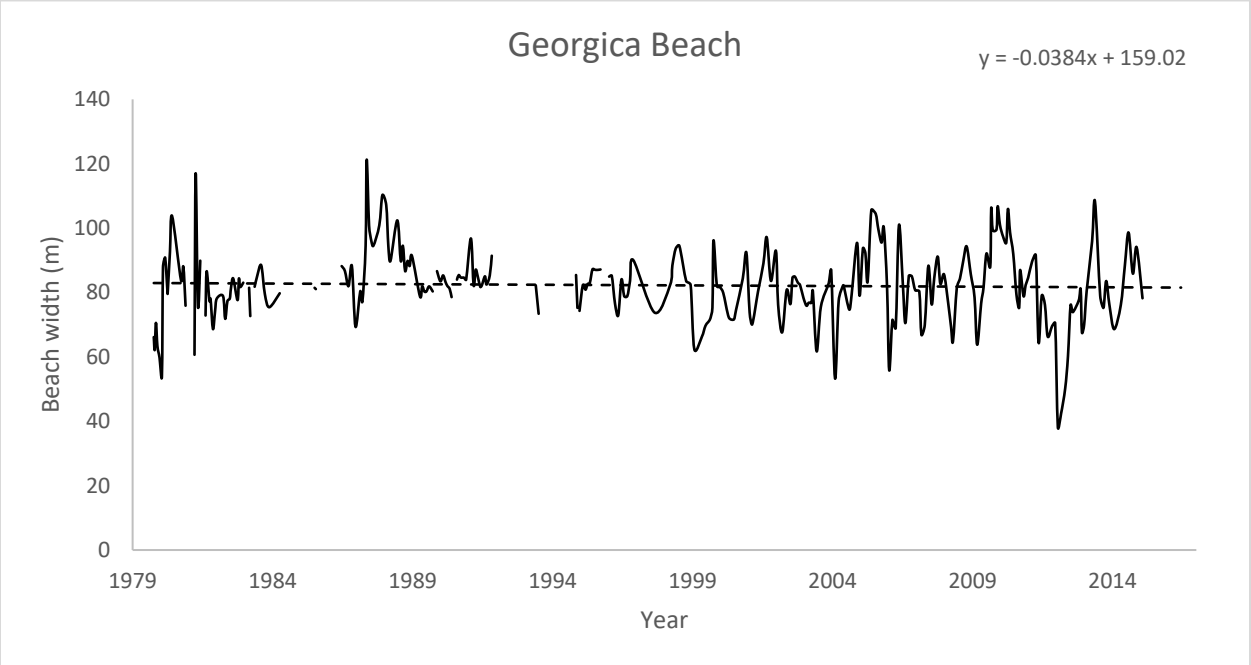

Figure 3. 27. Georgica beach width change since 1979 with linear regression trend.

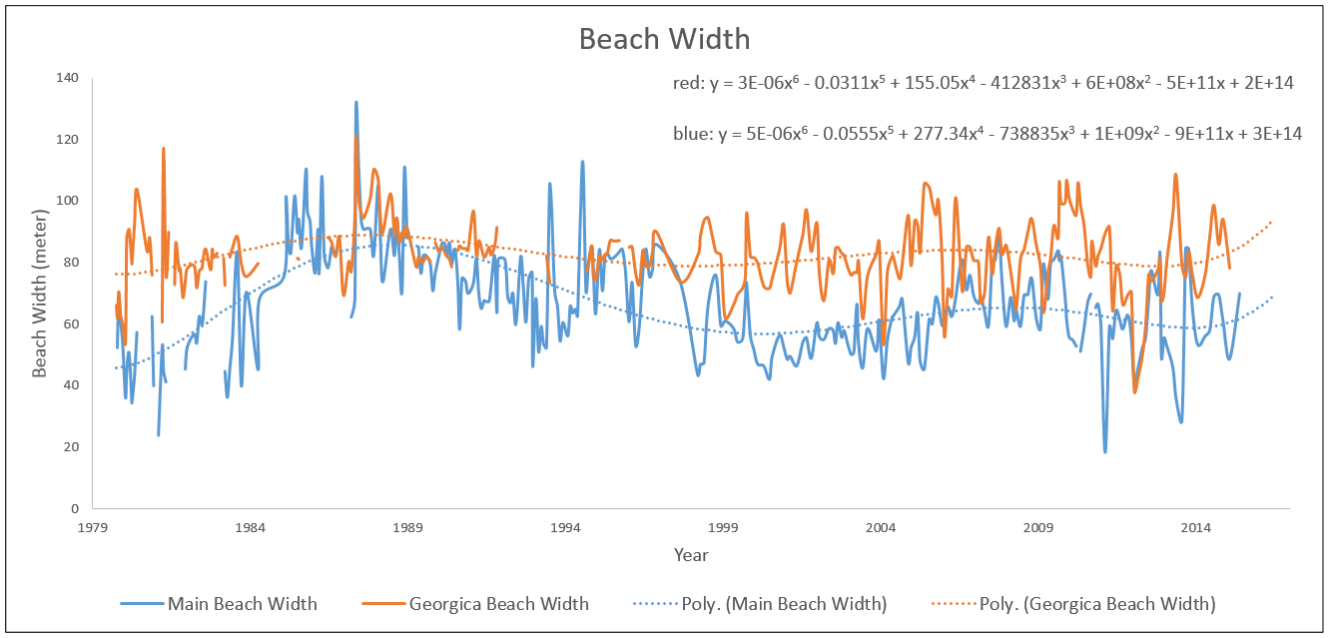

Figure 3. 28. Main beach and Georgica beach width change with the polynomial fit.

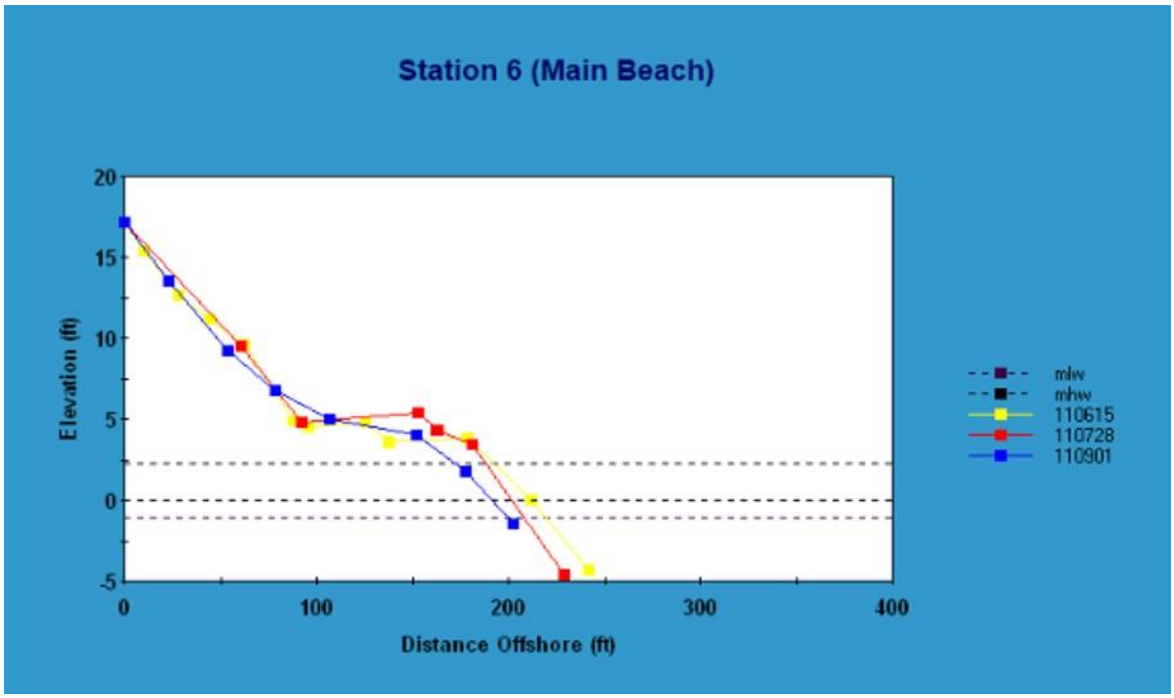

Figure 3. 29. After Irene Main Beach profile.

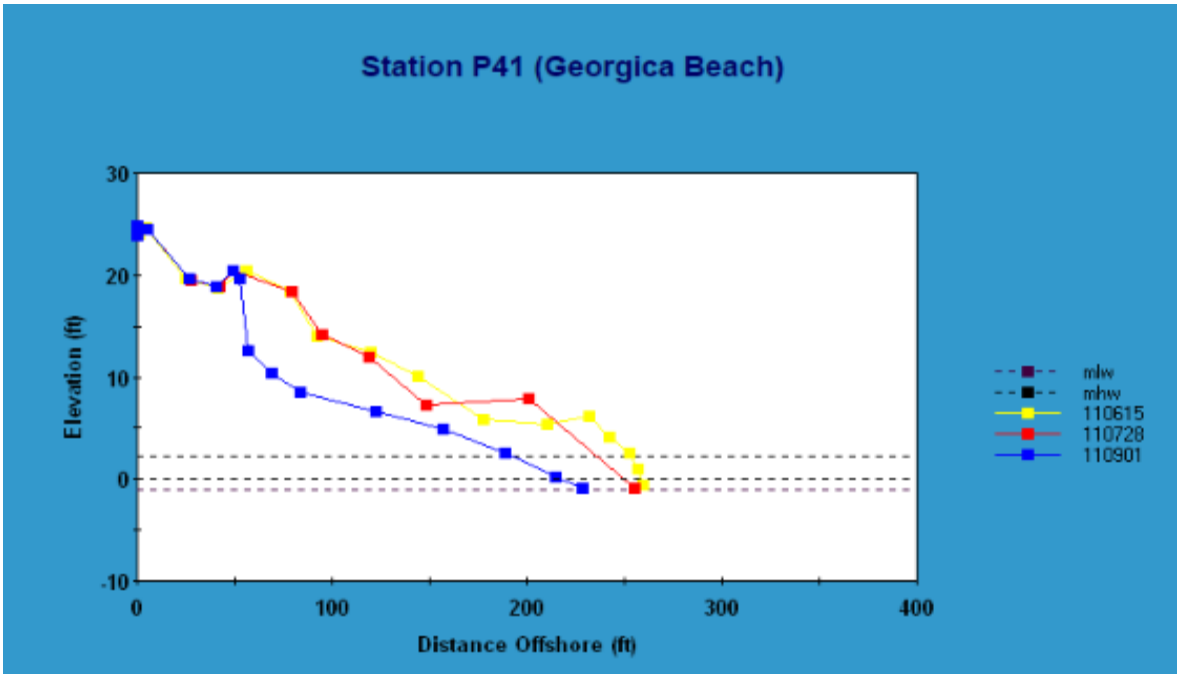

Figure 3. 30. After Irene Georgica Beach profile.

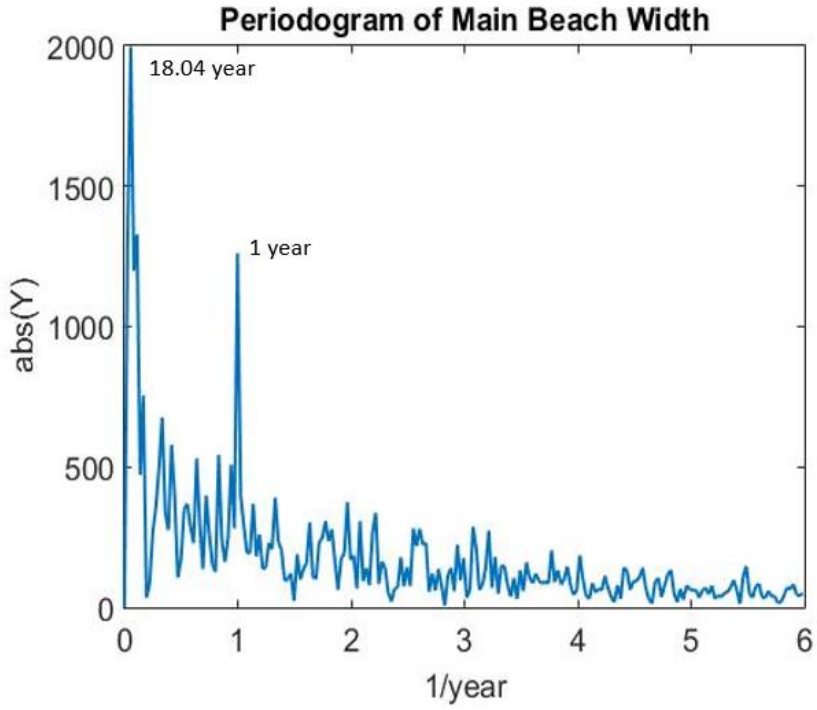

Figure 3. 31. Periodogram of Main Beach width.

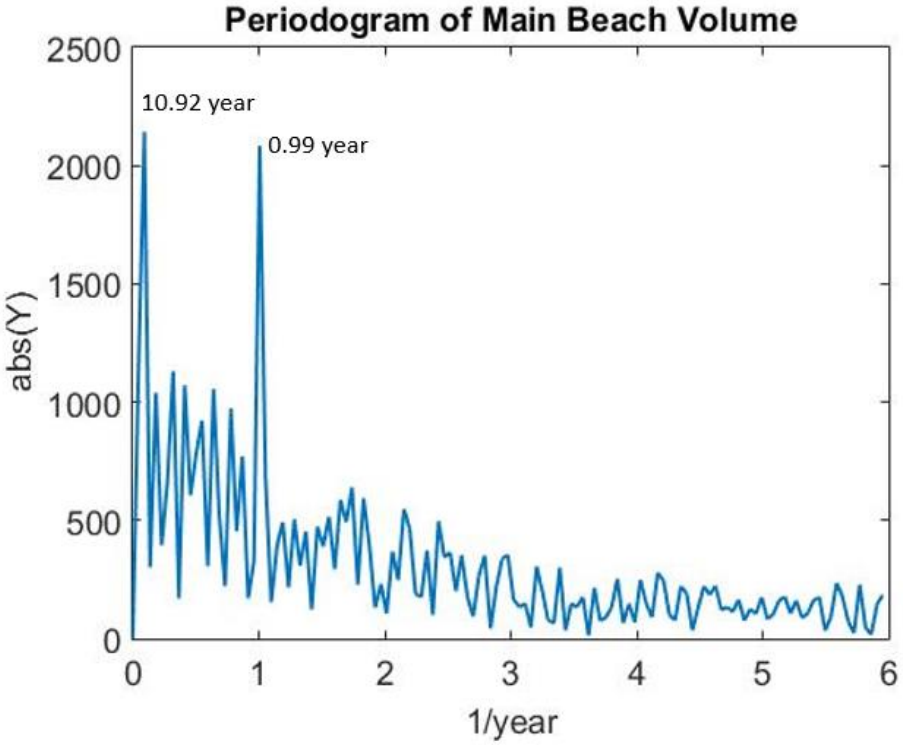

Figure 3. 32. Periodogram of Main Beach volume.

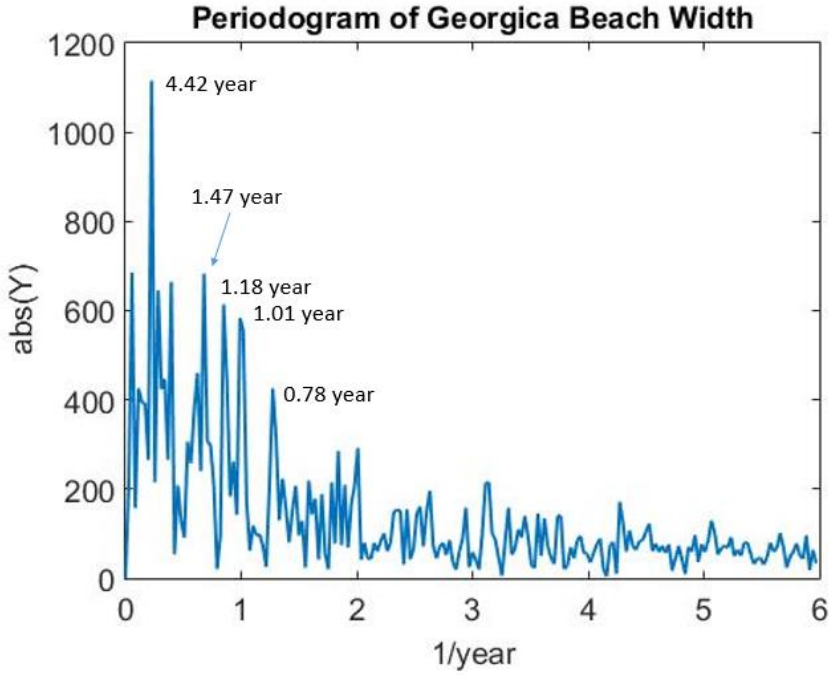

Figure 3. 33. Periodogram of Georgica Beach width volume.

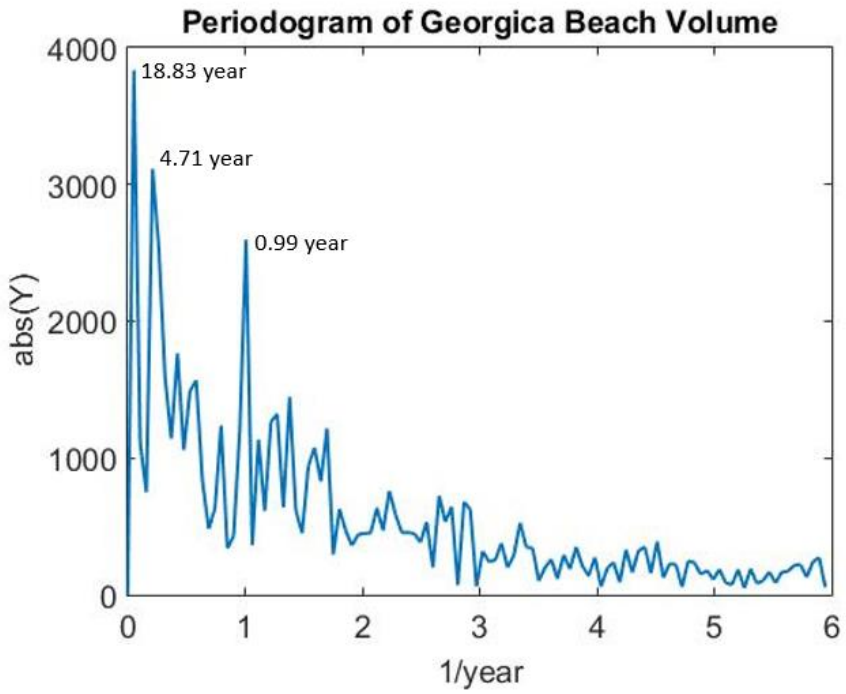

Figure 3. 34. Periodogram of Georgica Beach volume.

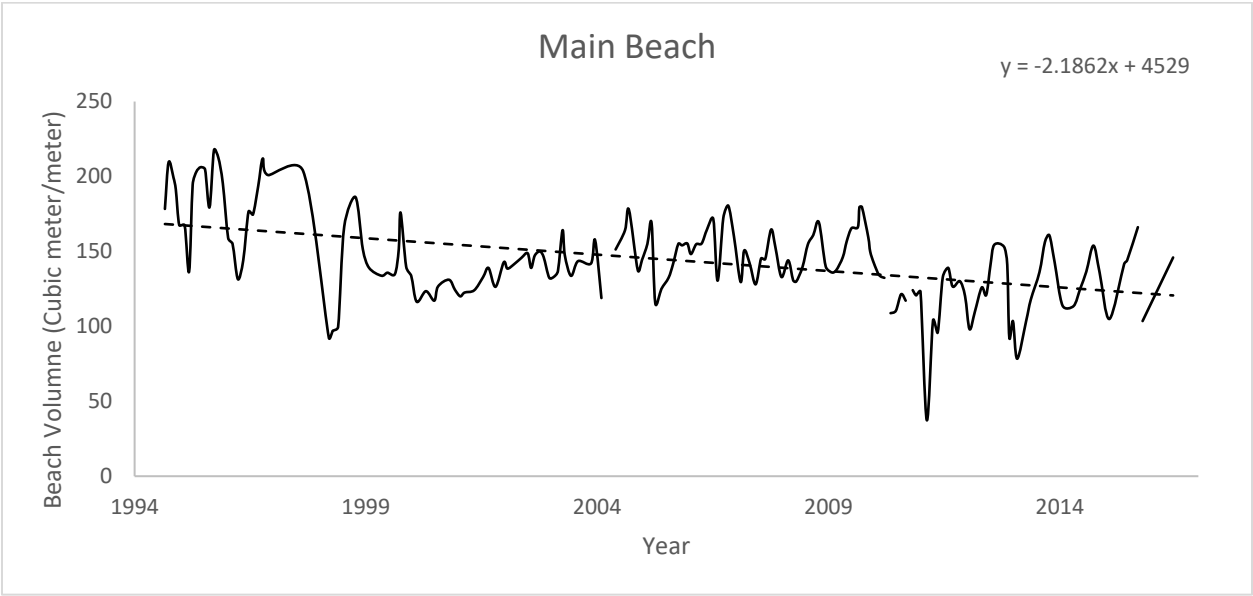

Figure 3. 35. Main Beach volume change with a linear fit.

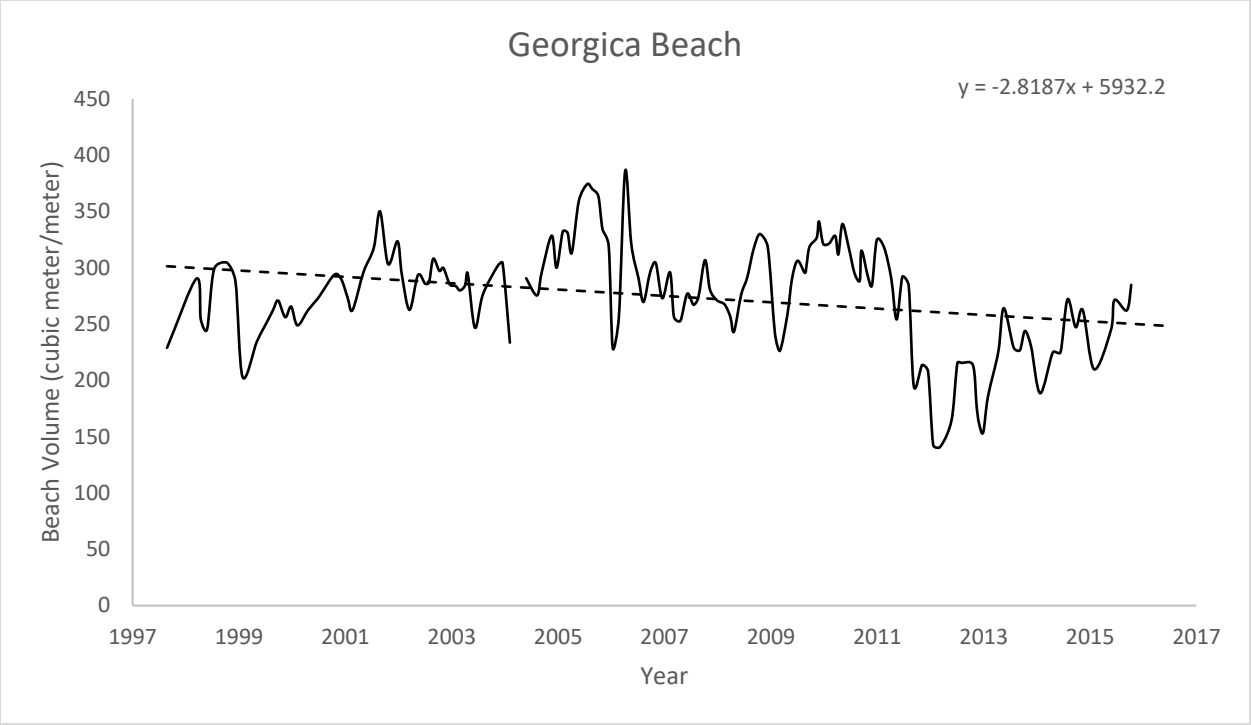

Figure 3. 36. Georgica Beach volume change with a linear fit.

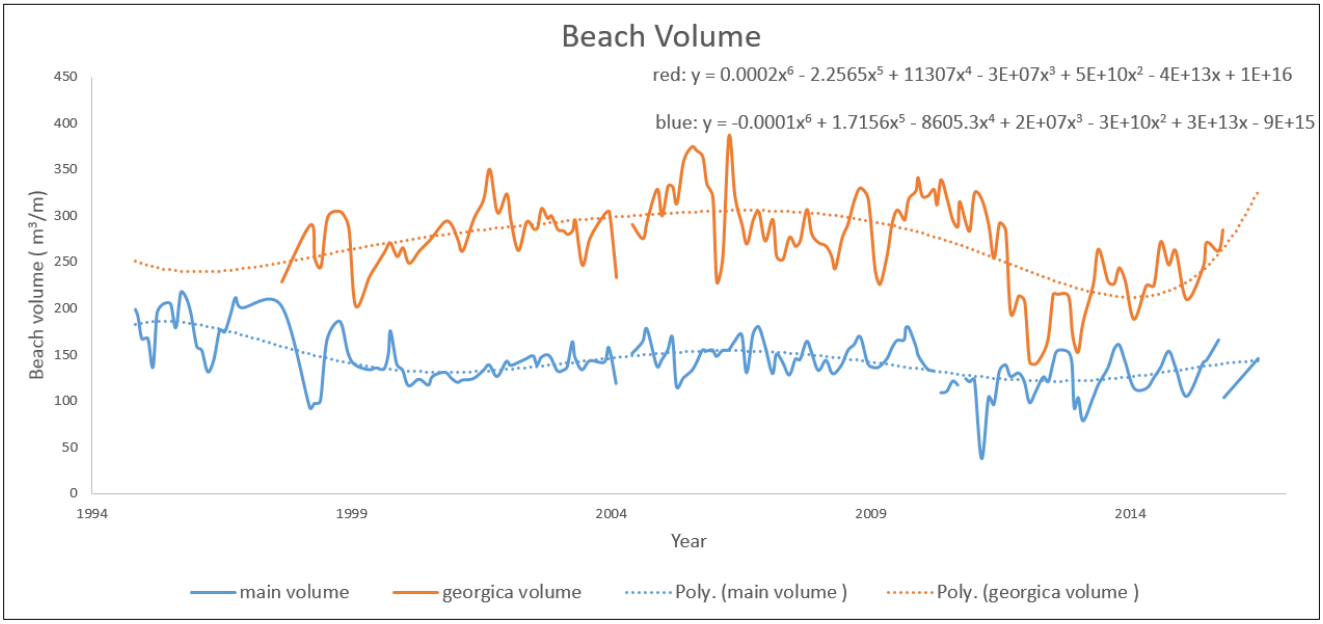

Figure 3. 37. Main beach and Georgica beach volume change with the polynomial fit.

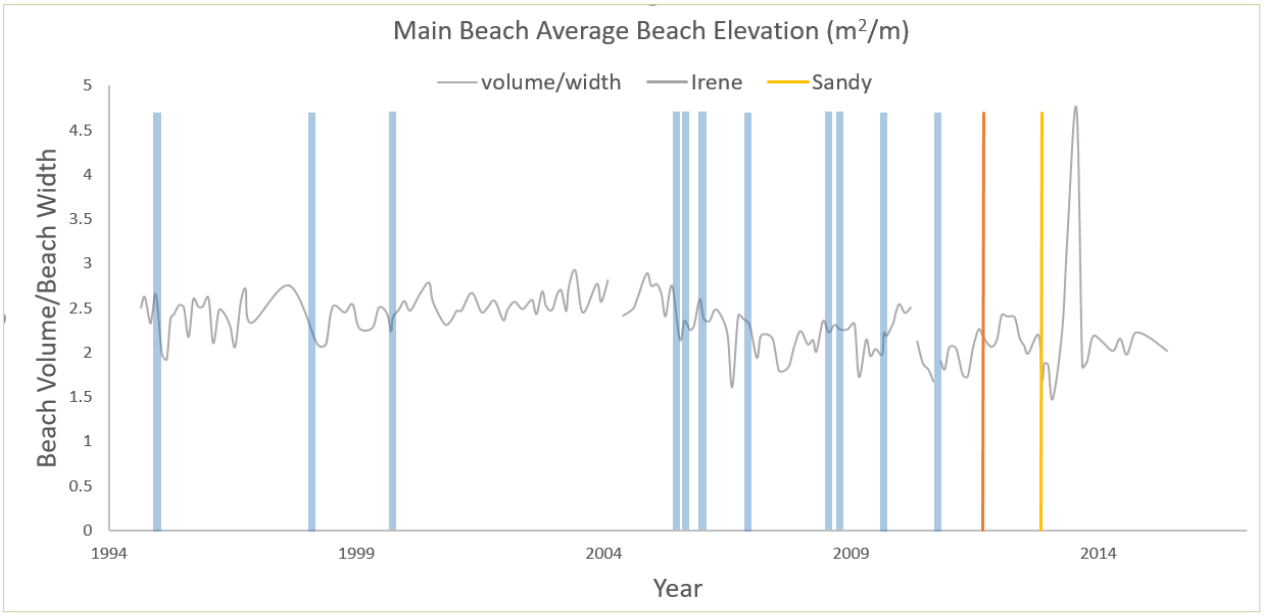

Figure 3. 38. Main beach average beach elevation with storm events.

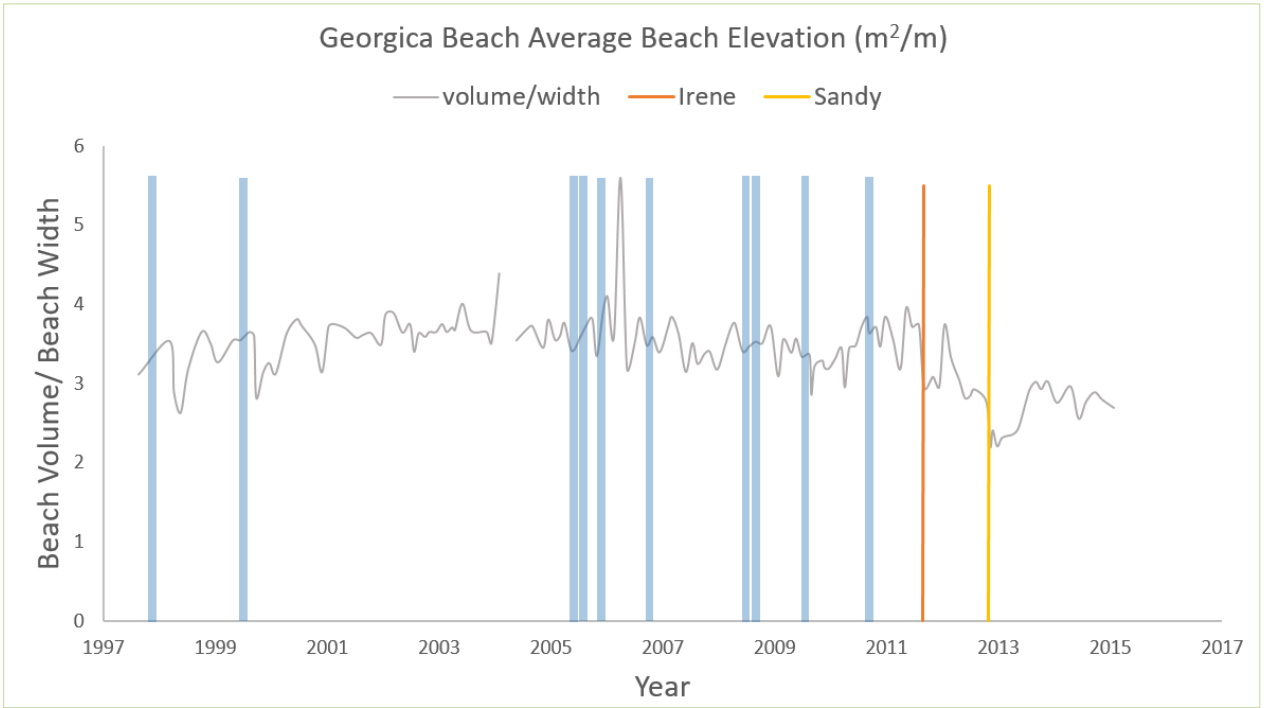

Figure 3. 39. Georgica beach average beach elevation with storm events.

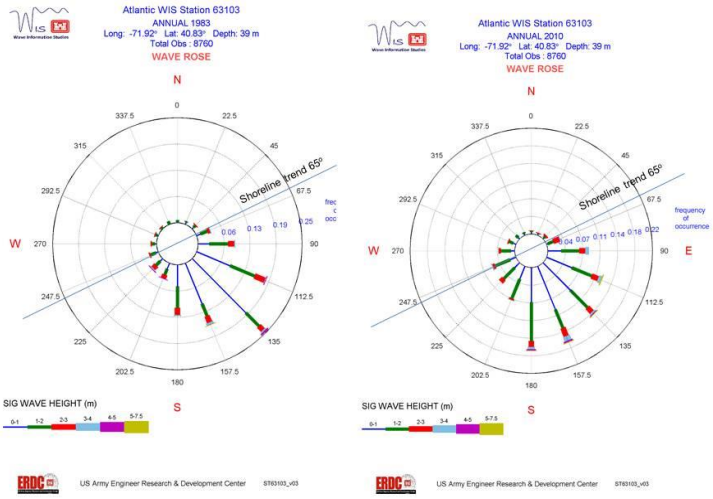

Figure 3. 40. Wave roses in 1983 and 2010, from < http://wis.usace.army.mil/wis.shtml >.

3.8 Tables

Date	Event	Time	Event
22-23,1,1980	Northeaster	16,9,1999	Tropical Storm Floyd
28-30,3,1984	Northeaster	19-24,9,1999	Hurricane Gert
9.27,1985	Hurricane Gloria	2005	Hurricane (Cindy, Irene, and Ophelia)
19,8,1991	Hurricane Bob	3,1,2006	Northeaster
30,10,1991	Northeaster (Halloween Storm)	22,11,2006	Northeaster
11-12,12,1991	Northeaster (Storm from Hell)	22,7,2008	Tropical Storm Cristobel
11-14,12,1992	Great Nor'easter	28,9,2008	Hurricane Kyle
13,3,1993	Northeaster	22,8,2009	Hurricane Bill
23,12,1994	Northeaster	23,9,2010	Hurricane Earl
27-28,1,1998	Northeaster	28,8,2011	Tropical Storm Irene
3-4,2,1998	Northeaster	22-31,10,2012	Hurricane (Superstorm Sandy)

Table 3. 1. Selected extreme events that have impacted New York's ocean shoreline.

Period	Average recession rate (m/yr)	Standard Deviation (m/yr)
1983-2010	-0.22	0.55
1983-2013	-0.21	0.50
1983-2010 (with 1999)	-0.17	0.55
1983-2013 (no 1999)	-0.19	0.50
1999-2010 (no 1983)	-0.12	1.07
1999-2013 (no1983)	-0.18	0.82

Table 3. 2. Recession rate with the new 1999 HWL, m/yr.

Section	Corresponding transects
1	602211-620941
2	620931-620191
3	620181-601341
4	601331-600591
5	600581-599841
6	599831-599091
7	599081-598341
8	598331-597591
9	597581-596861
10	596851-596101

Table 3. 3. Sections for sandwave analysis, from 1-2, the direction is from west to east.

Location ID	Recession rate between 1983-2013		Recession rate between 1983-2010	
m/yr	EP method	LR method	EP method	LR method
586001	-3.5	-2.8	-2.0	-2.1
585991	-4.0	-3.2	-2.1	-2.2
585981	-4.1	-3.3	-2.2	-2.4

Table 3. 4. Recession rates in m/yr for selected positions in the study area.

Section	Recession rate 1983 to 2010 (m/yr)	Recession rate 1983 to 2013 (m/yr)	Dominant wavelength 1983 to 2010 (m)	Dominant wavelength 1983 to 2013 (m)
West	-0.44	-0.39	1110	1388
Middle	-0.05	-0.06	1511	1511
East	-0.54	-0.46	1083	3250

Table 3. 5. Recession rate in m/yr and the dominant wavelength in m before and after Sandy.

	Before Sandy (m/yr)	After Sandy (m/yr)
Average	-0.37	-0.41
Standard Deviation	0.27	0.26

Table 3. 6. Recession rate in section 2.

Width (meter)	Average	Standard Deviation
Main Beach	66.80	24.52
Georgica Beach	82.25	33.34
Volume (m^3/m)	Average	Standard Deviation
Main Beach	144.65	36.89
Georgica Beach	274.61	60.35
Average Beach Elevation	Average	Standard Deviation
Main Beach	2.21	0.60
Georgica Beach	3.21	0.88

Table 3. 7. Beach survey statistic.

Wave Direction	Total Records	Sandwave	No Sandwave	Uncertain
Southeast	149	60	81	8
Southwest	71	33	35	3

Table 3. 8. Sandwave and wave direction records.

Section	Sandwave Existence	Section	Sandwave Existence
Section 1	22.7%	Section 6	68.2%
Section 2	54.5%	Section 7	59.1%
Section 3	45.5%	Section 8	31.8%
Section 4	54.5%	Section 9	0%
Section 5	81.9%	Section 10	0%

Table 3. 9. Sandwave appearance possibility in each section.

CHAPTER 4: CSHORE: Model Beach Profiles with Different Types of NPFs Under Extreme Weather Events

4.1 Introduction

The resilience of NPFs is their ability to naturally recover their protection functions after erosional losses. As discussed earlier, only dunes with an active source of sand can exhibit resilience, bluffs and relic dunes cannot. If the rate at which sand is resupplied after an erosion event is assumed to be constant, then, the resilience of dunes depends on the volume of sand lost. Erosional losses after an event, therefore, might be used to rank the resilience of dunes. With global warming, the frequency of Atlantic hurricanes may increase. (Mann and Emanuel 2006; Grinsted et al. 2013), and while the shoreline has repeatedly shown its capacity to recover after storm events, some events, like Superstorm Sandy are thought of as "game-changers", that is, impacts that permanently alter the resilience of the ocean shoreline. Resilience might be evaluated by the magnitude of erosional losses. If the NPF is a bluff or a relic dune, the losses are not recoverable; resilience, regardless of the loss, is zero. For dunes feed by wind-blow sand from the beach the time to recovering, that is the resilience, depends on the volume of sand that need to be restored, and whether or not the reconstructed dune has to climb a top a bluff.

However, to understand the resilience of NPFs, the evolution of the beach profiles under erosional stress might be modeled. Datasets from the period of time around Superstorm Sandy were chosen as an example of an extreme, potentially "game-chaning" event. Numerical models of coastal processes are routinely used to assess erosion impacts. Modeling in the study area used CSHORE, a simple and robust model that is suited for engineering applications. The initial CSHORE was developed in 1998 to predict the cross-shore transformation of irregular waves. However, the wave nonlinearity needs to be parameterized by empirical formulas and now CSHORE is based on linear wave theory and the Gaussian probability distribution (Kobayashi et al., 1998; Johnson and Kobayashi, 1998). Also, to expand the range of practical application, both impermeable and permeable version of CSHORE exists (Meigs and Kobayashi, 2004; Kobayashi et al., 2007). A part of MORPHOS project of US Army Engineer Research and Development Center is using the extended impermeable version of CSHORE to predict the cross-shore and longshore transport rates of suspended sand and bedload on beaches (Gencarelli et al., 2008; Zhao et al., 2005; Johnson et al., 2006). To predict wave overwash of dunes, a hydrodynamic model was coupled with the sediment transport model in CSHORE. On a permeable bottom, wave overtopping of rubble mound structures can also be calculated by the extended hydrodynamic model. Other than that this model is capable of predicting the evolution of damaged stone armor layers when coupled with the CSHORE bed load formula modified for stone (Kobayashi and Farhadzadeh, 2009; Johnson et al., 2009). Components of the model included (Table 4.1) a combined wave and current model based on time-averaged continuity; cross-shore and longshore momentum; wave action equations; roller energy equations; a sediment transport model for both suspended sand and bedload; a permeable layer model; empirical formulas for irregular wave run-up, overtopping and seepage; and a probabilistic model for an intermittently wet and dry zone.

As will be discussed below this exercise was only partially successful. Unexplained instabilities appeared in some of the simulations and attempted comparisons with the pre-and-post Sandy

LIDAR data were hampered because the modeled period was not the same as the period covered by LIDAR data.

4.2 Methods

CSHORE calculated the change in the beach profile during a period of interest based on the input wave height, wave period, water level and initial bathymetry. Because the available LiDAR data was only subaerial, the input bathymetry for the application of the model was based on a combination of topographic LiDAR data and offshore bathymetry provided by the Atlantic Coast of New York Monitoring Program (ACNYMP; http://dune.seagrant.sunysb.edu/nycoast/ accessed March 2016). The ACNYMP includes 348 locations that cover around 217 km of shoreline between Coney Island and Montauk Point (Figure 4.1). Data was collected spring and fall between 1995 and 2000 to a water depth of 10 meters. The study area includes 51 ACNYMP locations relative to the NGVD 1929 vertical datum. The subaerial profiles at these locations were extracted from the LiDAR data collected between November 2011 and April 2012 by New York State Department of Environmental Conservation and National Oceanic and Atmospheric Administration (NOAA) and georeferenced to North American Vertical Datum of 1988 (NAVD88). In order to connect two datasets VDatum from NOAA was used to convert the vertical and horizontal coordinates to be consistent. VDatum is a free software tool being developed jointly by NOAA's National Geodetic Survey, Office of Coast Survey, and Center for Operational Oceanographic Products and Services (http://vdatum.noaa.gov/ accessed February 2016). To convert the datum, the coordinate information of each point is required, only the LiDAR dataset had that information, so LiDAR data had been converted to a reference to NGVD 1929 vertical datum (Figure 4.2). Post-Sandy LiDAR data was collected by NOAA on November 14 and 15, 2012, a little over two weeks after the storm (https://coast.noaa.gov/dataviewer/ accessed March 2016). Pre-and post-Sandy LiDAR on 72 transects were compared in the study area.

Bathymetry was incorporated based on the distance between the LiDAR station and ACNYMP station (Table B4). The time period is from October 20th, 2012 to October 31th, 2012, 12 days in total. The water level data (Figure 4.3) is from National Data Buoy Center Station MTKN6 near Montauk Point, the wave height and wave period data (Figure 4.4) is from Station 44025 (near the western boundary of the study site), the wave period is the dominant wave period for the model requirement (Figure 4.5). During Sandy, waves reached heights of 9.7 m at the wave buoy and the storm tide reached 1.5 m. Data from Station 44025, far offshore was adjusted for wave shoaling to a 10-meter bathymetric contour by:

$$H_{10} = H_o [\{1+2kd/\sinh(2kd)\}\tanh(kd)]^{0.5} \qquad [1]$$

Where H_0 is the offshore wave height and H_{10} is the wave height in 10-meter water depth, k is the wave number and d, the water depth.

An attempt was made to compare the model results to the post-Sandy LiDAR profiles. Only the subaerial part of the profile (from sea-level NAVD88 out to 300 meters from the shoreline) had been used for sand lost in this part because the post-LiDAR data did not include the bathymetry. The "coastal zone" is defined by New York State to be one thousand feet from the shoreline.

4.3 Results

Five of the model calculations showed (unexplained) instabilities, these may have been due to the predetermined smoothing of the profiles or an insufficiently small spatial step. 19 of 24 of the trials ran well, but others show some instability (Figure 4.6): 2 in single dune group; 1 in multiple dune groups; 2 in dune-on-top group. Profiles representing dunes in front of a bluff were accommodated by the model without instabilities developing. The average sand lost for single dune was 238 m^3/m, for multiple dunes was 246 m^3/m, for dune in front of the bluff is 274 m^3/m and for dune on top of the bluff was 265 m^3/m (Table 4.2). The average amount of sand lost was 257 m^3/m (the instability trials were not included), with a standard deviation of 40.38 m^3/m. In all 24 trials (Figure 4.7), the offshore bar eroded. Almost all the dune features eroded although some of them reformed under post-Sandy's wave conditions. Larger erosional losses were interpreted to represent a lower resilience, that is, with a greater loss of sand, more time would be needed for the system to recover. So the resilience of NPFs was highest for the dune, followed by multiple dunes, then dune atop a bluff with dunes in front of a bluff showing the lowest resilience.

In all the cases (Figure 4.8-4.11, Figure A1-A4), sand was moved offshore, scarping the dune displacing the foot of the dune landward. In 95% of the trials, however, the elevation of the dune crest was also reduced. Only one of the trials representing a single dune did not have the crest elevation lowered by the storm (Figure A1, transect 600351). The original dune height in this exception was around 8 m. With others have a dune height around 4 m – 6 m. Dune heights for dunes found in front of a bluff were around 5 m.

To better capture the recovery after Sandy, the storm conditions were shifted to the middle of the 12-day simulation period, that is from October 25th, 2012 to November 5th, 2012.The corresponding trials' distribution and their water level and height data are in Figure 4.12-4.14. The bathymetry combination between the LiDAR station and ACNYMP station is in Table B5. In all the trials no instability showed up (Figure 4.15-18, Figure A5-A11), the average volume of sand lost by single dunes was 222 m^3/m; for profiles with multiple dunes, 230 m^3/m; for dunes in front of a bluff, 254 m^3/m; and for dunes on top of a bluff, 244 m^3/m (Table 4.3). The average volume of sand lost is 237 m^3/m, with a standard deviation of 42.65 m^3/m. In all 48 trials, the offshore bar eroded substantially. Based on the volume of sand lost, the ranking of resiliency among sections remained the same. The resilience of NPFs was highest for the dune, followed by multiple dunes, then dune atop a bluff with dunes in front of a bluff showing the lowest resilience.

The least amount of sand loss occurred for the single dunes. Combinations of NPFs do not seem to necessarily equate to high resilience because the combination of features had a more sand lost under the model conditions. The dune height, width, and volume are the control factor. Comparison with the post-LiDAR data will be discussed in next section.

In almost all cases (94%), the sand was moved offshore, scarping the dune and displacing the foot of the dune landward. In 71% of the trials, however, the elevation of the dune crest was also reduced. The decrease of the dune height is related to both the original height of the dune and the wave height. For example, the dune elevation in Transect 620181 stayed at 6.5 m during Sandy period, while dune elevation in Transect 599671, at 5 m, decreased (Figure 4.19). The eroded dune may recover after an extreme event, as long as the sand source area is sufficient. However, as discussed earlier, if the dune is compromised, the bluff itself provides protection against flooding and resistance to landward migration of the shoreline. In the face of a long-term rise in sea-level, the dune may be less important as an NPF. Rather, the bluff provides protection and controls the shoreline response. Bluffs and relic dunes will not recover as NPFs if compromised by erosion.

In all of the trials, the offshore (longshore) bar eroded substantially. For multiple dune features, all the dune fields suffered erosion, but, in some cases, the second dune survived the storm unscathed, apparently because the waves were not high enough to reach the second dune. Although some features of the multiple dune fields were lost and the crest height reduced, the dune field itself survived. When dune was found on top of a bluff, a trough tended too form at the foot of the dune. This was attributed to model showed instability which could not be explained. Dunes in front of a bluff tended to have crest heights less than about around 5m. Under the conditions seen during Sandy, the offshore bar eroded, and the seaward toe of the dune was scarped, but the dunes survived the storm.

Out of the 66 stable trials used for the pre-and post-Sandy comparisons (Figure 4.20-23, A12-A23), single dunes lost an average of 9.23 m^3/m, compared to the modeled sand losses of 68.77 m^3/m (Table 4.4); for multiple dunes, the measured average volume of sand lost was 20.20 m^3/m, while the model predicted an average of 62.07 m^3/m; for dunes in front of a bluff, the average sand lost was 20.88 m^3/m, but average modeled losses was 63.15 m^3/m; for dune on top of a bluff, the average sand lost was 4.13 m^3/m, with average model sand lost as 76.96 m^3/m (Figure 4.24). In total, the model predicted that the beach profile would have lost an average volume of 67.50 m^3/m with the standard deviation of 26.31 m^3/m. In almost all cases (95%), this sand was moved offshore, scarping the dune and displacing the foot of the dune landward. In almost all cases, however, the offshore bar was also eroded. In 83% of the trials, however, the elevation of the dune crest was also reduced. The LiDAR data predicted an average volume loss of 53.50 m^3/m ranged with the standard deviation of 34.74 m^3/m.

As well be discussed the comparison were flawed and interpretation could not be definitive but the comparisons indicate important direction to future research. From the comparisons of the LIDAR profiles the resilience of NPFs was highest for dunes formed on top of a bluff, followed by that of single dunes, then multiple dunes with dunes in front of a bluff showing the lowest resilience. The model calculations yielded a different sequence. The most resilient features, that is those showing the smallest loss of sand, were multiple dunes followed by dunes situated in front of a bluff, single dunes and dunes formed on top of a bluff in that order.

4.4 Discussion

From the LiDAR data after Sandy, losses ranged from less than one cubic meter per meter of beach to 100.50 m^3/m, but gains in sand volume occurred at 22 locations (33%), but these changes were only for the subaerial beach. Sand losses from the offshore sandbar were very large. The average change in dune volume was 14 m^3/m including those stations with volume increases. Considering the erosional losses only, the average loss was 33 m^3/m. The average value of the model results is 68 m^3/m, or twice the LiDAR result.

Dunes perched on top of bluffs (n = 16) fared better than dunes located in front of bluffs (n = 18). Those on top lost an average volume of 4.13 m^3/m and almost half of the locations gained sand. Dunes located in front of the bluff lost an average of 20.88 m^3/m although five (27.8%) gained sand. When only the losses of sand were considered, the disparity was reduced. Dunes in front of bluffs lost 34.68 m^3/m and while those formed on top of a bluff crest lost 42.20 m^3/m.

Comparisons with pre-Sandy and post-Sandy LiDAR data were encouraging although the use of smoothed profiles by CSHORE hampered direct comparisons. The smoothed profiles used by CSHORE looked substantially different from the input measurements. In an attempt to improve the comparison, the distance-step used in the model was reduced. Smoothing of the profile was redone after reducing. The smoothed profiles using a spacing of 0.5 meter and 0.1 meter were closer to the original ones, but the improvement is fairly small and the run-time increase a great deal. The model will not accept smaller values of Δ x, like 0.05 or 0.01 meter.

Historical offshore profiles used for the modeling may not have been accurate representations of conditions immediately before Sandy. In addition, the LiDAR data was taken a month after the storm when some recovery could have already occurred. Nevertheless, the modeled losses were larger than those recorded by the data by a factor of two to as much as six.

4.5 Conclusion

Although "Superstorm" Sandy was a historic event, the primary dunes were proof against the storm in the study area. CSHORE models of storm erosion yield an average loss of 67.5 m^3/m or about 41% of the FEMA criteria of 540 square-meters in the dune reserve for surviving a 100-year storm. Only losses at one location exceeded the FEMA criteria of 165 m^3/m. Direct comparison of pre- and post-Sandy LiDAR profiles showed smaller erosional losses, but those dunes formed in front of the coastal bluff experiencing the greatest average loss of 20.9 m^3/m. The erosion of the subaerial bluffs seems to contribute only an uncertain fraction of the longshore sand in transport alongshore, perhaps 40% but maybe as little as 2% based on previous studies. On the other hand, the role played by the offshore bar in the response of the beached to storms suggests to me that bars should be recognized as NPFs in the future. As a practical matter, however, it would be difficult to determine the distribution of bar characteristic at sufficient resolution all along the shore.

4.6 Figures

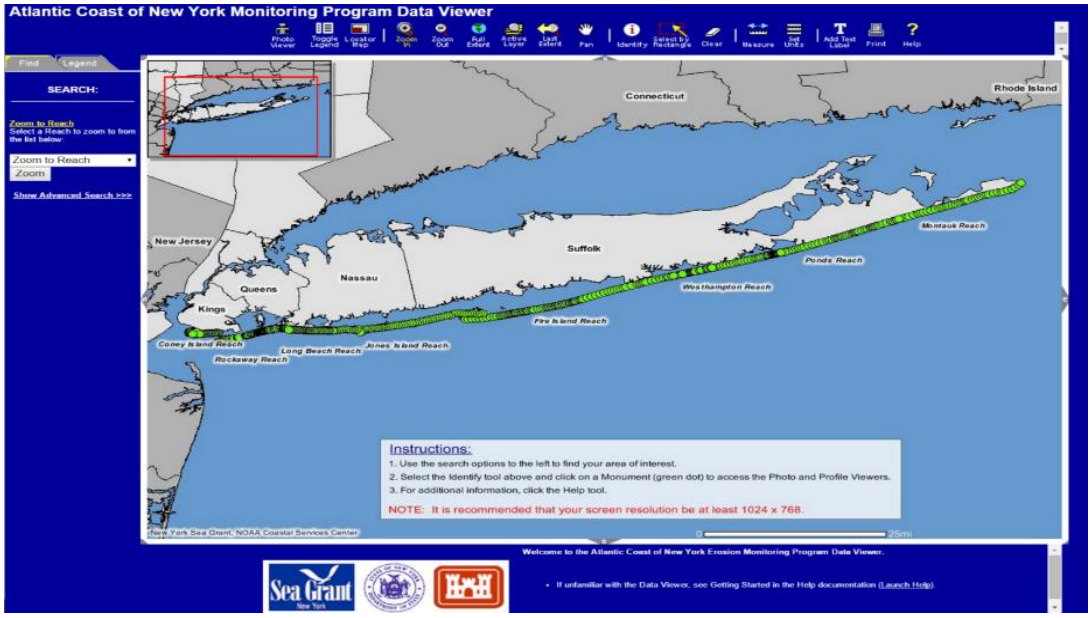

Figure 4. 1. Atlantic Coast of New York Monitoring Program Data Viewer.

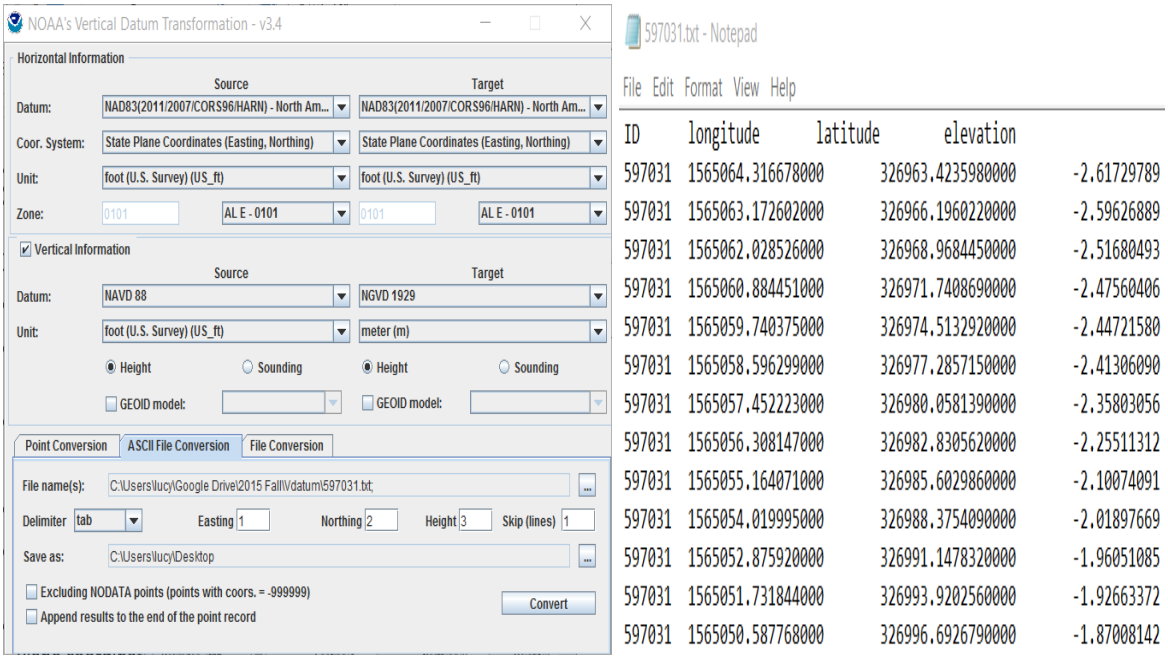

Figure 4. 2.Vertical datum conversion using VDatum tool.

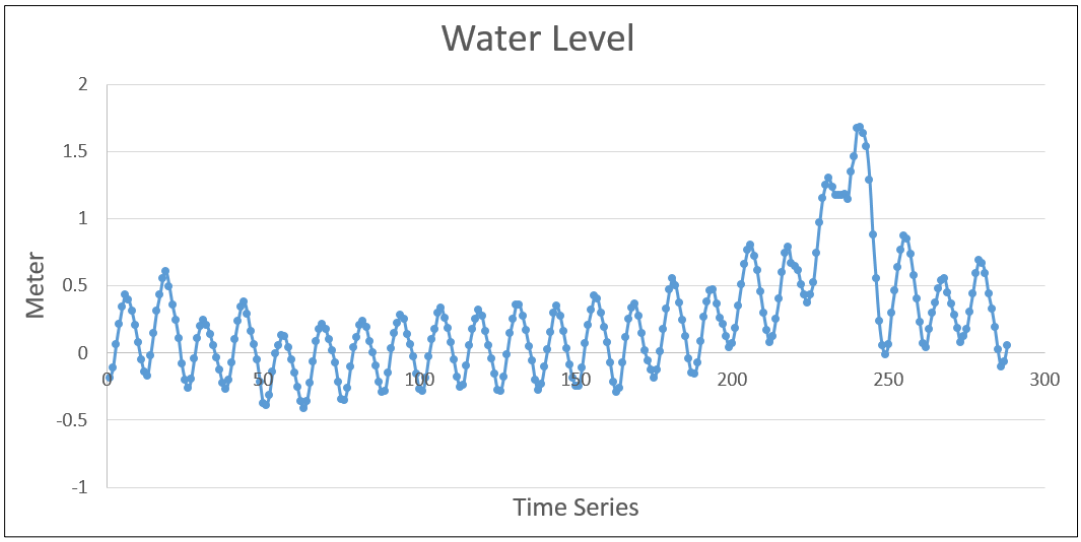

Figure 4. 3. Water level data during October 20th, 2012 to October 31th, 2012.

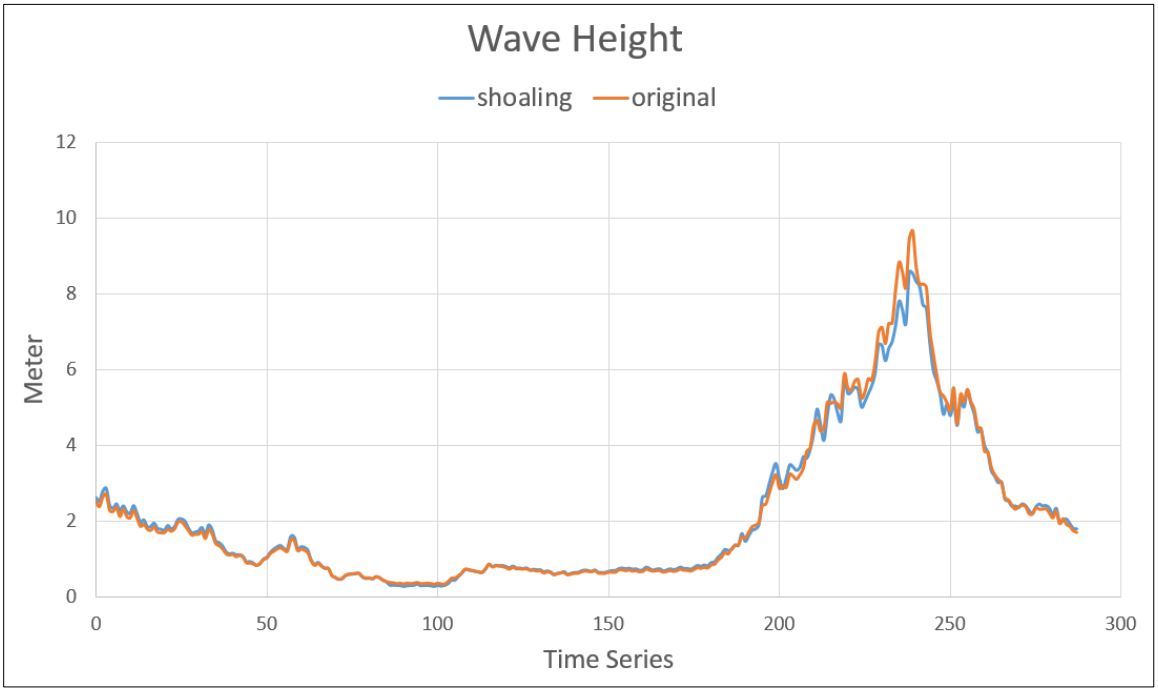

Figure 4. 4. Wave height data during October 20th, 2012 to October 31th, 2012, red line is wave height before shoaling, blue line is wave height after shoaling.

Figure 4. 5. National Buoy Center Station MTKN6 and Station 44025.

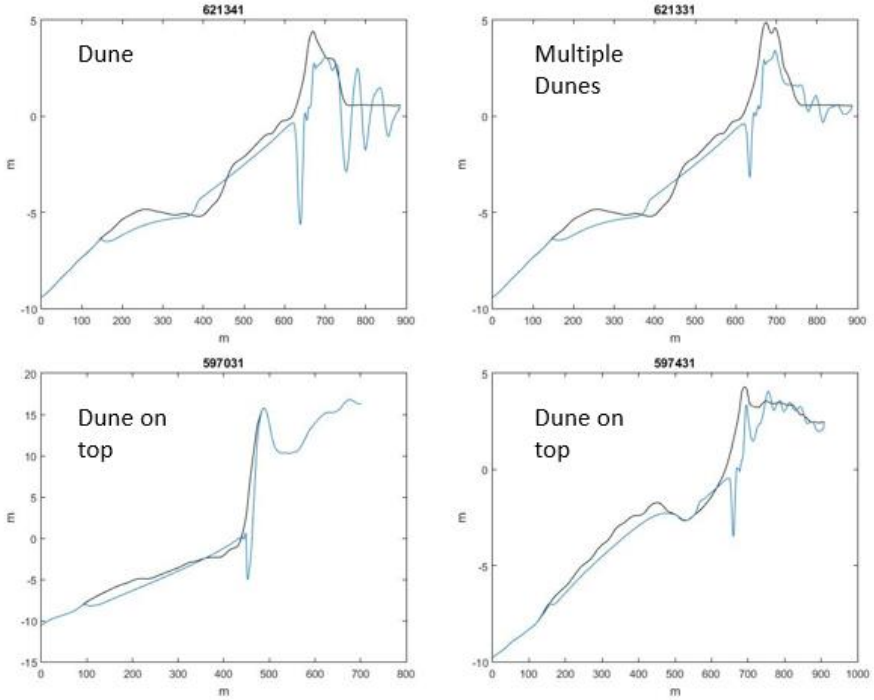

Figure 4. 6. An example of instability in model trials. 1 example from subclass “dune”, 1 example from subclass “multiple dunes” and 2 examples from subclass “dune on top”. The black line is the original profile, the blue line is the model results. All of them showed instability on the landward side of the profile.

Figure 4. 7. Model trials distribution map during October 20th, 2012 to October 31th, 2012.

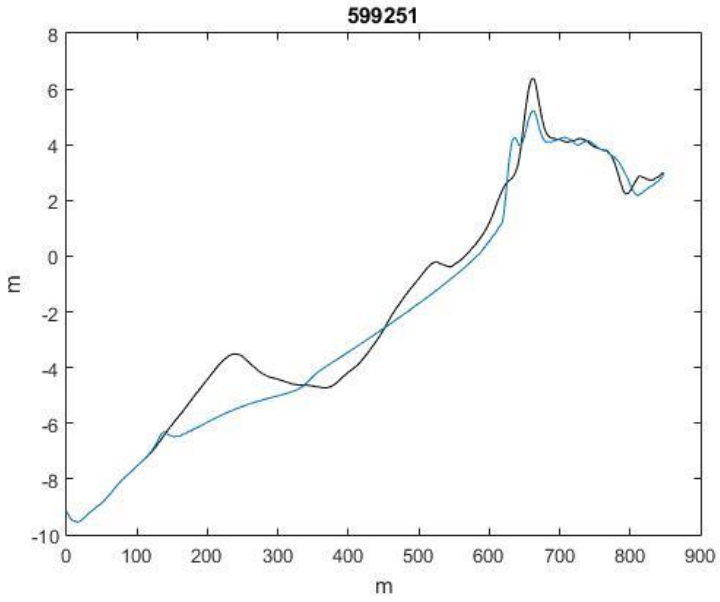

Figure 4. 8. Example of dune trials during October 20th, 2012 to October 31th, 2012, the black line is the original profile, the blue line is the model results after Sandy.

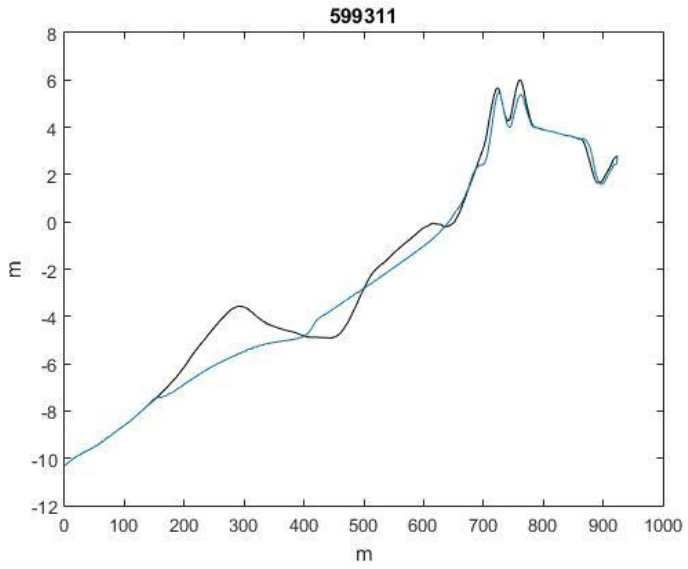

Figure 4. 9. Example of multiple dunes' trials during October 20th, 2012 to October 31th, 2012, the black line is the original profile, the blue line is the model results after Sandy.

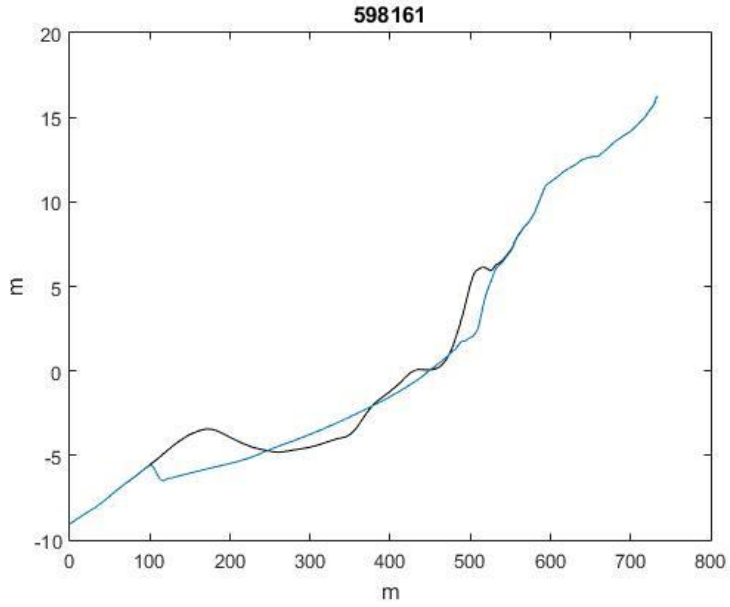

Figure 4. 10. Example of dune in front trials during October 20th, 2012 to October 31th, 2012, the black line is the original profile, the blue line is the model results after Sandy.

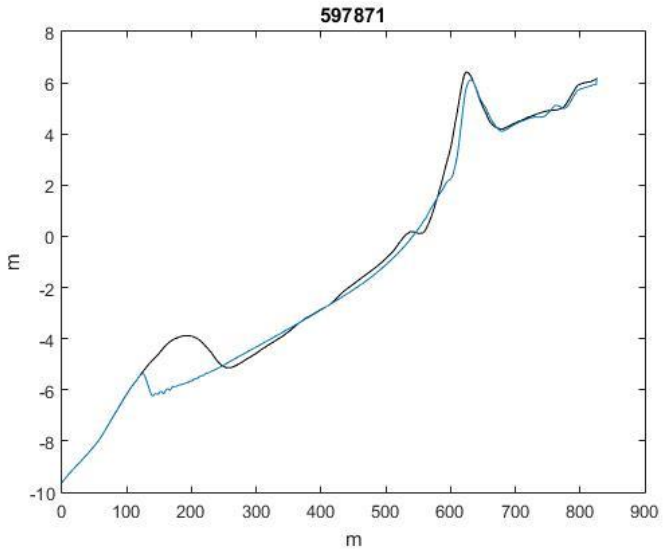

Figure 4. 11. Example of dune on top trials during October 20th, 2012 to October 31th, 2012, the black line is the original profile, the blue line is the model results after Sandy.

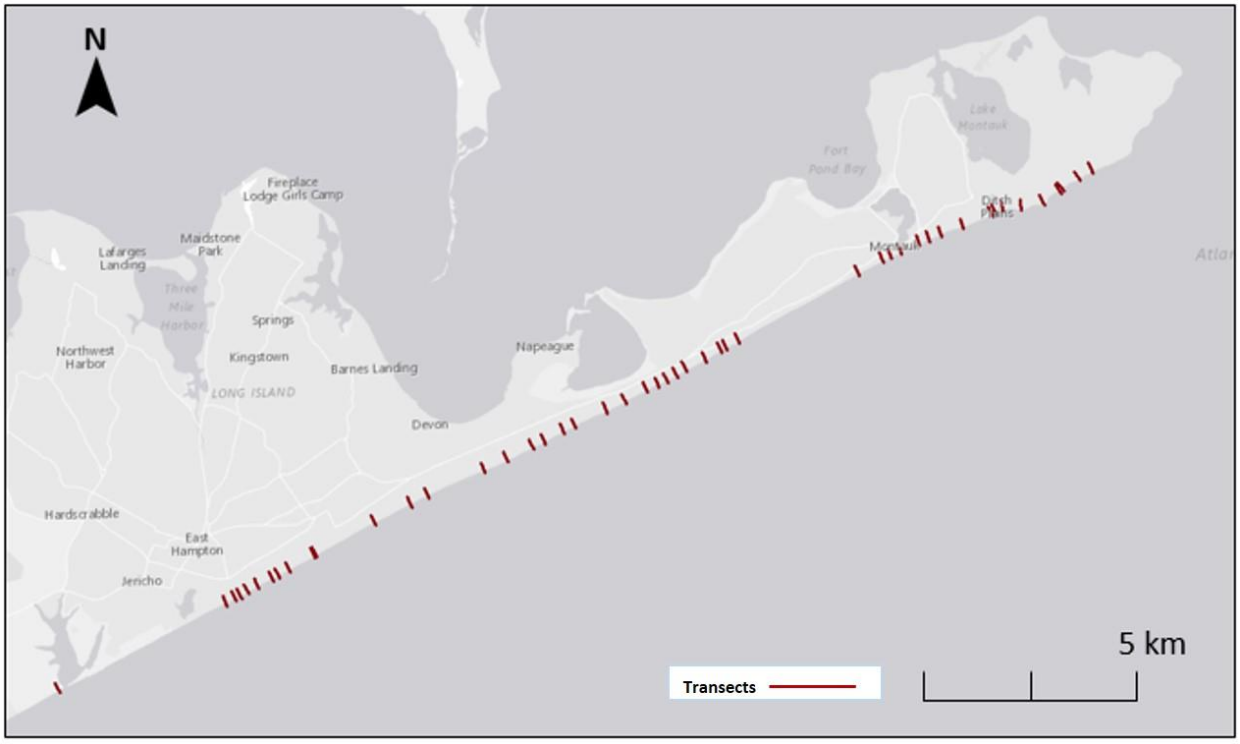

Figure 4. 12. Model trials distribution map during October 25th, 2012 to November 5th, 2012.

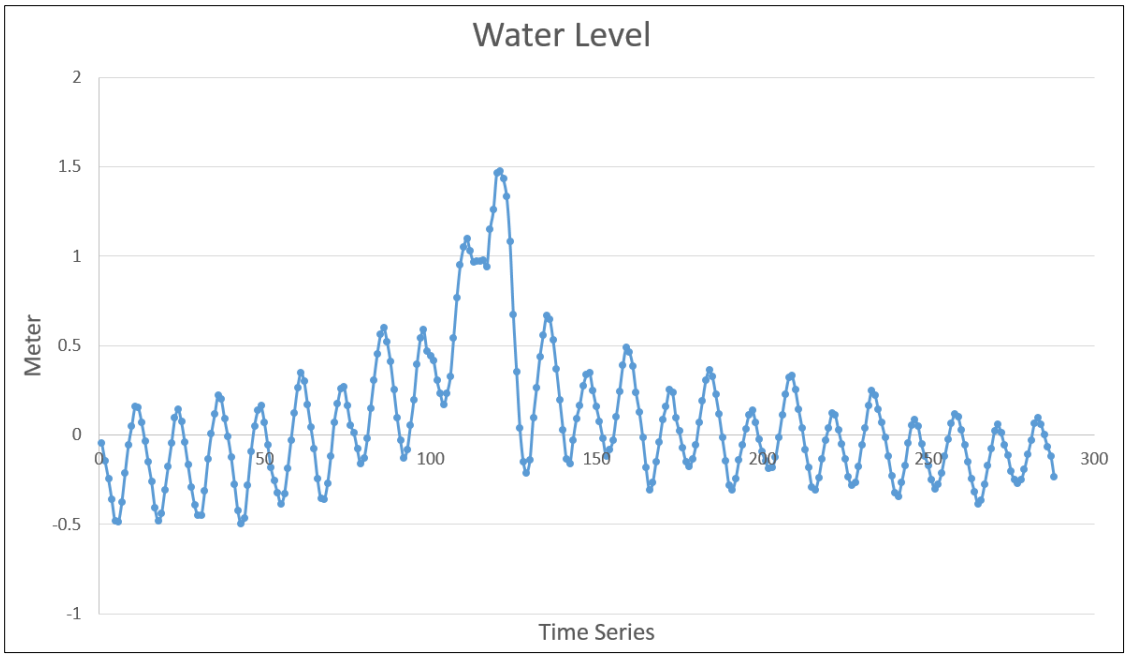

Figure 4. 13. Water level data during October 25th, 2012 to November 5th, 2012.

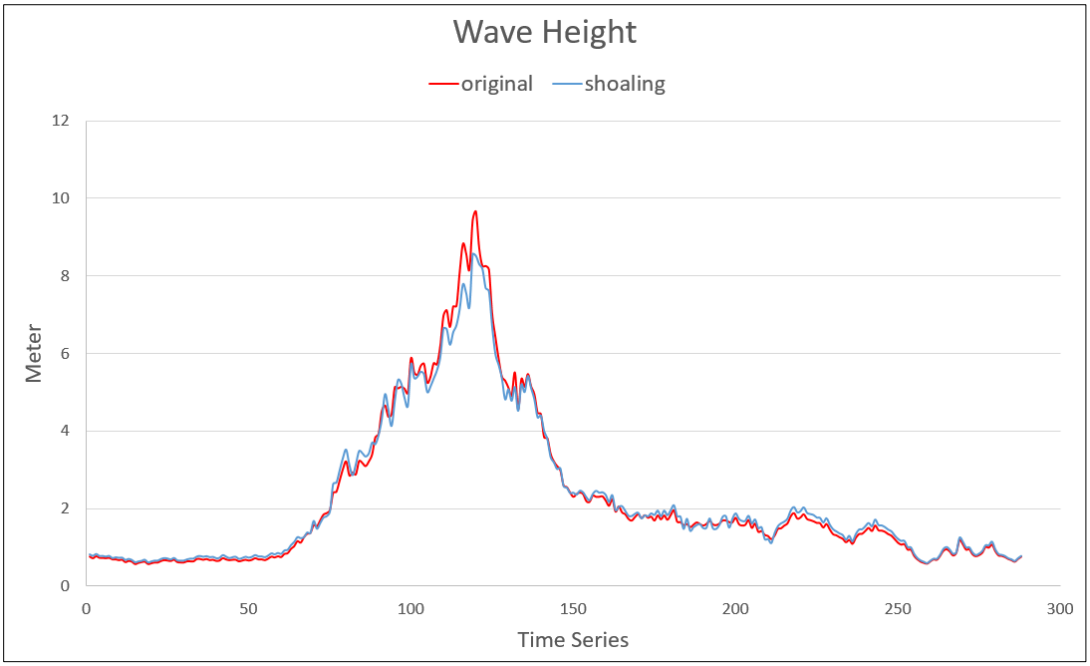

Figure 4. 14. Wave height data during October 25th, 2012 to November 5th, 2012, the red line is wave height before shoaling, the blue line is wave height after shoaling.

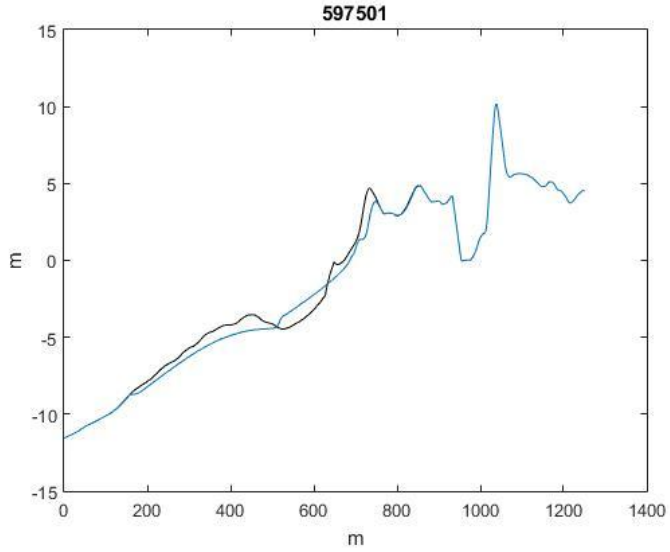

Figure 4. 15. Example of dune trials during October 25th, 2012 to November 5th, 2012, the black line is the original profile, the blue line is the model results after Sandy.

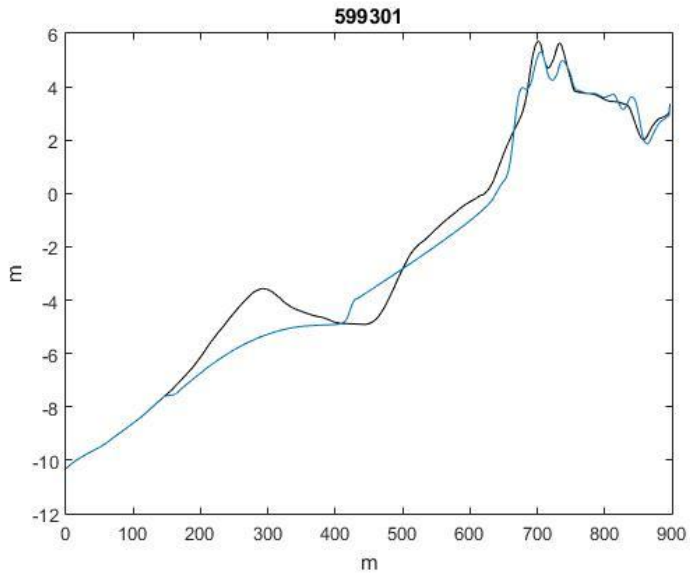

Figure 4. 16. Example of multiple dunes' trials during October 25th, 2012 to November 5th, 2012, the black line is the original profile, the blue line is the model results after Sandy.

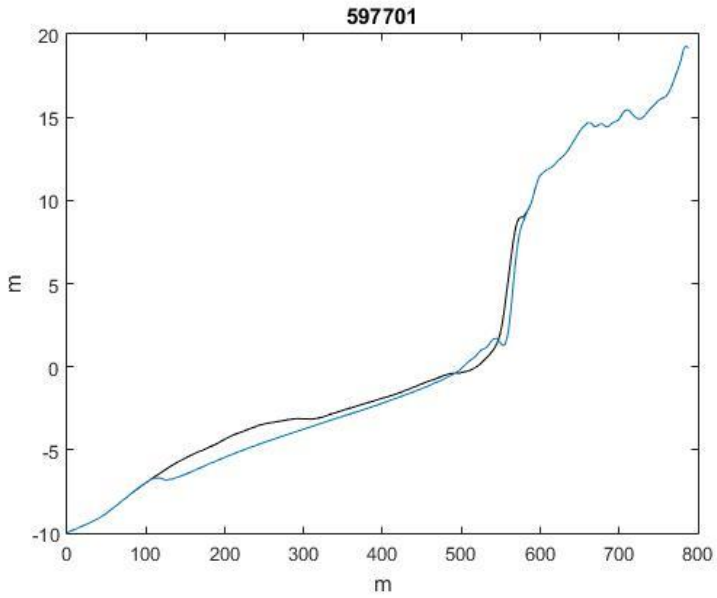

Figure 4. 17. Example of dune in front trials during October 25th, 2012 to November 5th, 2012, the black line is the original profile, the blue line is the model results after Sandy.

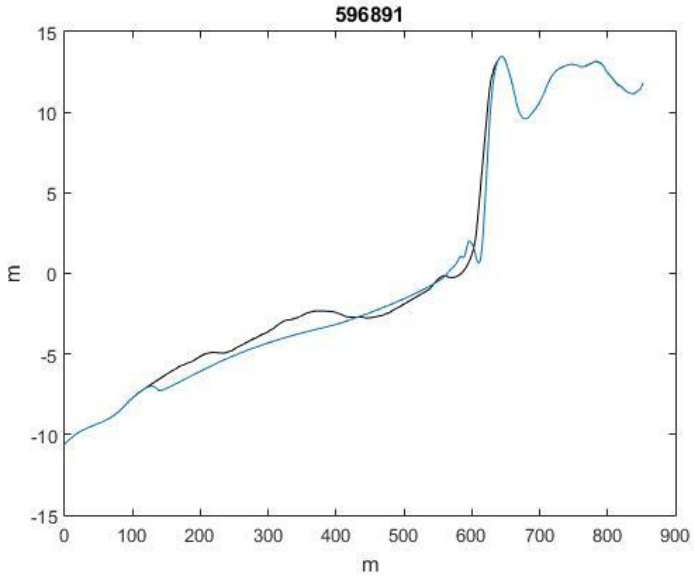

Figure 4. 18. Example of dune on top trials during October 25th, 2012 to November 5th, 2012, the black line is the original profile, the blue line is the model results after Sandy.

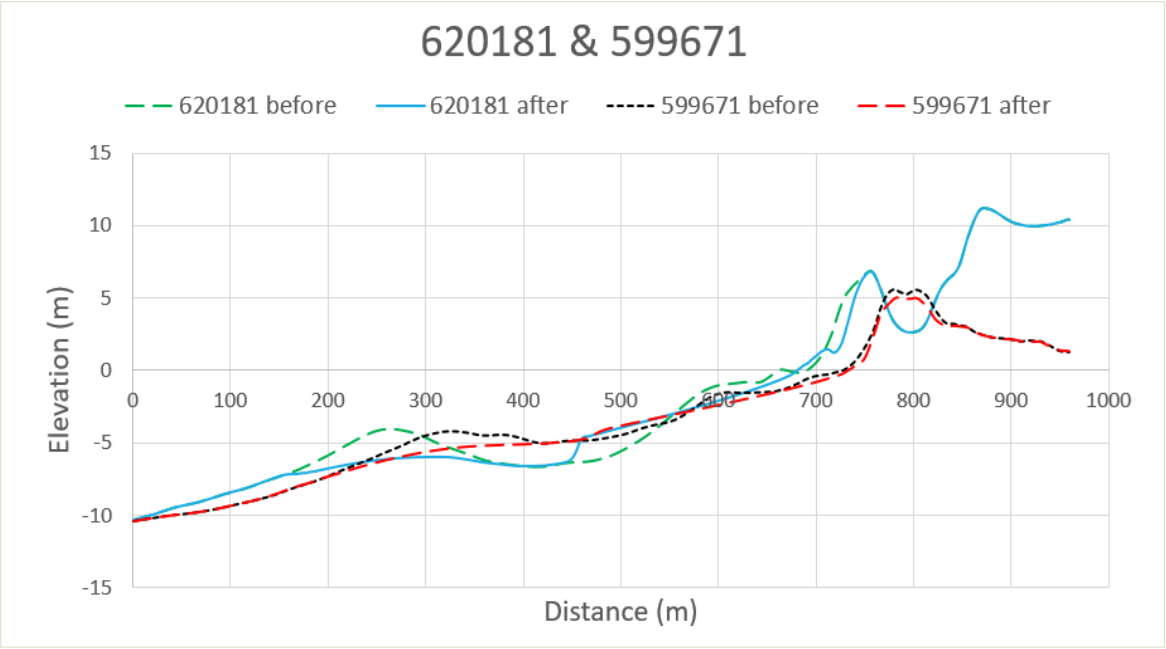

Figure 4. 19. Dune elevation got decreased vs. dune elevation stayed the same.

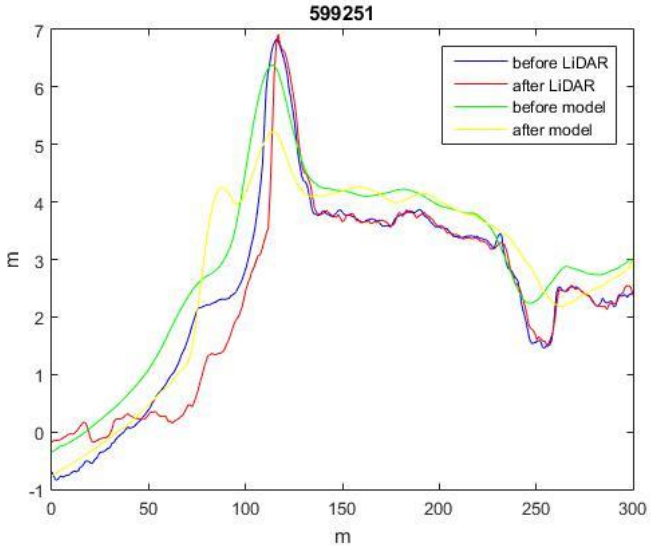

Figure 4. 20. Example of sand lost comparison in dune trials, model results are green and yellow line before and after Sandy, LiDAR data are blue and red line before and after Sandy.

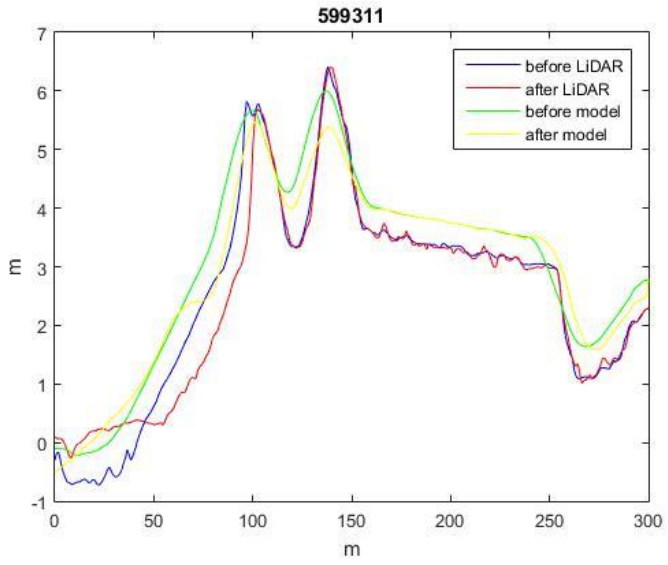

Figure 4. 21. Example of sand lost comparison in multiple dunes' trials, model results are green and yellow line before and after Sandy, LiDAR data are blue and red line before and after Sandy.

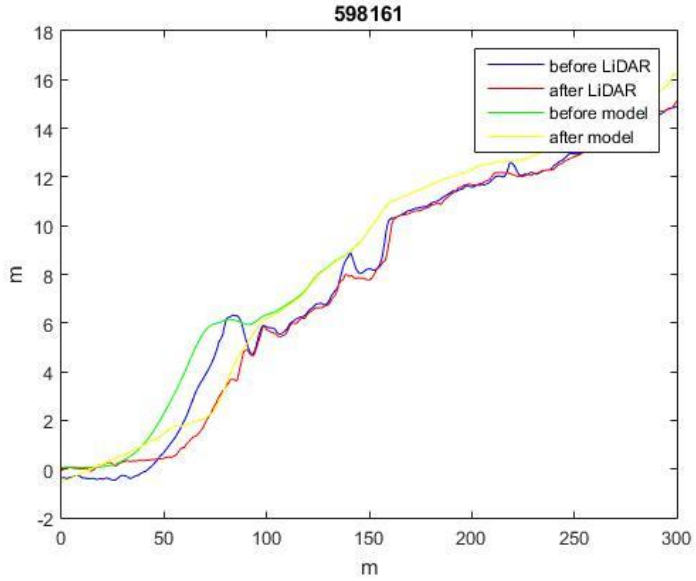

Figure 4. 22. Example of sand lost comparison in dune in front trials, model results are green and yellow line before and after Sandy, LiDAR data are blue and red line before and after Sandy.

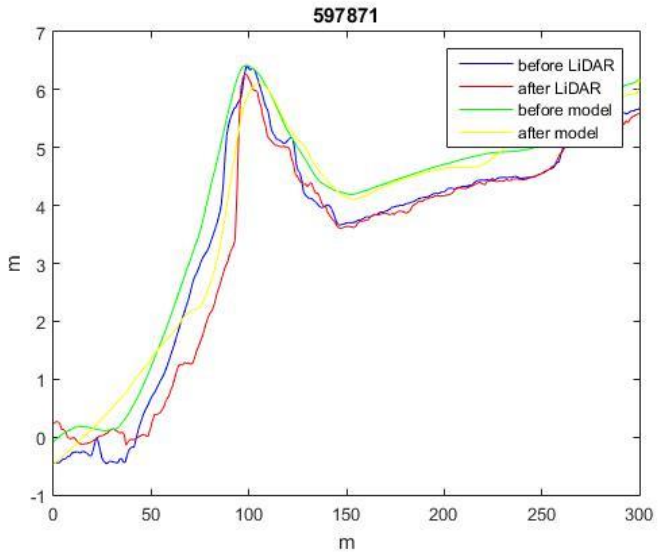

Figure 4. 23. Example of sand lost comparison in dune on top trials, model results are green and yellow line before and after Sandy, LiDAR data are blue and red line before and after Sandy.

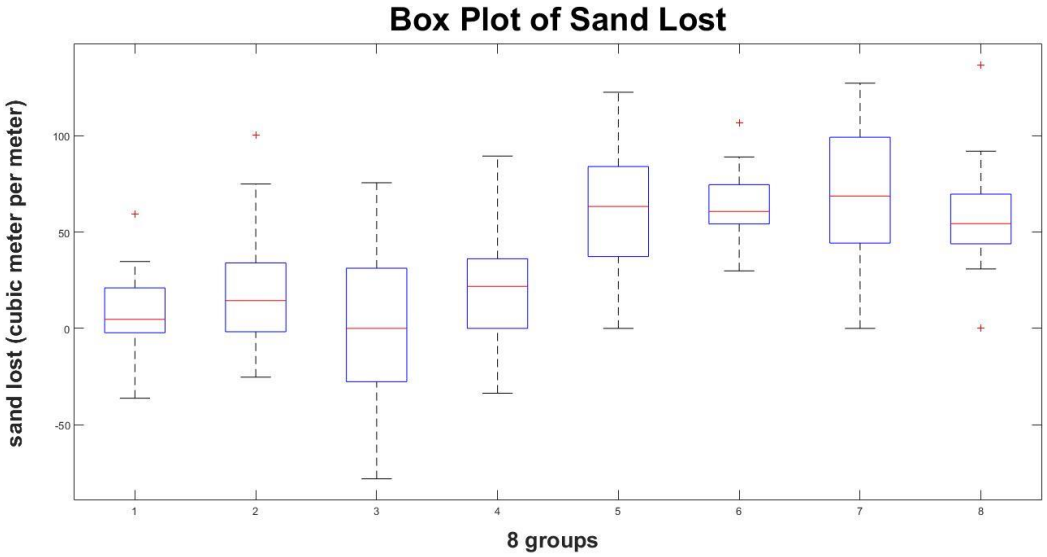

Figure 4. 24. Box plot for the sand lost in all trials. Number 1-4 are LiDAR results for dune, dune in front, dune on top and multiple dunes; Number 5-8 are model results in the same sequence.

4.7 Tables

1	A combined wave and current model (time-averaged continuity)
2	Cross-shore and longshore momentum equations
3	Wave action equations
4	Roller energy equations
5	A sediment transport model (suspended sand and bedload)
6	A permeable layer model (porous flow, energy dissipation)
7	Empirical formulas for irregular wave runup, overtopping and seepage
8	A probabilistic model for wet and dry zone (wave overwash, structural damage progression)

Table 4. 1. The components of CSHORE.

Dune	Sand lost	Multiple	Sand lost	In Front	Sand lost	On Top	Sand lost
620521	226.52	601741	261.79	620351	254.56	598121	260.92
				620121	237.23	598051	266.12
		600051	222.64	599121	262.65	597971	316.81
600351	183.01	599871	174.97	599011	288.87	597871	218.08
600151	265.55	599351	291.67	598221	336.08		
599251	276.01	599311	277.83	598161	264.83		
Average	237.77	Average	245.78	Average	274.04	Average	265.48

Table 4. 2. Sand lost results for model trials during October 20th, 2012 to October 31th, 2012, the unit is m^3/m.

Dune	Sand lost	Multiple	Sand lost	In Front	Sand lost	On Top	Sand lost
597501	203.69	599301	259.63	597701	266.69	596891	246.99
599201	278.95	599421	199.03	597831	195.93	596971	248.34
600181	212.77	599481	209.56	598181	317.48	597081	250.82
600301	101.07	599541	248.47	598331	338.05	597101	243.01
600371	134.11	599601	241.06	599171	270.92	597221	188.27
600531	220.69	599671	186.11	599091	263.77	597361	207.60
600671	229.19	599801	198.39	620091	223.52	597461	246.27
601121	268.56	599921	194.46	620181	220.75	597521	247.68
601011	209.38	600111	238.08	620241	229.31	597901	211.10
601341	271.50	601721	297.84	620291	230.21	597961	308.99
601711	300.41	620051	244.72	620321	244.53	598071	273.37
601881	231.29	601961	242.01	620381	246.77	598131	251.24
Average	221.80	Average	229.95	Average	253.99	Average	243.64

Table 4. 3. Sand lost results for model trials during October 25th, 2012 to November 5th, 2012, the unit is m^3/m.

Sand Lost Comparison					
Transect	Sand Lost		Transect	Sand Lost	
Dune	LiDAR	Model	Multiple	LiDAR	Model
599251	34.72	61.47			
600151	2.34	86.71	601741	21.73	69.68
600351	19.90	55.51	600051	32.26	71.92
			599871	33.74	55.94
			599351	-10.55	49.02
620521	31.06	95.99	599311	21.84	30.84
601881	59.29	72.46	601961	-6.74	136.73
601711	-21.11	88.97	620051	37.12	81.25
601341	6.98	122.59	601721	-24.27	91.98
601121	32.98	37.11	600111	-33.70	69.19
601011	-2.27	67.14	599921	42.68	39.84
600671	-20.05	43.35	599801	89.45	51.46
600531	-14.08	84.02	599671	0.62	54.08
600371	11.58	69.05	599601	20.75	65.17
600301	-36.25	44.79	599541	24.73	50.55
600181	12.38	65.08	599481	36.10	43.90
			599421	19.67	38.96
599201	21.02	37.30	599301	37.91	54.65
Average	9.23	68.77	Average	20.20	62.07
Dune in Front	LiDAR	Model	Dune on Top	LiDAR	Model
620351	43.58	60.27			
620121	33.94	78.15			
599121	9.07	57.47	598051	-29.47	96.78
599011	-21.71	74.58	597871	53.02	53.36
598221	-1.77	88.96	597971	28.58	105.73
598161	63.37	106.78	598121	71.31	98.21
620381	74.94	61.13	598131	72.22	94.24
620321	-6.83	67.64	598071	0.74	106.02
620291	28.11	54.40	597961	-0.79	99.20
620241	22.40	54.19	597901	75.60	4.85
620181	-19.35	54.36	597521	4.94	127.30
620091	-25.35	72.12	597461	31.21	124.19
599171	11.53	37.63	597361	-33.34	42.42
599091	28.63	50.80	597221	-26.19	44.26
598331	17.26	81.09	597101	-21.82	48.97
598181	100.50	71.76	597081	-54.16	83.96
597831	11.25	35.58	596971	-27.69	50.90
597701	6.31	29.85	596891	-78.11	50.92
Average	20.88	63.15	Average	4.13	76.96

Table 4. 4. Sand lost results for all model trials, the unit is m^3/m.

Chapter 5: Recommendations for Future Work

The occurrence of oscillations in the longshore recession rates was linked to the occurrence of alongshore sand waves in one or more of the aerial photographs. Spectral analysis may offer a way to mitigate the influence of these features in recession rate calculations. Spectral analyses showed dominant wave lengths of one to 1.5 km and, perhaps, for the assessment of long-term recession rates, running averages over this distance should be used as a filter.

The common use of visual interpretation of aerial photographs to delineate HWL's might be tested and improved with modern technology. Shorelines determined by recognition of wrack-lines, vegetation lines or wetted perimeter, by eye or by "Beach Tools" or GIS pixel discrimination might be checked with LIDAR data. Although the time period covered by LIDAR is much shorter than that covered by aerial photographs and simultaneous LIDAR and photographic surveys are not generally available. LIDAR shorelines can be based directly on surface elevation rather than relying on visual discrimination in two dimensions. Additional shoreline identification using satellite imagery (e.g. WorldView-3) or unmanned (drone) aerial surveys could be useful.

Explaining the occurrence of sand waves remains problematic. Future research based on wave climate may be most promising. As discussed earlier, the angle of wave attack, the offshore wave steepness and the divergence (or convergence) of waved produced by offshore bathymetry are all possible causes of shoreline morphology. Comparing wave conditions with documented occurrences of sand waves could help and two-dimensional wave modeling would be an appropriate approach.

Erosional losses might be used to quantify resilience of the shoreline, but combinations of NPFs do not necessarily equate with high (or low) resilience. Model simulations done here were not adequate to resolve this issue, but the relative ranking of the resilience of NPFs may provide a framework to further investigate aspects of dune position, height and volume on coastal resilience. Despite unsatisfying results here from the use of CSHORE, the model is widely used and successful in many applications. In this case, shortcomings of CSHORE simulations might be mitigated by using a smaller time step to reduce the influence of smoothing.

References

Agarwal, A., Kobayashi, N., and Johnson, B.D. 2006. Longshore suspended sediment transport in surf and swash zones. *Proc. 30th Coastal Eng. Conf., World Scientific,* 2498-2510.

Allen, J., and Labash, C. 1996. Measuring shoreline change on Fire Island. *Maritimes*, 39, 13–16.

Ashton, A.D and A.B. Murray. 2006. High-angle wave instability and emergent shoreline shapes: 1. Modeling of sand waves, flying spits and capes. *Journal of geophysical Research* 111. doi:10.1029/2005JF000422.

Batten, B.K. 2003. Morphologic typologies and sediment budget for the ocean shoreline of Long Island, New York. *Stony Brook University Ph.D. Dissertation*, 116 pp.
Bokuniewicz, H. J. 2003. Isolated groins at East Hampton, NY. *Journal of Coastal Research,* 33:215-222.

Bokuniewicz, H.J. and J. Tanski. 1980. Managing localized, episodic erosion of coastal bluffs. In W. Edge, ed. Coastal Zone '80, Proceedings of the Second Symposium on Coastal and Ocean Management, Vol. III. *American Society of Engineers*, New York: 1883-1898.

Bokuniewicz, H.J., B. Batten and J. Plummer. 2016. Coastal Erosion Areas (CEHA) Delineation Pilot, Fi*nal Report to the New York State Energy Research and Development Authority*, 37 pp.

Bruun, P. 1962. Sea level rise as a cause for shore erosion. American Society of Civil Engineers Proceedings, *Journal of Waterways and Harbors Division 88*, 117-130.

Crowell, M., Stephen P. L., and Michael K. B. 1991. Historical shoreline change: error analysis and mapping accuracy. *Journal of coastal research*. 839-852.

Dolan, Robert, Michael S. F., and Stuart J. H. 1991. Temporal analysis of shoreline recession and accretion. *Journal of coastal research*. 723-744.

Dubois, R.N. 1977. Predicting beach erosion as a function of rising water level. *Journal of Geology 85*, 470-476.

Fenster, Michael S., Robert D., and Robert A. M. 2001. Coastal storms and shoreline change: signal or noise? *Journal of Coastal Research*. 714-720.

Fisher, J.J. 1982. Barrier islands and the Bruun Rule. *Geological Society of America Abstracts with Programs,* Northeastern and Southeastern Combined Sections Meeting 14, 17.

Fuller, M. L. 1914. The geology of Long Island, New York. *United States Geological Survey Professional Paper 82*, 231.

Gencarelli, R., Tomasicchio, G.R., Kobayashi, N., and Johnson, B.D. 2008. Beach profile evolution and dune erosion due to the impact of Hurricane Isabel. *Proc. 31th Coastal Eng. Conf., World Scientific*, 1697-1709.

Gravens, M. 1999. Periodic shoreline morphology, Fire Island, New York. *Proceedings of Coastal Sediments*, ASCE Press, 1613-1626.

Grinsted, A., J. C. Moore and S. Jevrejeva. 2013. Projected Atlantic hurricane surge threat from rising temperatures, *Proceedings of the National Academy of Sciences* 110, 5369-5373.

Hallermeier, R. J. and P. E. Rhodes. 1986. Description and Assessment of Coastal Dune Erosion. *Dewberry and Davis*, Fairfax, VA.

Halverson, J. B., and T. Rabenhorst. 2013. Hurricane Sandy: the science and impacts of a superstorm. *Weatherwise*, 66(2), 14-23.

Hands, E.B. 1980. Prediction of shore retreat and nearshore profile adjustments to rising water levels on the Great Lakes. U. S. Army Corps of Engineers, *Coastal Engineering Research Center, Ft. Belvoir, Virginia, Technical Paper No. 80-7*, 119pp.

Hapke, Cheryl J., et al. 2011. National assessment of shoreline change; historical shoreline change along the New England and Mid-Atlantic coasts. *US Geological Survey*. No. 2010-1118.

Inman, D.L. 1987. Accretion and erosion waves on beaches. *Shore and Beach*, v. 55, n. 3-4, 61-66.

Intergovernmental Panel on Climate Change. 2013. Managing the Risks of Extreme Events and Disasters to Advance Climate Change Adaptation, A Special Report of Working Groups I and II of the Intergovernmental Panel on Climate Change, Cambridge University Press, Cambridge, UK, and New York, NY, USA, 582 pp.

Jennings, J. N. 1967. Cliff-Top Dunes. *Australian Geographical Studies5.1*, 40-49.

Johnson, B., Gravens, M., Wamsley, T., and Kobayashi, N. 2009. A predictive model for beach profile evolution. *Proc. Coastal Dynamics 2009*, Tokyo, Japan, Paper No. 64.

Johnson, D.W. 1919. Shore processes and shoreline development. *John Wiley & Sons Inc*, NY: 584 pp.

Johnston, S. and H. J. Bokuniewicz. 2001. Seasonal Beach on Long Island's Ocean Shorelines, (New York). *Shore and Beach*, 69:3-6.

Kobayashi, N., and Farhadzadeh, A. 2009. Dune erosion and overwash. *Proc. Coastal Dynamics 2009*, Tokyo, Japan, Paper No. 81.

Kobayashi, N., and Johnson, B.D. 1998. Computer program CSHORE for predicting cross-shore transformation of irregular breaking waves. *Res. Rep. No. CACR-98-04, Center for Applied Coastal Research,* Univ. of Delaware, Newark, Del.

Kobayashi, N., Herrman, M.N., Joshnson, B.D., and Orzech, M.D. 1998. Probability distribution of surface elevation in surf and swash zones. *J. Waterway, Port, Coastal and Ocean Eng*., 124 (3), 99-107.

Kobayashi, N., Meigs, L.E., Ota, T., and Melby, J.A. 2007. Irregular breaking wave transmission over submerged porous breakwaters. *J. Waterway, Port, Coastal, Ocean Eng*., 133 (2), 104-116.

Kobayashi, N., Zhao, H., and Tega, Y. 2005. Suspended sand transport in surf zones. *J. Geophys. Res., 110, C12009, doi*: 10.1029/2004JC002853.

Komar, P. D. 1998. *Beach Processes and sedimentation*, Prentice-Hall, Upper Saddle river, NJ: 544p.

Kunz, M., et al. 2013. Investigation of superstorm Sandy 2012 in a multi-disciplinary approach. *Natural Hazards and Earth System Sciences* 13.10: 2579-2598.

Leatherman, S.P. 2003. Shoreline change mapping and management along the U.S. East Coast. *Journal of Coastal Research,* SI (38), 5-13.

Leatherman, S.P., and J.R. Allen. 1985. Analysis Fire Island Inlet to Montauk Point Long Island, New York. *Final Report to the U.S. Army Corps of Engineers.* New York District. 298 pp.

Mann, M.E. and K. A. Emanuel. 2006. Atlantic hurricane trends linked to climate change, *EOS, Transactions American Geophysical Union* 87, 233-241.

Mauermeyer, E. M., and R. G. Dean. 1982. Sea level rise and barrier island migration: An extension of the Bruun Rule to account for landward sediment migration. *Geological Society of America Abstracts with Programs, Northeastern and Southeastern Combined Sections*, 14.

Meigs, L.E., and Kobayashi, N. 2004. Time-averaged model for irregular breaking waves on porous structures and beaches. *Res. Rep. No. CACR-04-02, Center for Applied Coastal Res.,* Univ. of Delaware, Newark, Del.

New York State Coastal Erosion Hazard Area Mapping, Report to the New York Department of Environmental Conservation, Project No. S8239.

Plummer, J.P., B. Batten, and M. Chlebus. 2015. Using Geospatial Tool to Objectively Identify Coastal Features for Regulatory Mapping. *Coastal Sediments '15*, San Diego.

Rector, R.L. 1954. Laboratory study of the equilibrium profile of beaches. *U.S. Army Corps of Engineers Beach Erosion Board,* Technical Memorandum No. 41.

Rich, C.A. 1975. Effects of storms and construction activities on beach accretion and recession rates from Moriches Inlet to Amagansett, Long Island, New York. Master's Thesis. *Department of Earth and Environmental Sciences, Queens College,* City University of New York, NY, 95 pp.

Rosen, P.S. 1978. A regional test of the Bruun Rule on shore erosion. *Marine Geology 26*, M7-M16.

Schwartz, M.L. 1967. The Bruun theory of sea level rise as a cause of shore erosion. *Journal of Geology*, vol. 75, 76-92.

Seaver, K., Bokuniewicz, H. and Buoniauto, F. 2006. Evolution of erosional hot spots on a barrier island: Fire Island, New York. *Proceedings of Coastal Sediments '07*, ASCE Press, 1722-1730.

Shalowitz, A. L. 1964. Shore and Sea Boundaries. (Two vols.), Volume Two: Interpretation and Use of Coast and Geodetic Survey Data, Publication 10-1, U.S. Department of Commerce, *Coast and Geodetic Survey*, Washington, D.C., 749 pp.

Smith, George L., and Gary A. Z. 1990. Calculating long-term shoreline recession rates using aerial photographic and beach profiling techniques. *Journal of Coastal Research*. 111-120.

Sonu, C.J. 1968. Collective movement of sediment in littoral environment. *In ASCE, Proceedings 11th CEC*, p. 373-400.

Taney, N.E. 1961. Geomorphology of the south shore of Long Island, New York. *Coastal Engineering Research Center Vicksburg MS*, No. TM128.

Thevenot, M.M., & Kraus, N.C. 1995. Longshore sand waves at Southampton Beach, New York: observation and numerical simulation of their movement. *Marine Geology*, v. 126, p. 249-269.

Walton Jr, Todd L. 1999. Shoreline rhythmic pattern analysis. *Journal of coastal research*, 379-387.

Watts, G.M. 1954. Laboratory study on the effect of varying wave periods on beach profiles. *U.S. Army Corps of Engineers Beach Erosion Board*, Technical Memorandum No. 53.

Weggel, J. R. 1979. A method for estimating long-term erosion rates from a long-term rise in water level. U.S. Army Corps of Engineers, *Coastal Engineering Research Center, Ft. Belvoir, Virginia, Coastal Engineering Technical Aid No*. 79-2, 16 pp.

Williams, S.J. 1976. Geomorphology, Shallow Subbottom Structure, and Sediments of the Atlantic Inner Continental Shelf Off Long Island, New York. *US Army Corps of Engineers, Coastal Engineering Research Center Technical Paper No*. 76-2: 125.

Zimmerman, M.S. 1983. Coastal Facets as Indicators of Shoreline Response to Rising Sea Level. *Stony Brook University M.S. Dissertation*, 91 pp.

Appendix A. Figures

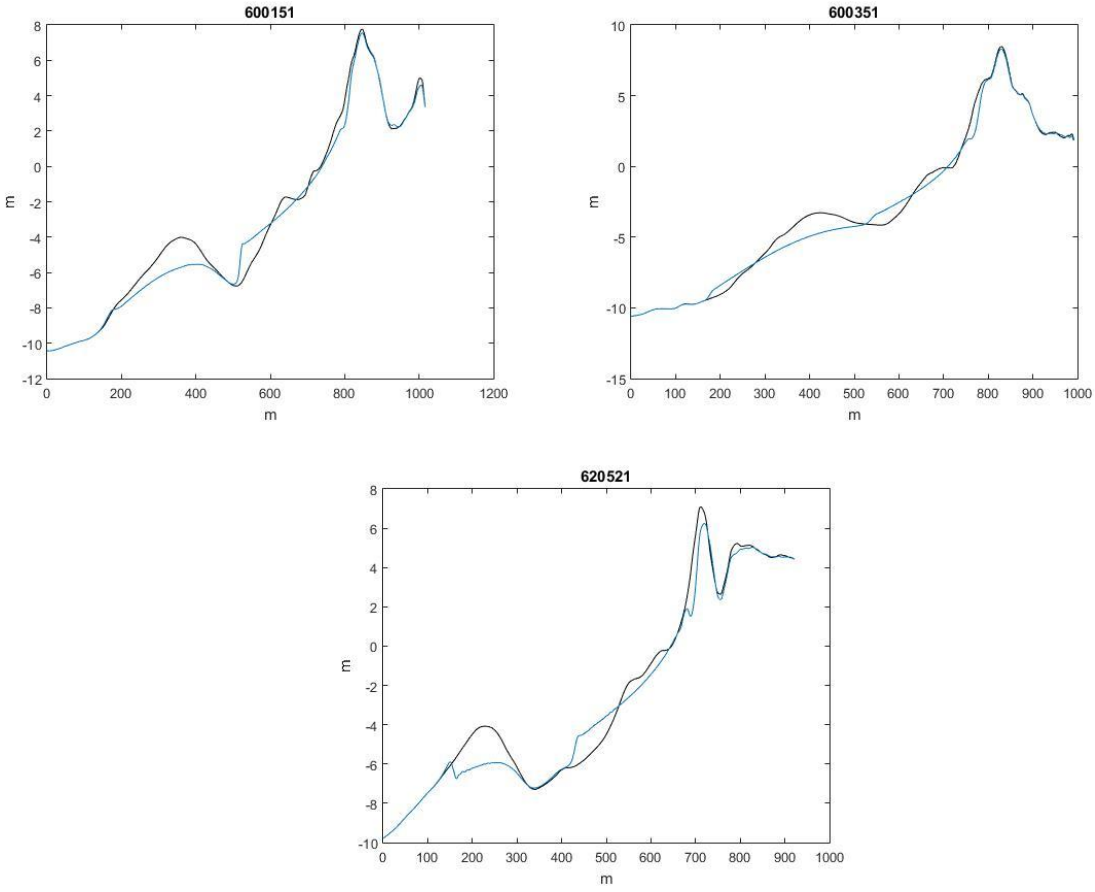

A1. The rest trials of dune NPFs during October 20th, 2012 to October 31th, 2012, the black line is the original profile, the blue line is the model results after Sandy.

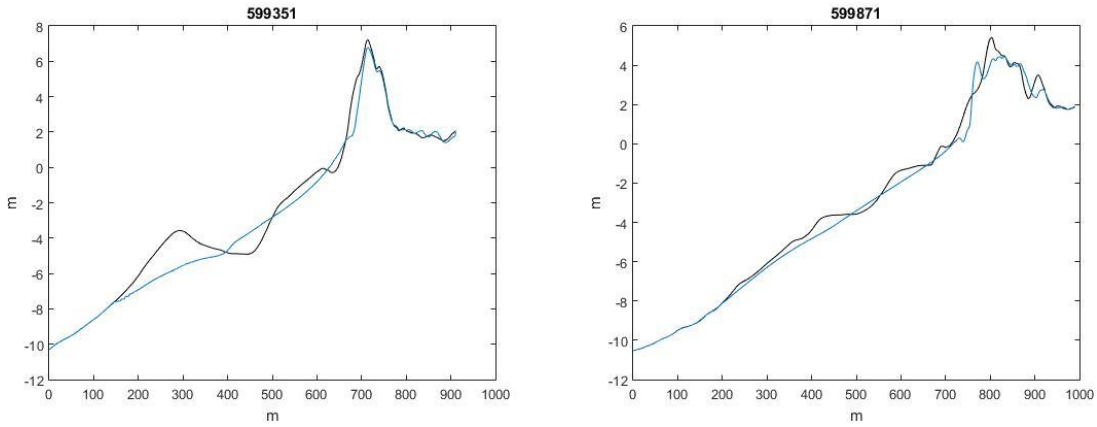

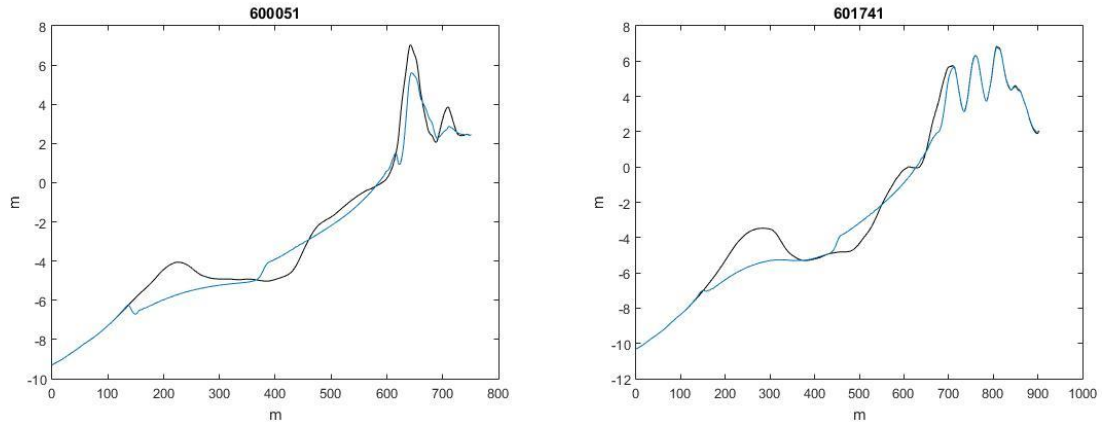

A2. The rest trials of multiple dunes NPFs during October 20th, 2012 to October 31th, 2012, the blue line is the model results after Sandy.

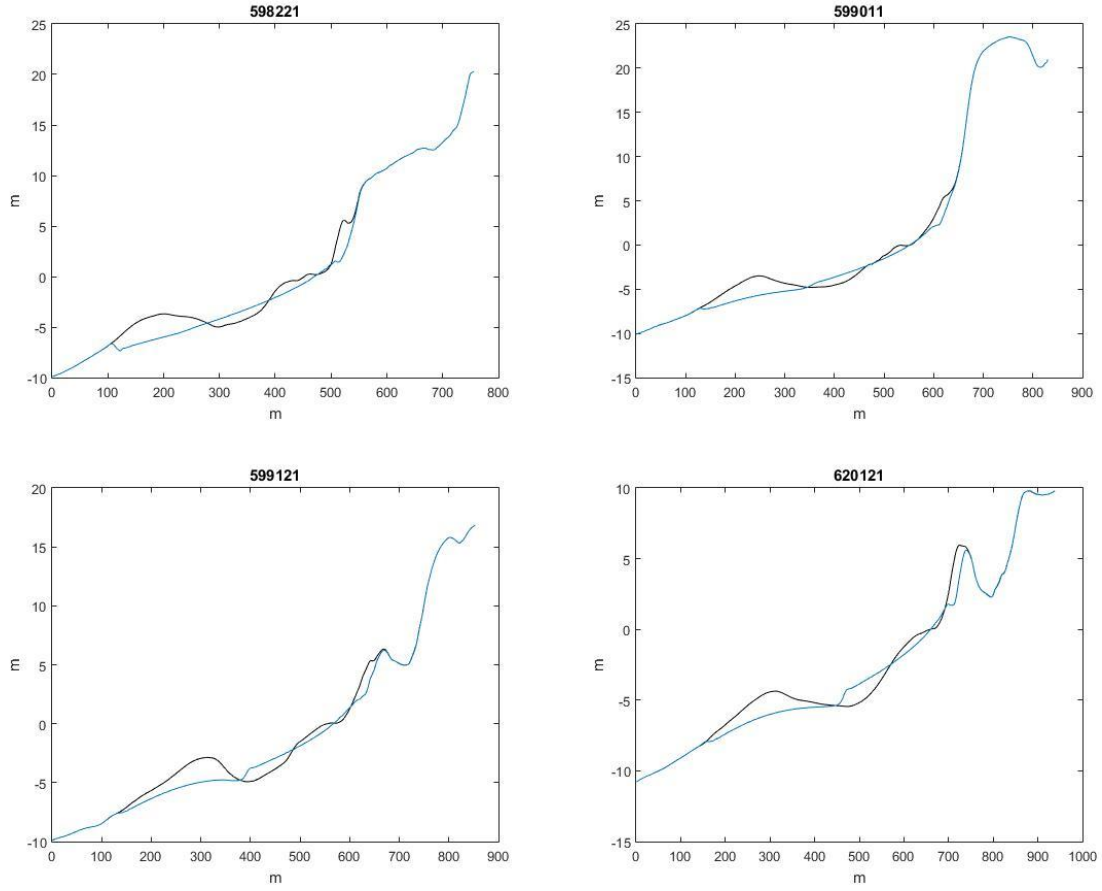

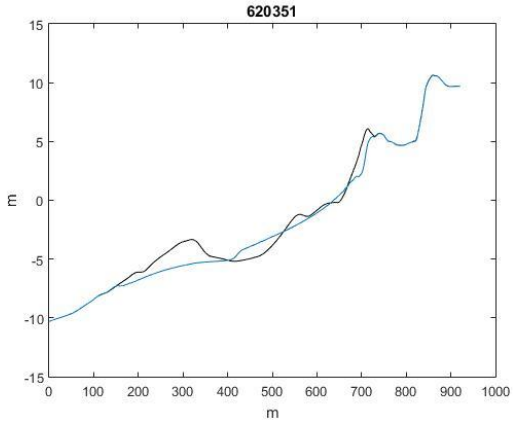

A3. The rest trials of dune in front of bluff NPFs during October 20th, 2012 to October 31th, 2012, the blue line is the model results after Sandy.

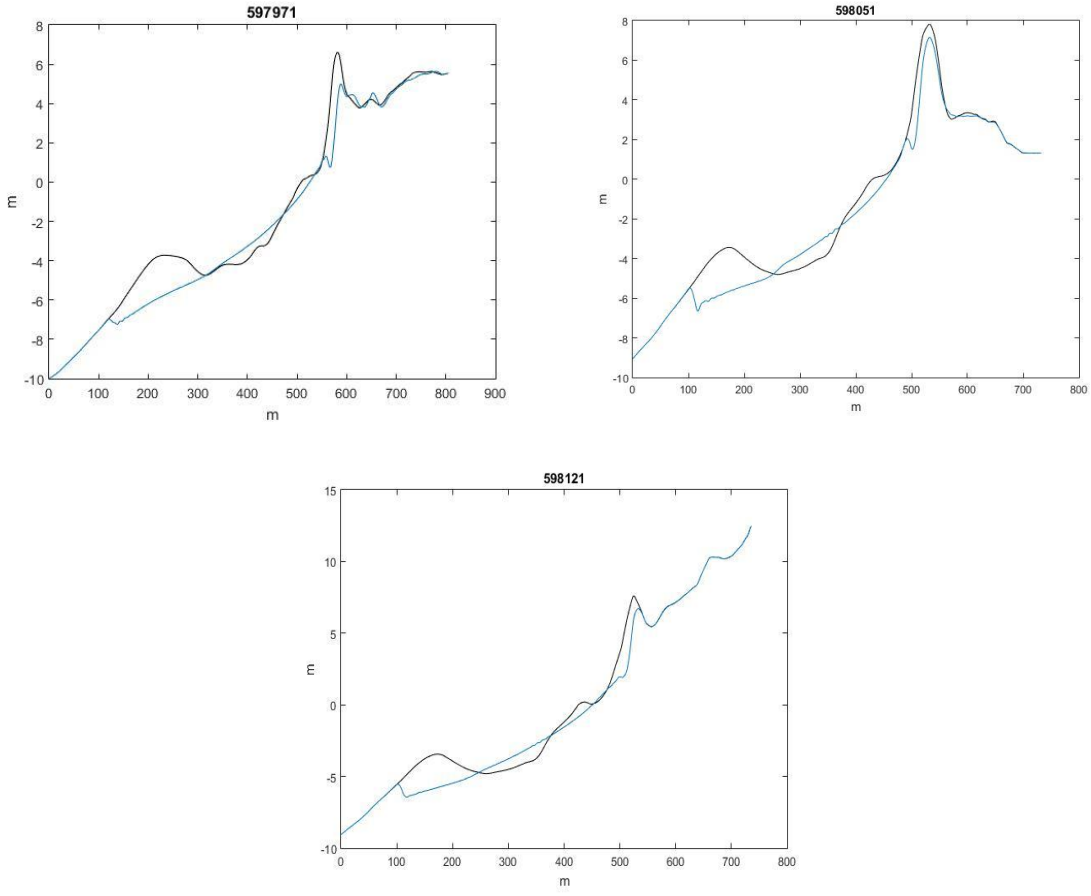

A4. The rest trials of dune on top of bluff NPFs during October 20th, 2012 to October 31th, 2012, the blue line is the model results after Sandy.

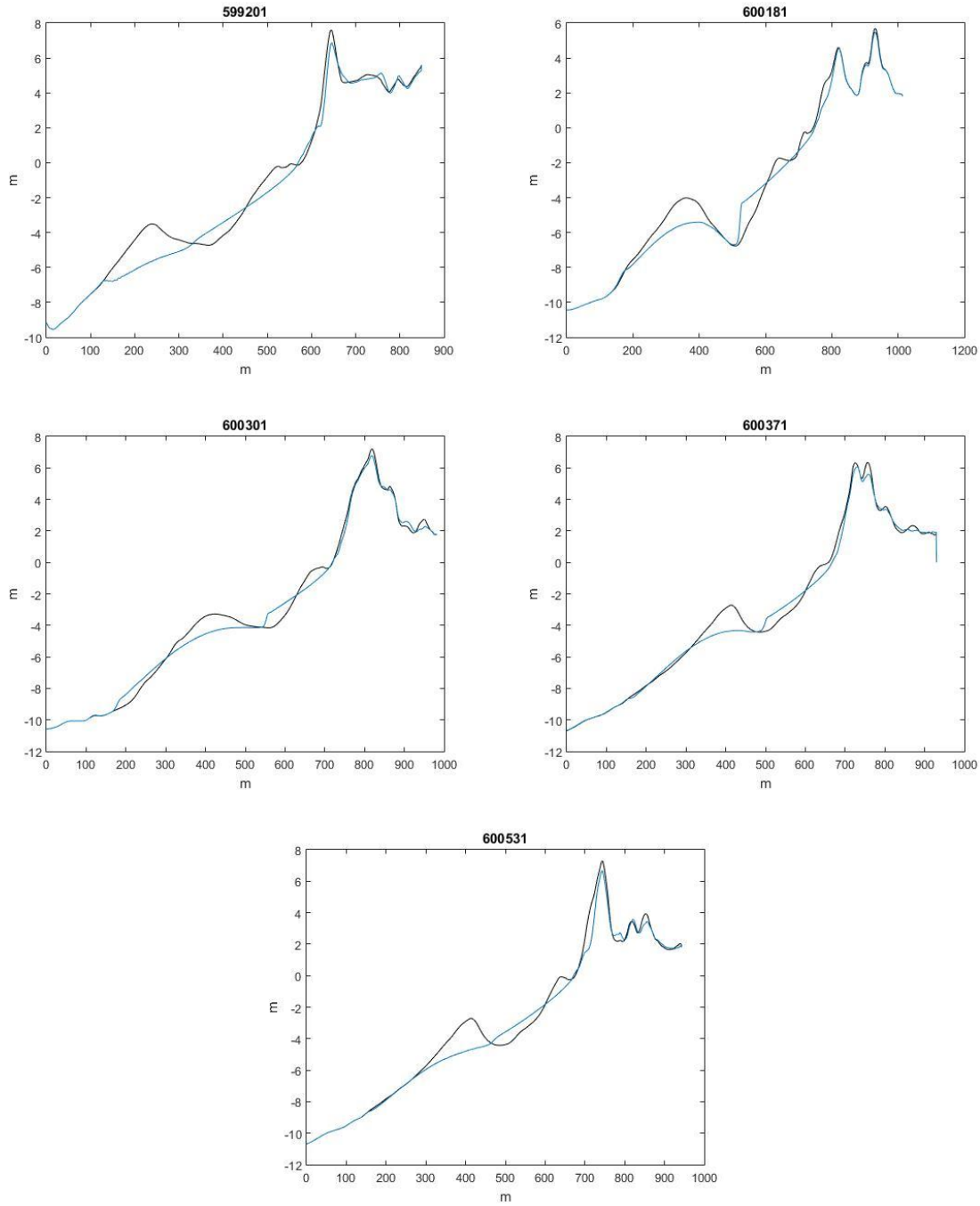

A5. The rest trials of dune NPFs during October 25th, 2012 to November 5th, 2012, the blue line is the model results after Sandy.

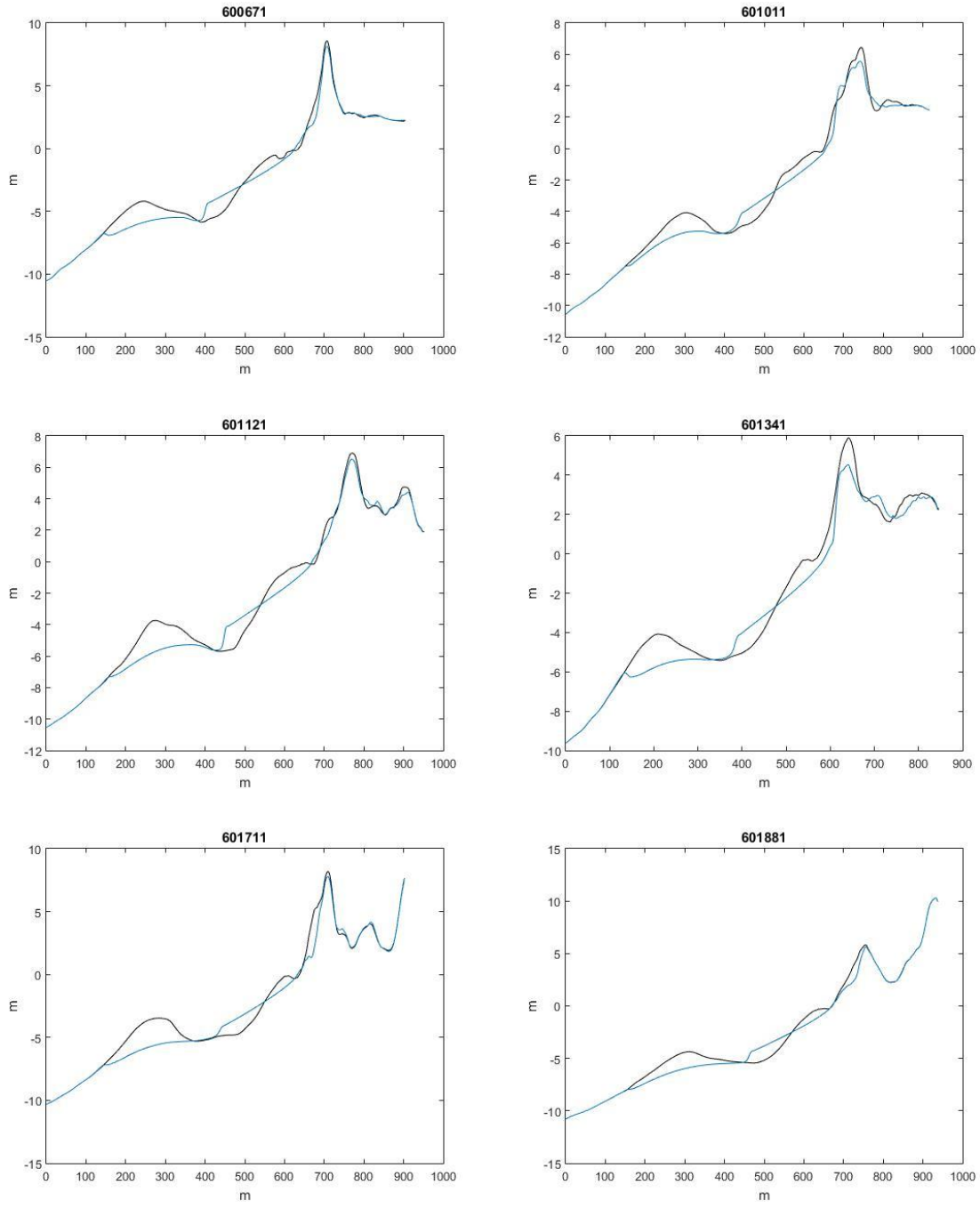

A6. The rest trials of dune NPFs during October 25th, 2012 to November 5th, 2012 continue, the blue line is the model results after Sandy.

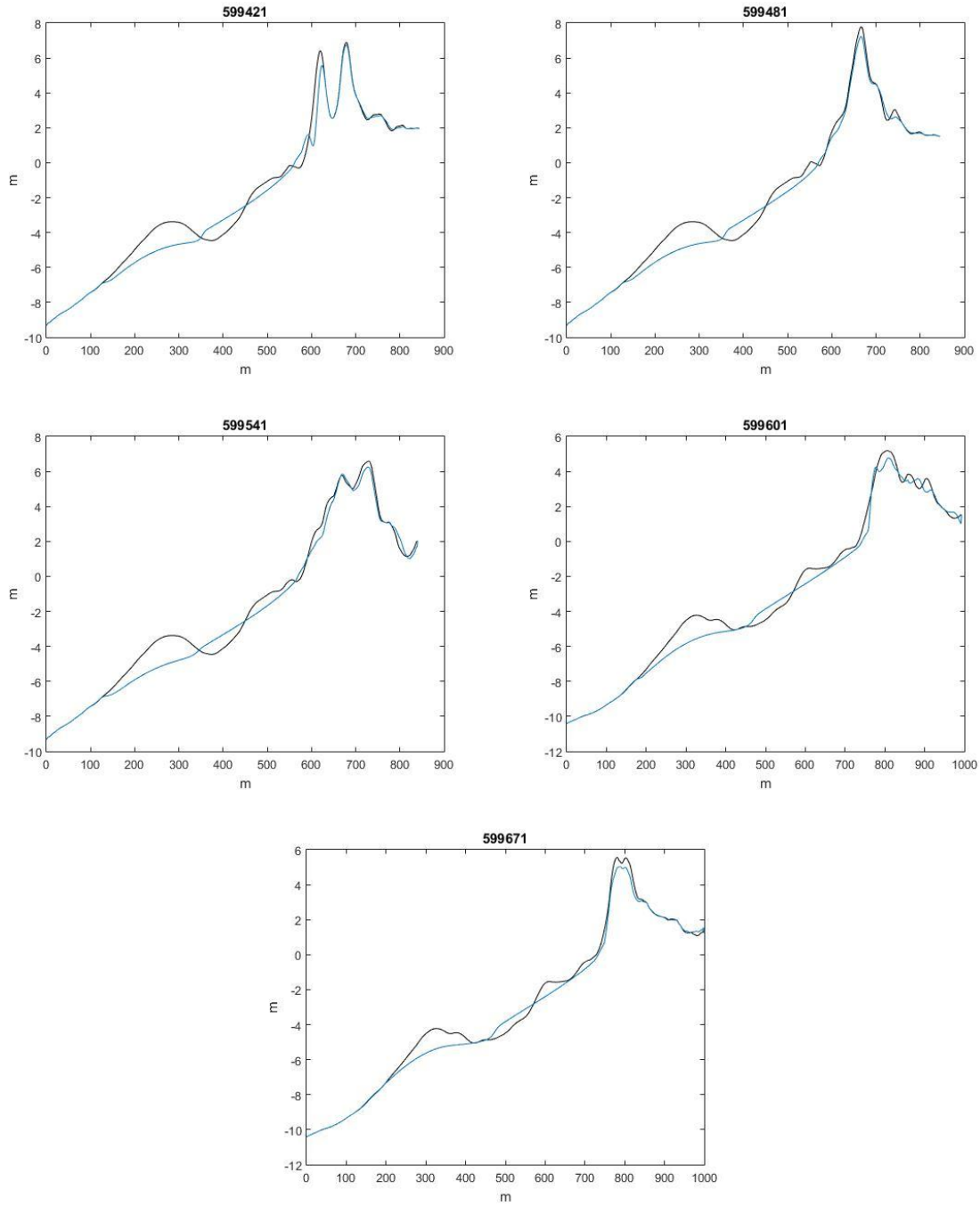

A7. The rest trials of multiple dunes NPFs during October 25th, 2012 to November 5th, 2012, the blue line is the model results after Sandy.

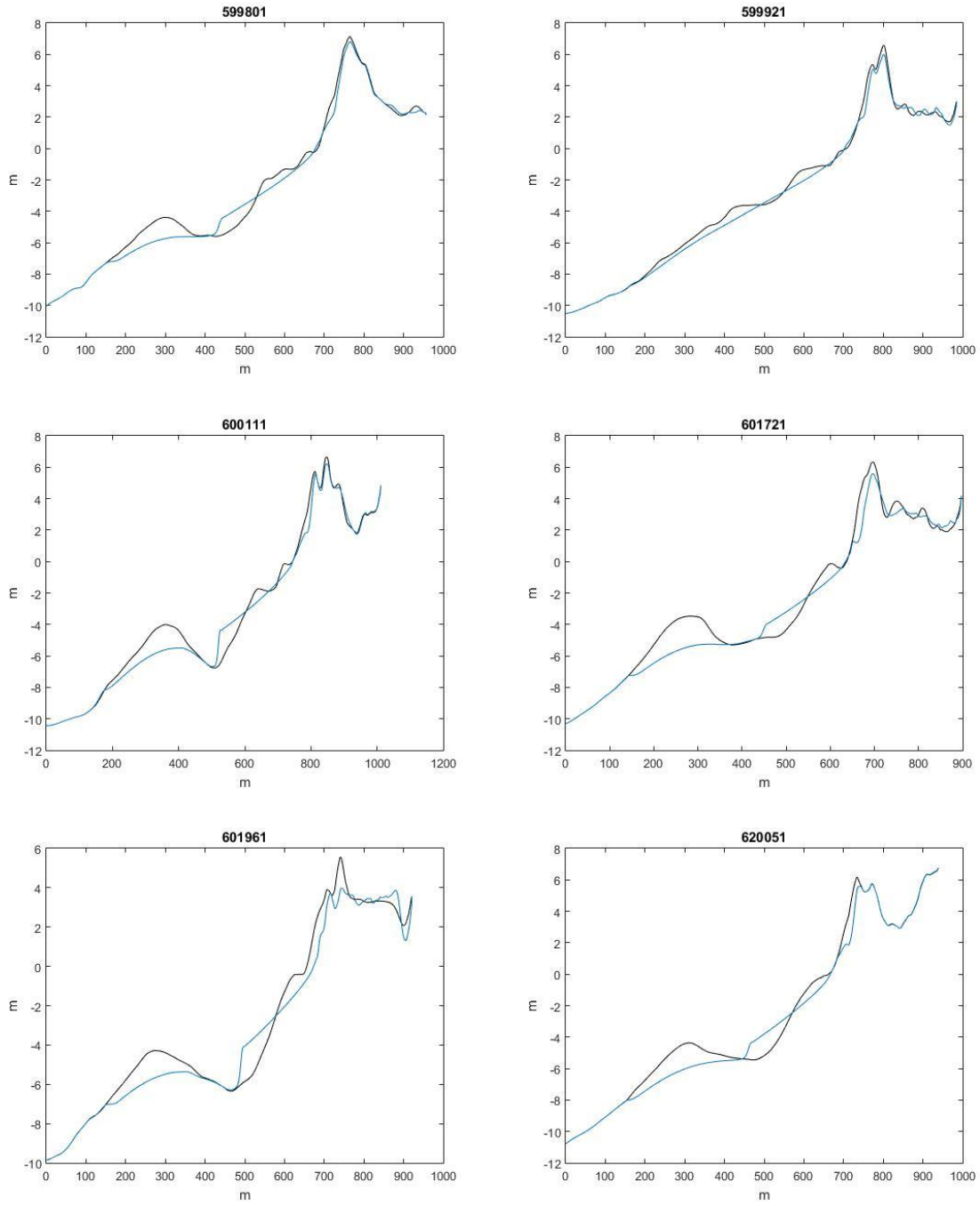

A8. The rest trials of multiple dunes NPFs during October 25th, 2012 to November 5th, 2012 continue, the blue line is the model results after Sandy.

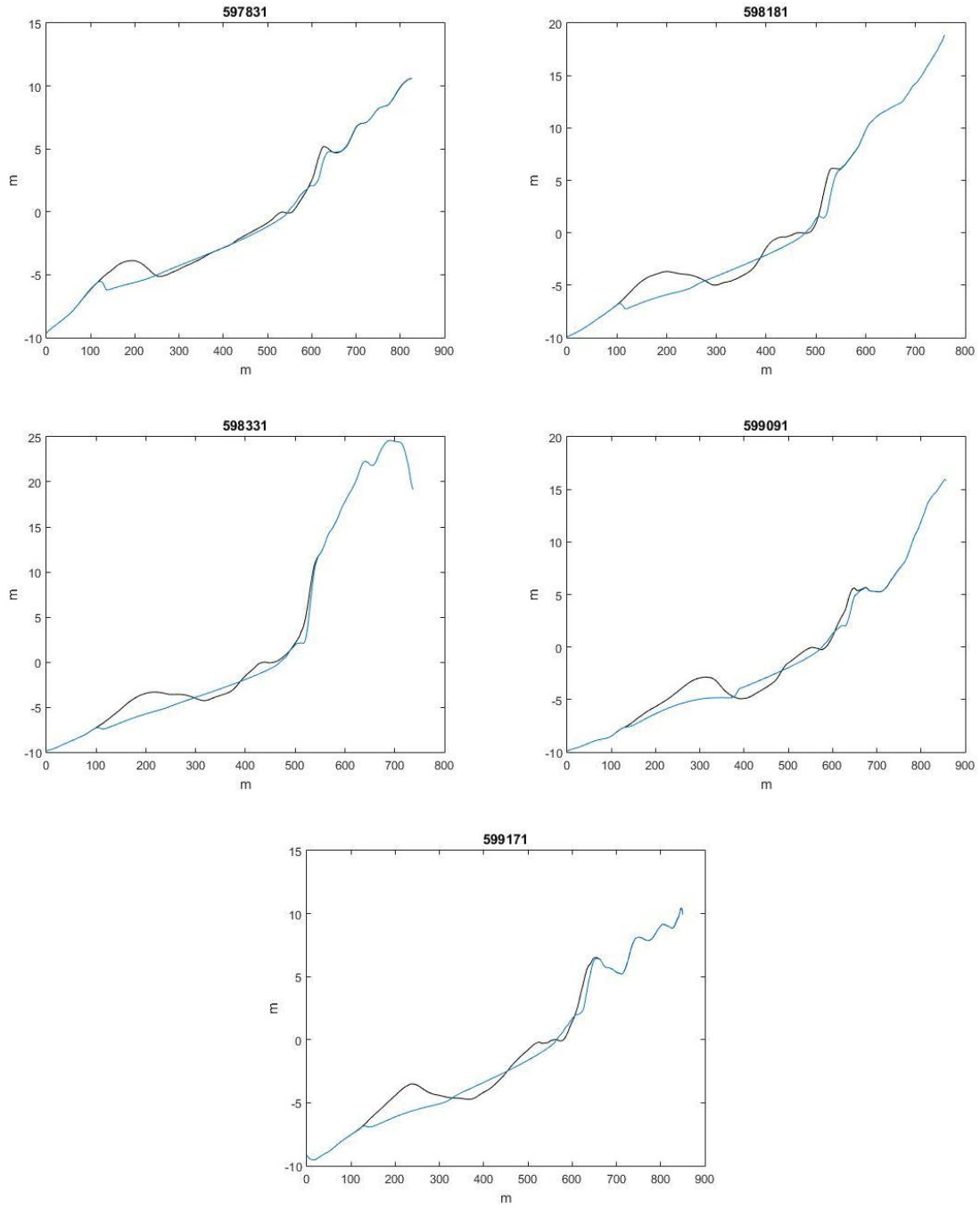

A9. The rest trials of dune in front of bluff NPFs during October 25th, 2012 to November 5th, 2012, the blue line is the model results after Sandy.

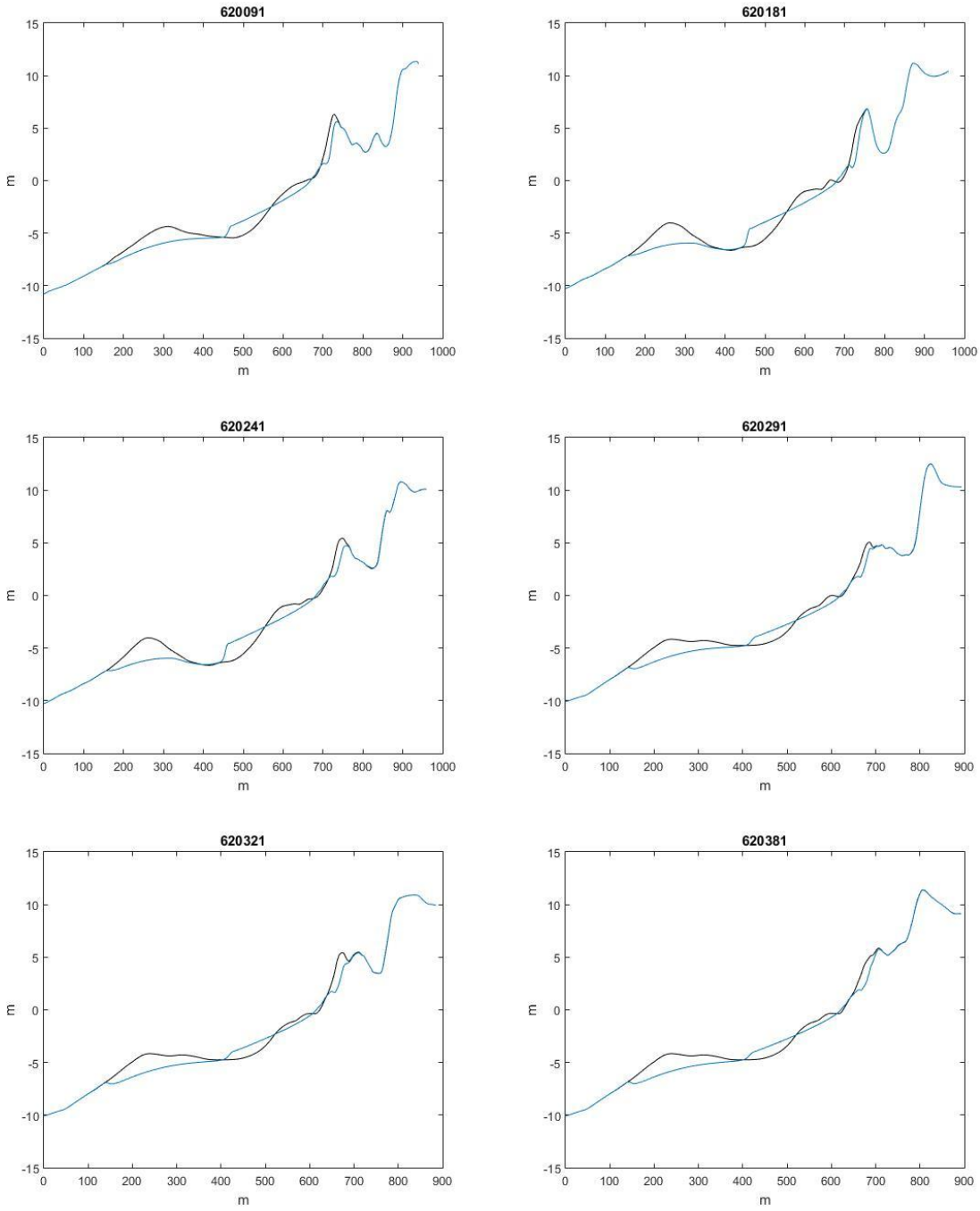

A10. The rest trials of dune in front of bluff NPFs during October 25th, 2012 to November 5th, 2012 continue, the blue line is the model results after Sandy.

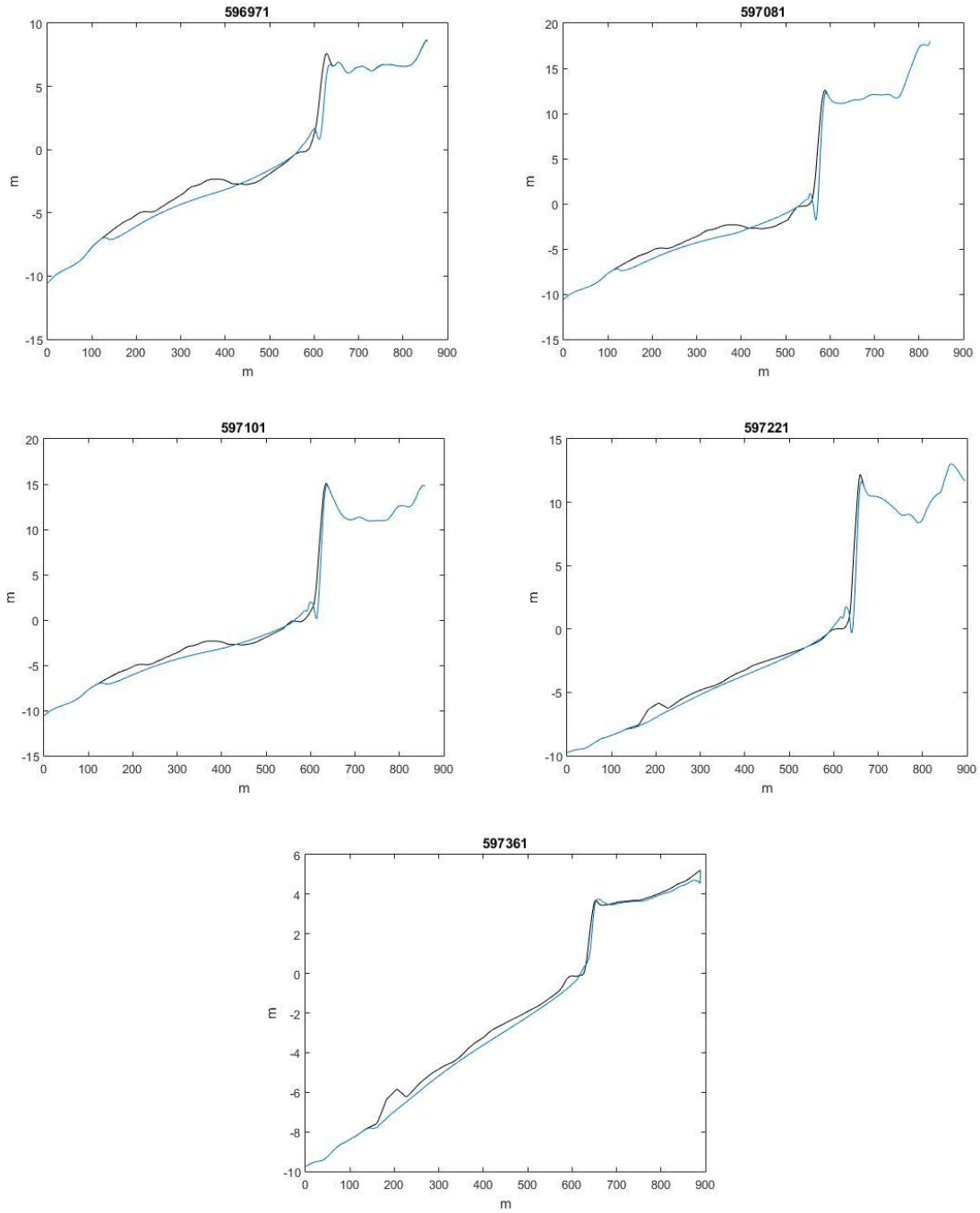

A11. The rest trials of dune on top of bluff NPFs during October 25th, 2012 to November 5th, 2012, the blue line is the model results after Sandy.

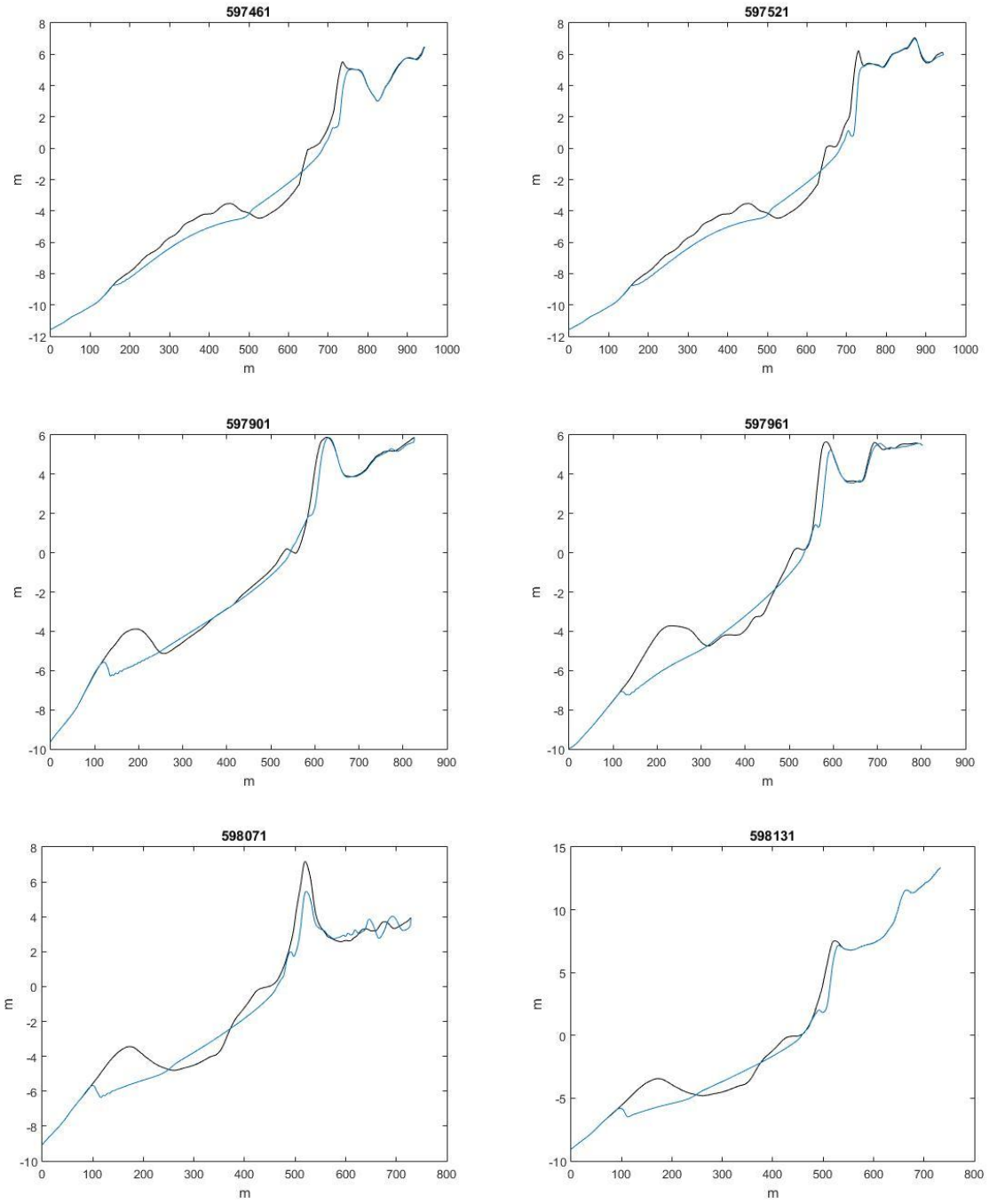

A11. The rest trials of dune on top of bluff NPFs during October 25th, 2012 to November 5th, 2012 continue, the blue line is the model results after Sandy.

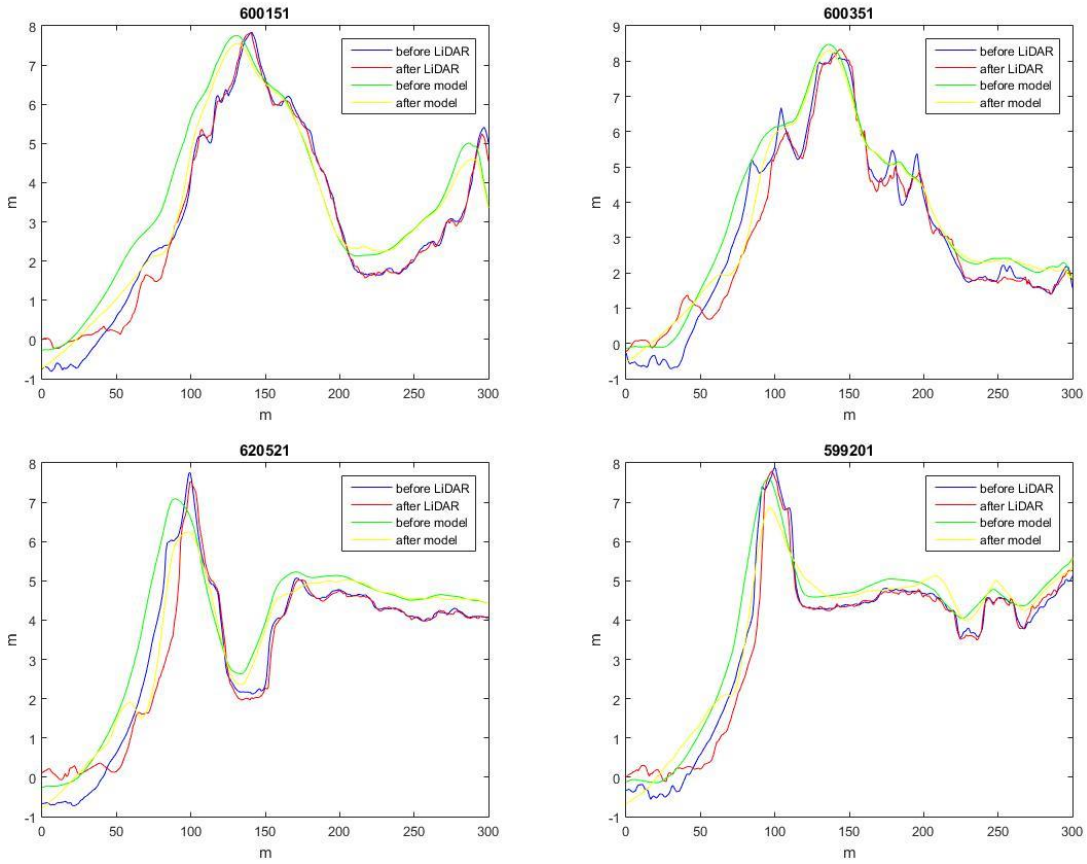

A12. The rest trials of sand lost comparison in dune NPFs, model results are green and yellow line before and after Sandy, LiDAR data are blue and red line before and after Sandy.

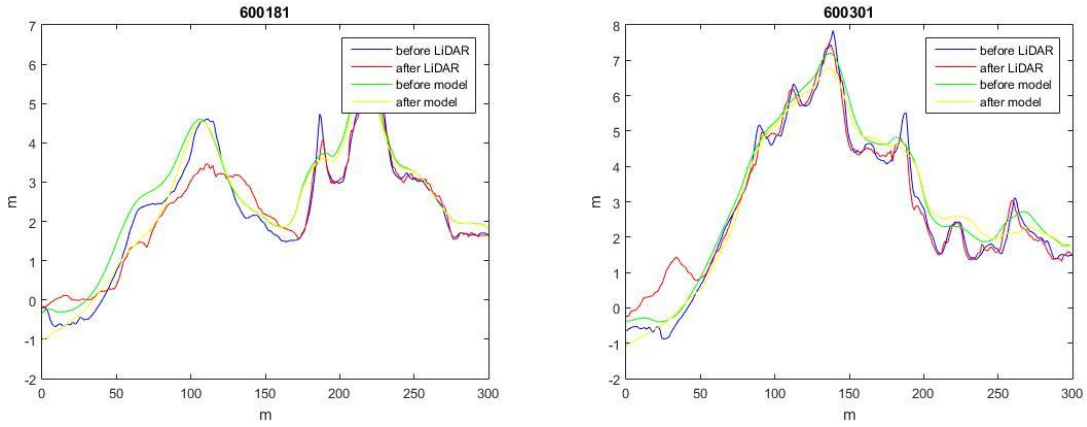

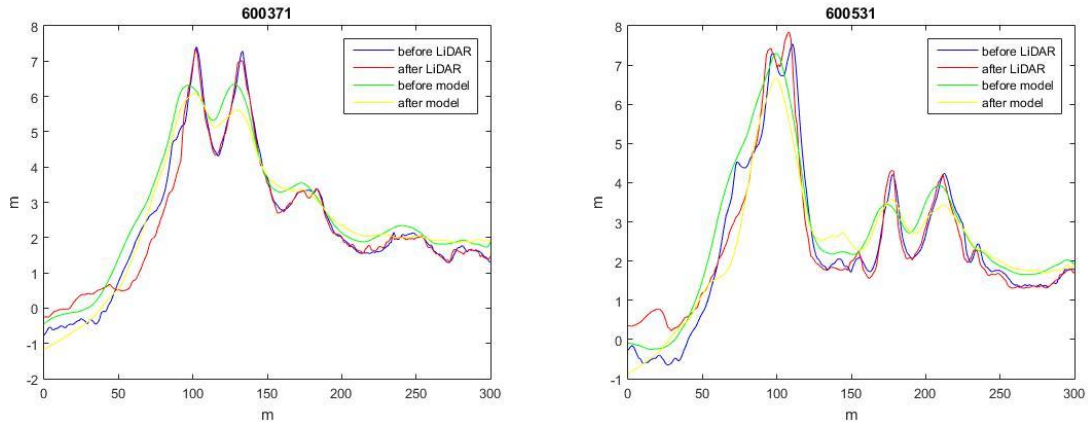

A13. The rest trials of sand lost comparison in dune NPFs continue 1, model results are green and yellow line before and after Sandy, LiDAR data are blue and red line before and after Sandy.

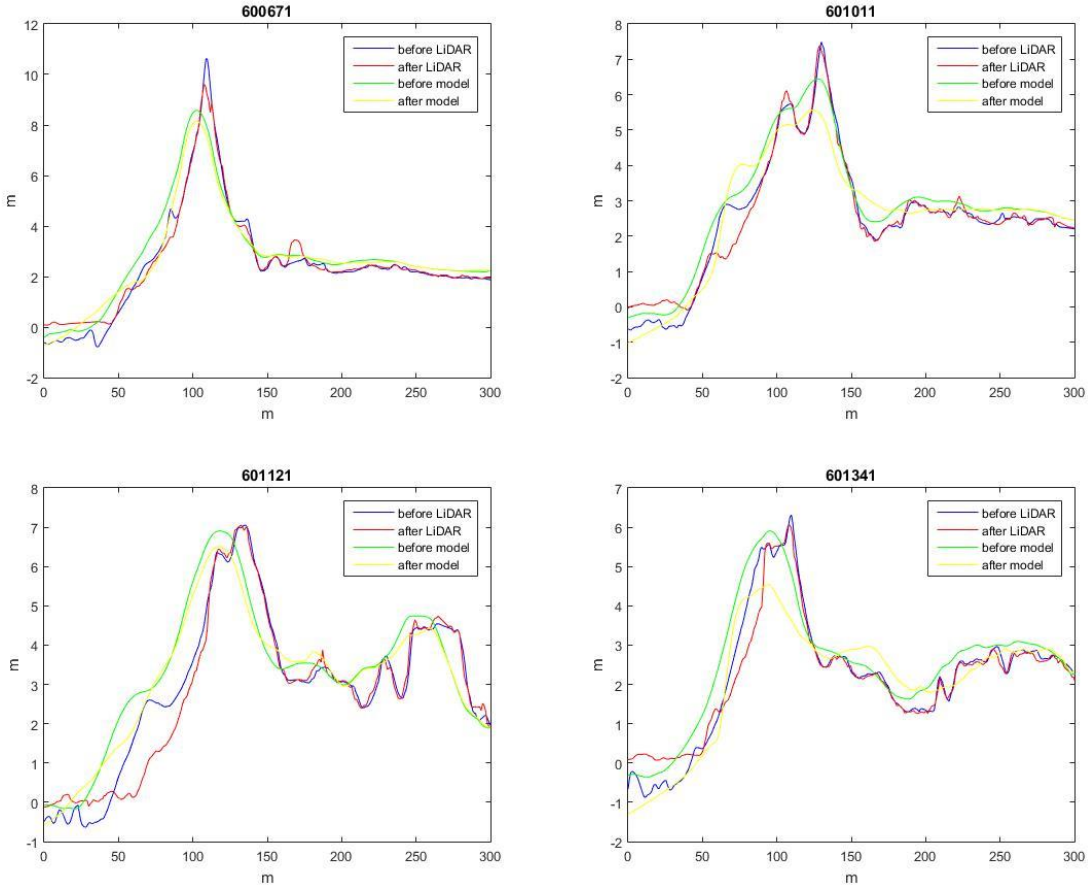

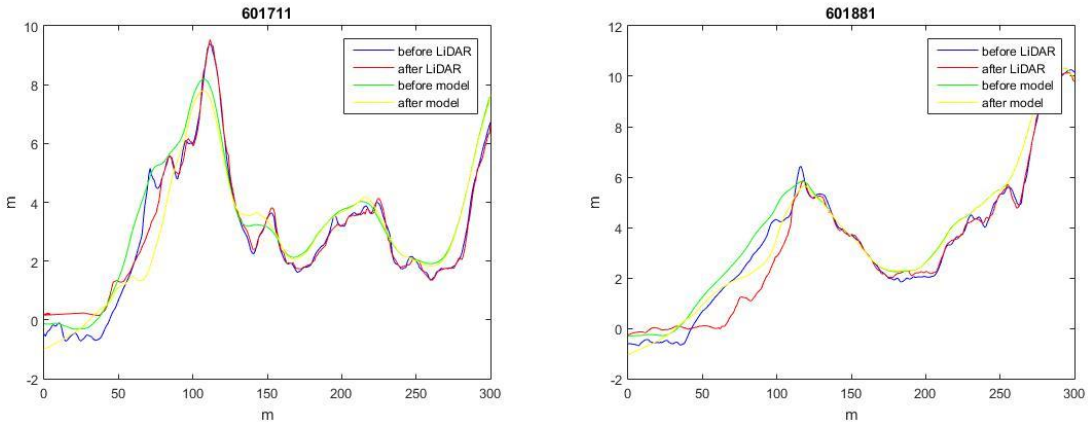

A14. The rest trials of sand lost comparison in dune NPFs continue 2, model results are green and yellow line before and after Sandy, LiDAR data are blue and red line before and after Sandy.

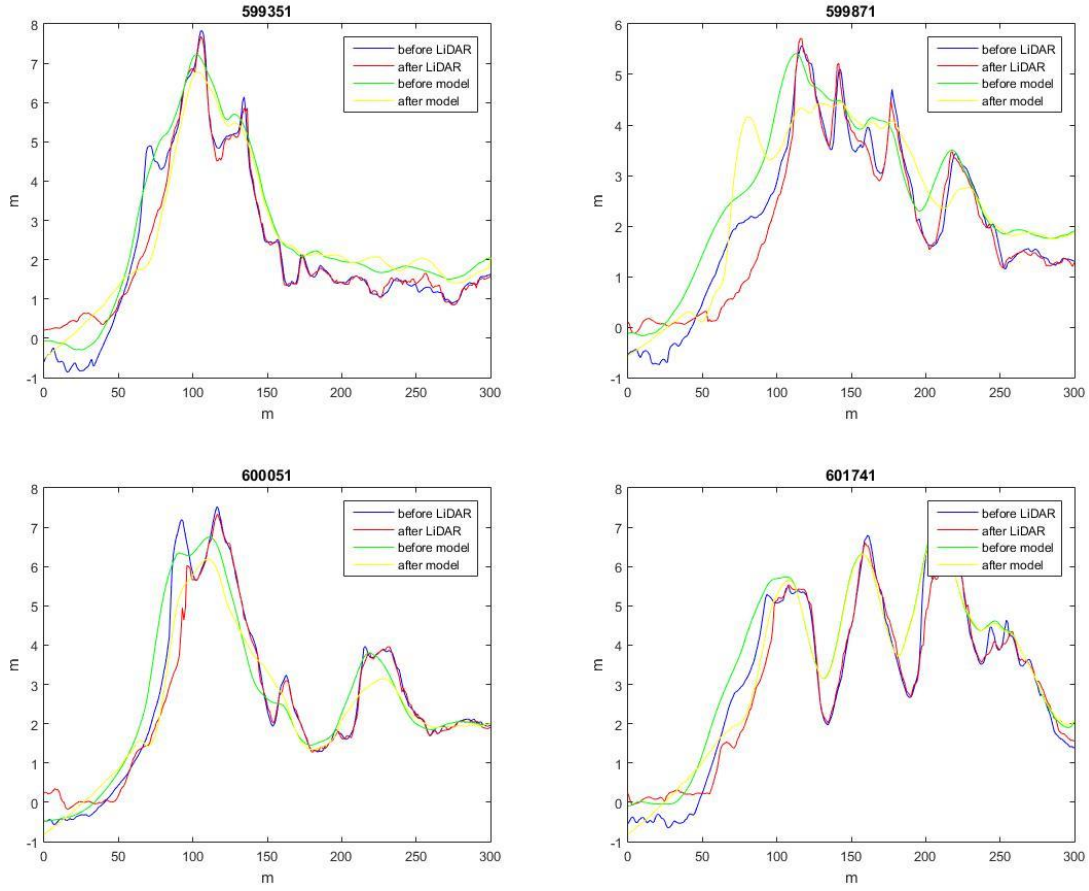

A15. The rest trials of sand lost comparison in multiple dunes NPFs, model results are green and yellow line before and after Sandy, LiDAR data are blue and red line before and after Sandy.

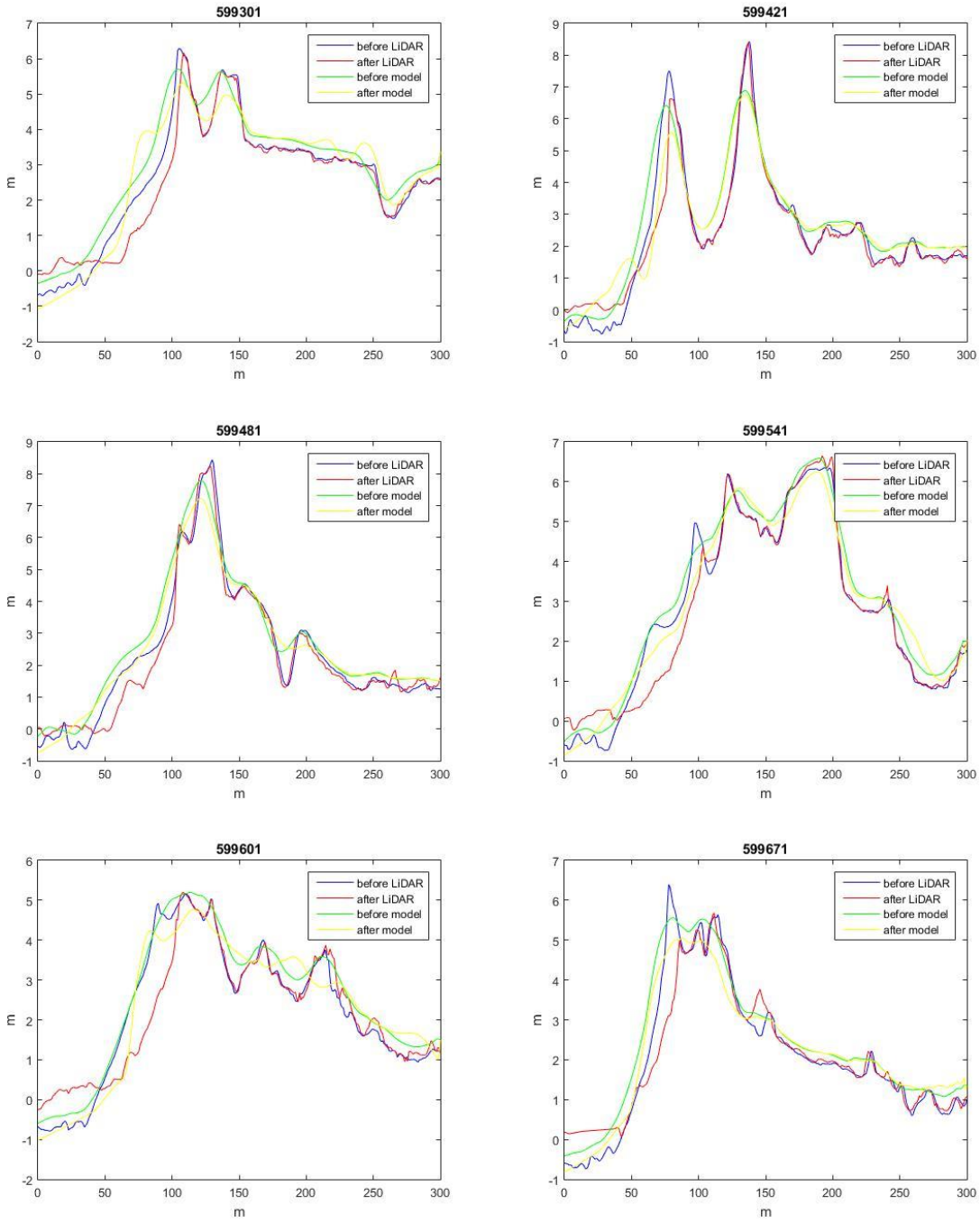

A16. The rest trials of sand lost comparison in multiple dunes NPFs continue 1, model results are green and yellow line before and after Sandy, LiDAR data are blue and red line before and after Sandy.

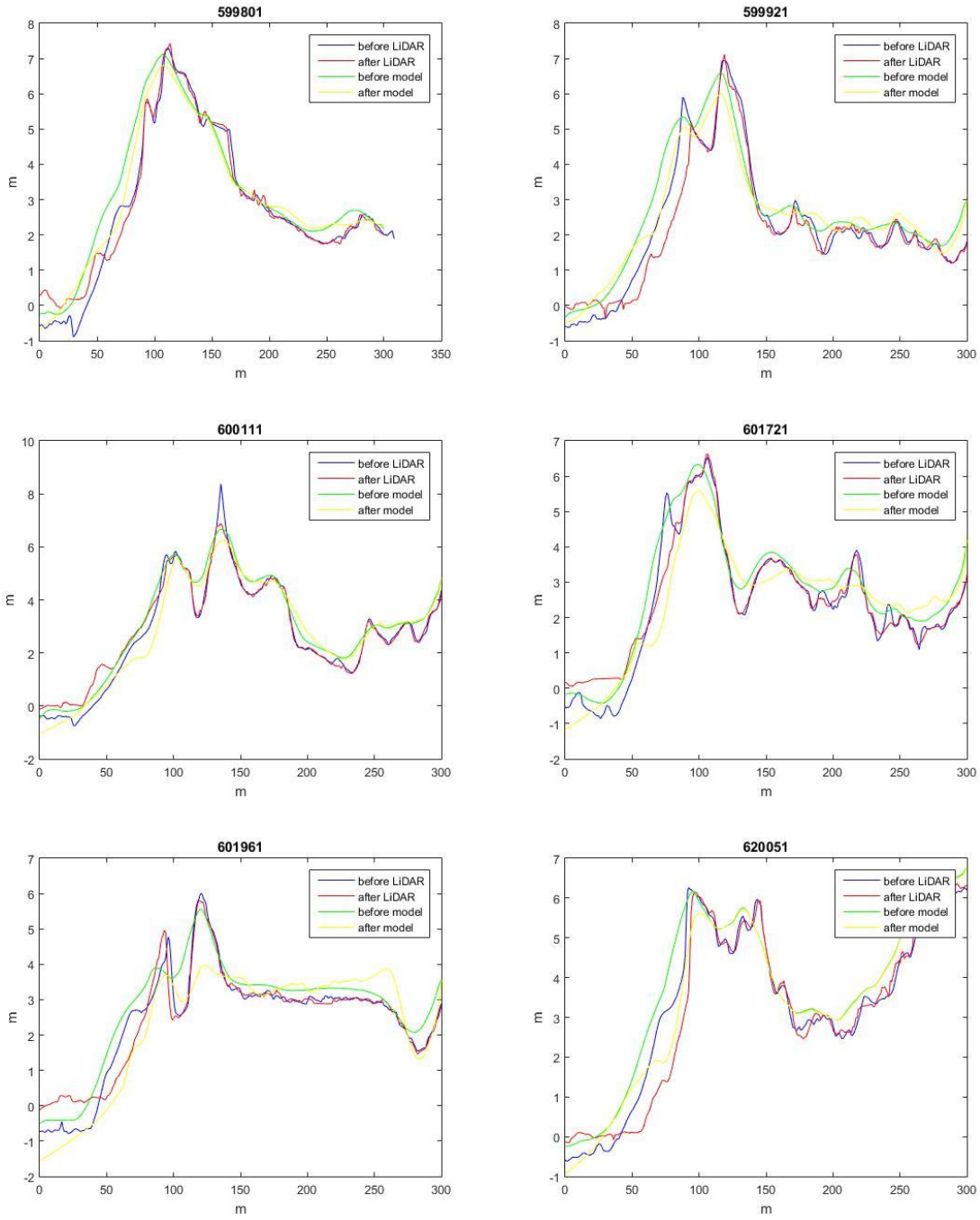

A17. The rest trials of sand lost comparison in multiple dunes NPFs continue 2, model results are green and yellow line before and after Sandy, LiDAR data are blue and red line before and after Sandy.

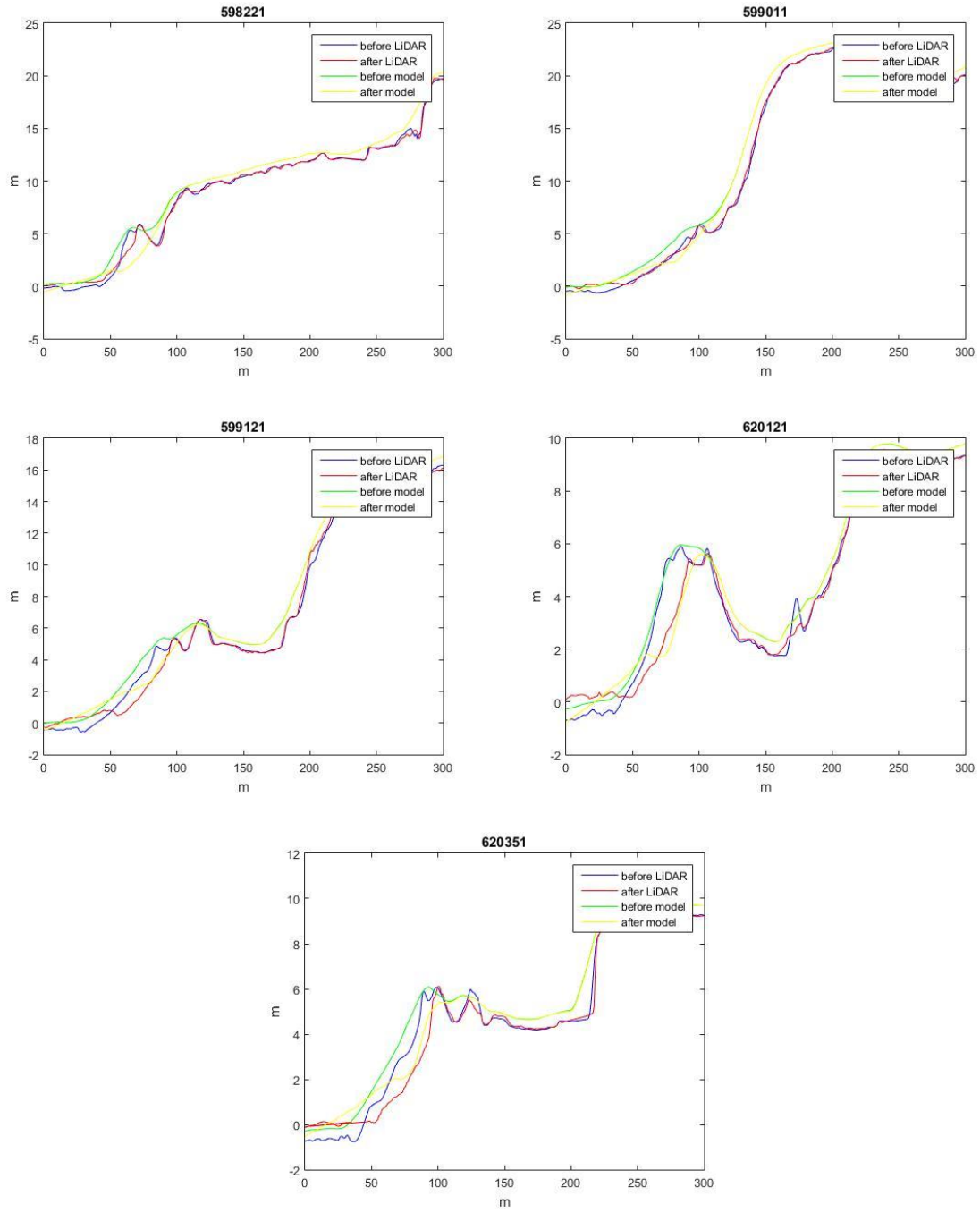

A18. The rest sand lost comparison in dune in front of bluff NPFs, model results are green and yellow line before and after Sandy, LiDAR data are blue and red line before and after Sandy.

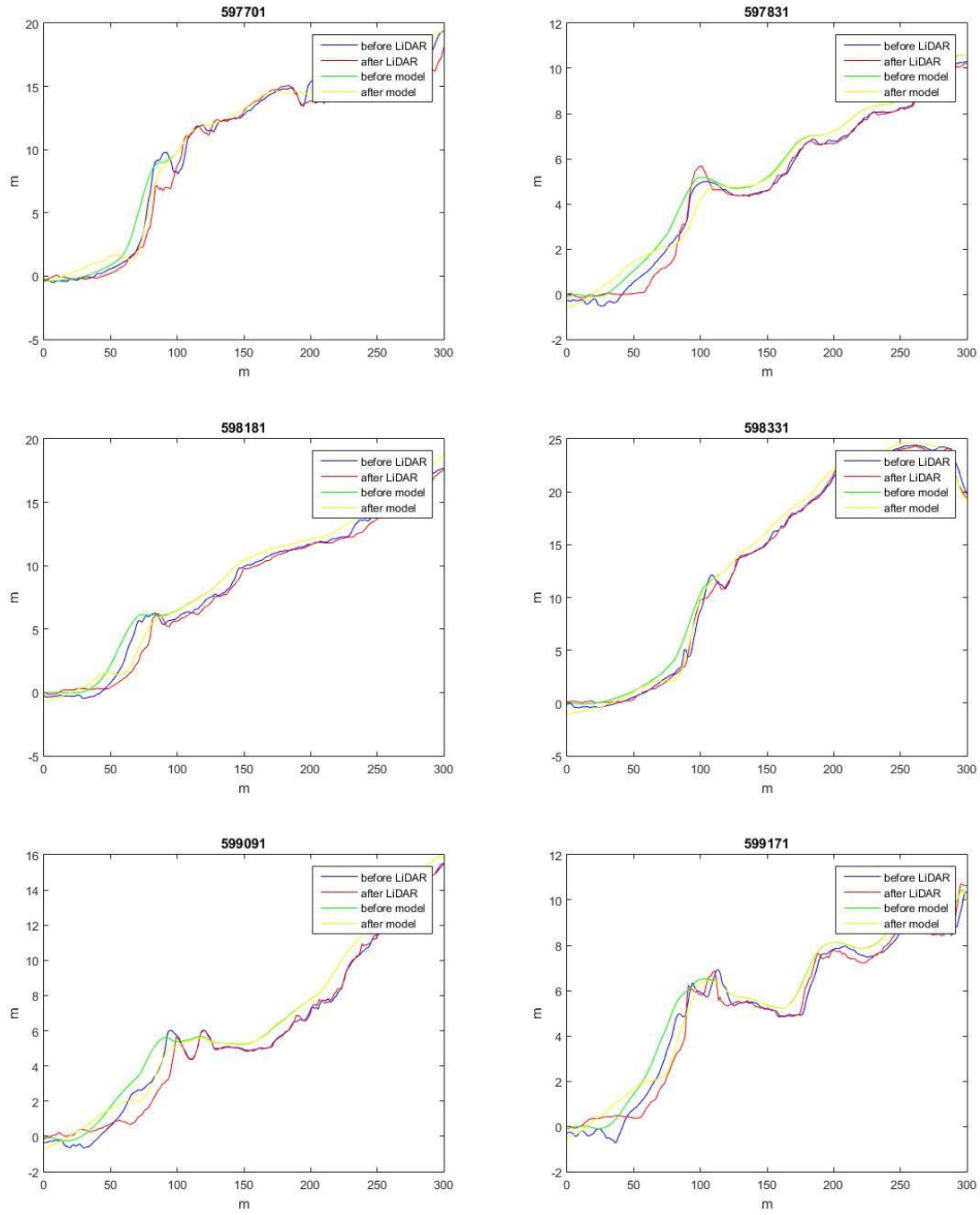

A19. The rest trials of sand lost comparison in dune in front of bluff NPFs continue 1, model results are green and yellow line before and after Sandy, LiDAR data are blue and red line before and after Sandy.

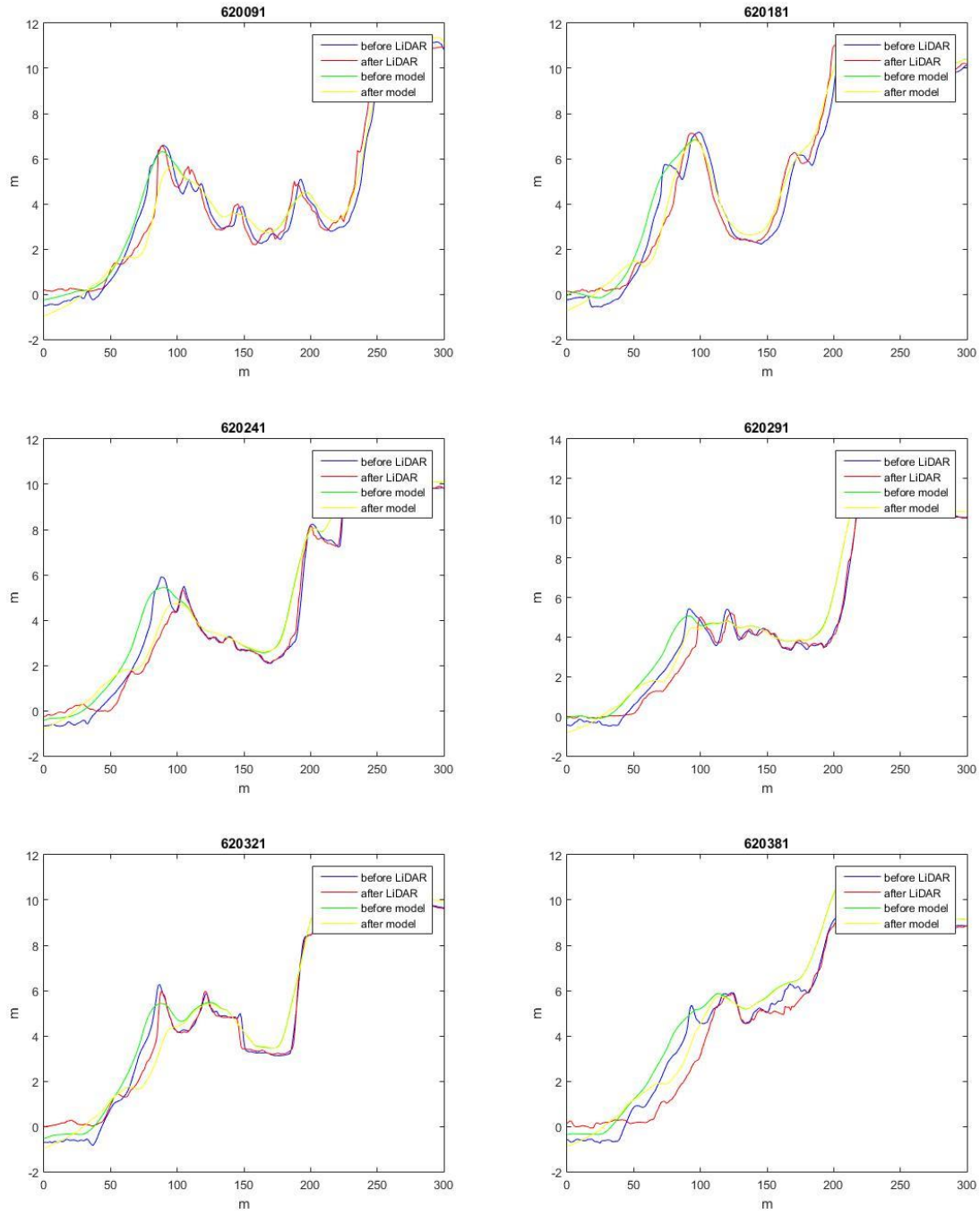

A20. The rest trials of sand lost comparison in dune in front of bluff NPFs continue 2, model results are green and yellow line before and after Sandy, LiDAR data are blue and red line before and after Sandy.

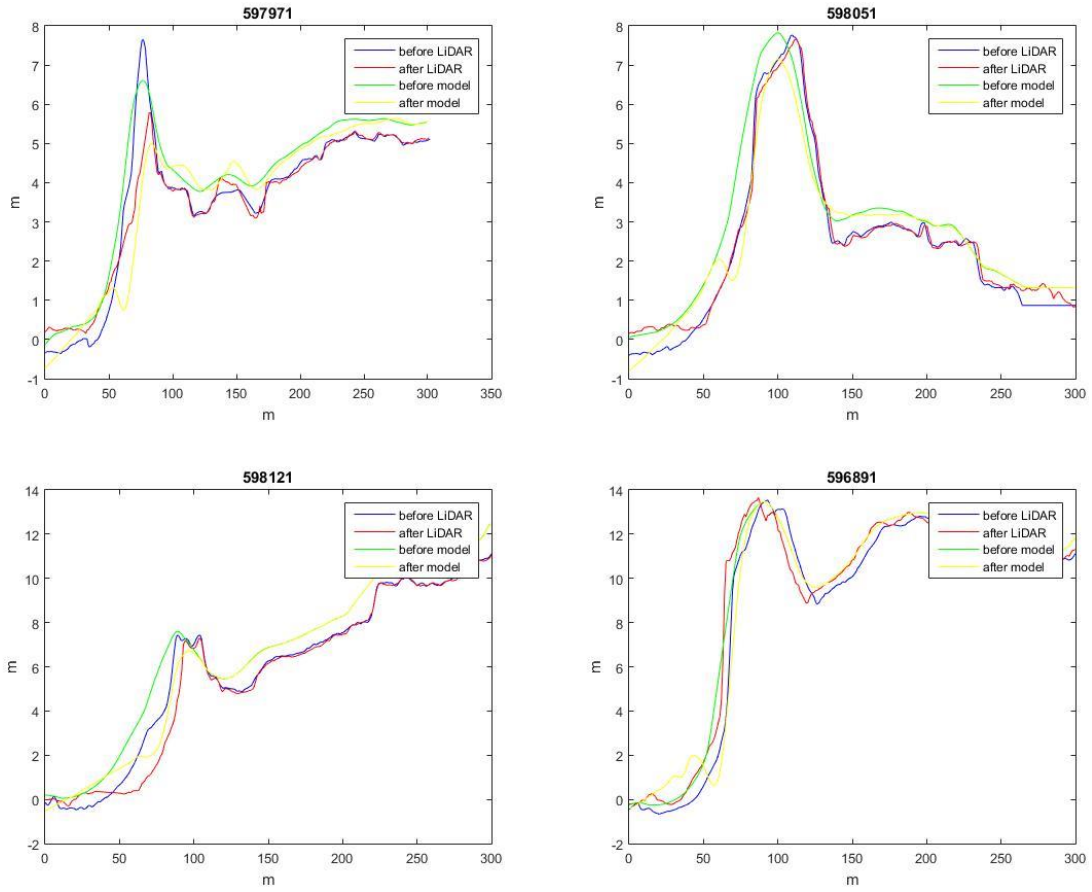

A21. The rest trials of sand lost comparison in dune on top of bluff NPFs, model results are green and yellow line before and after Sandy, LiDAR data are blue and red line before and after Sandy.

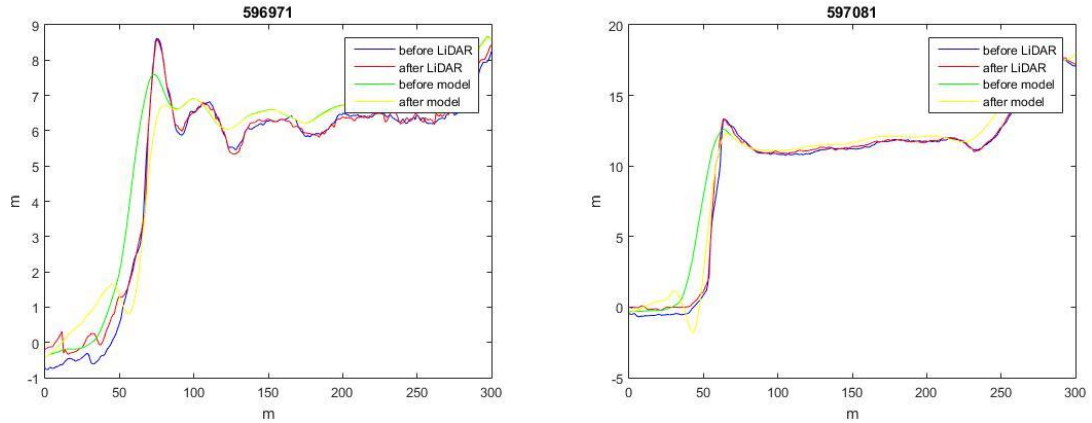

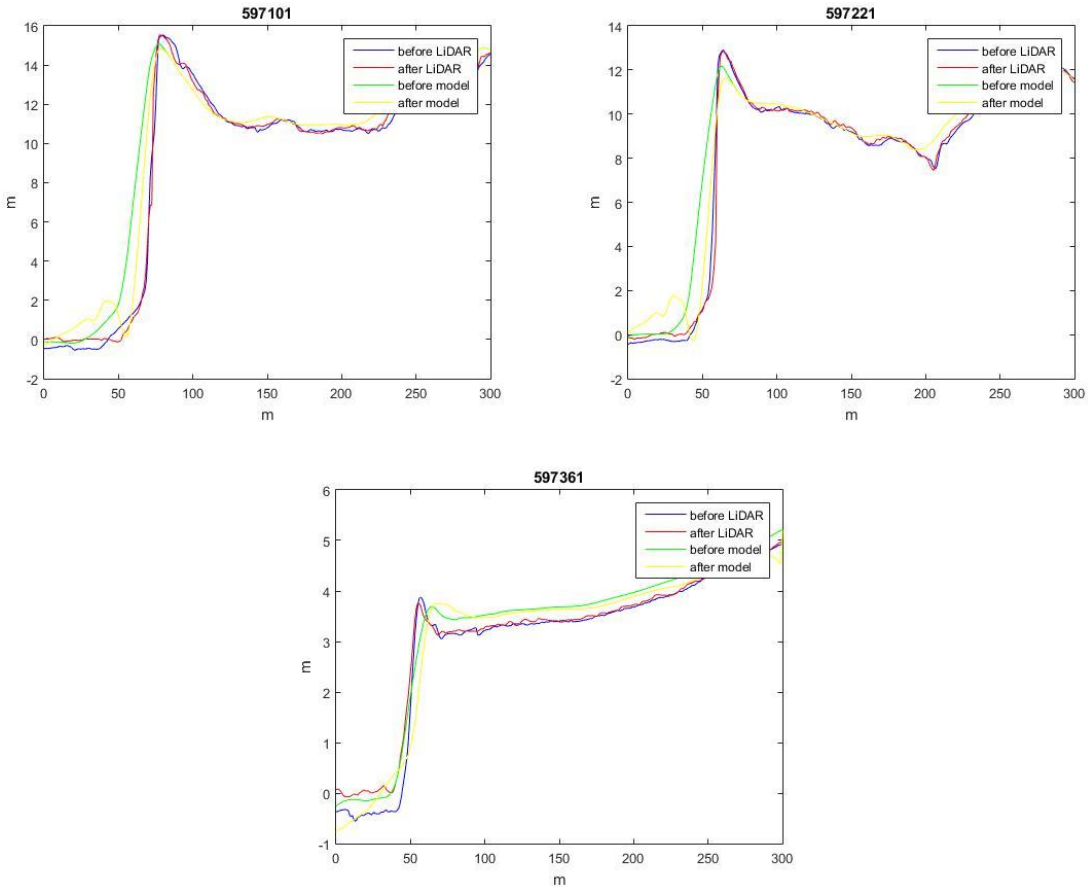

A22. The rest trials of sand lost comparison in dune on top of bluff NPFs continue 1, model results are green and yellow line before and after Sandy, LiDAR data are blue and red line before and after Sandy.

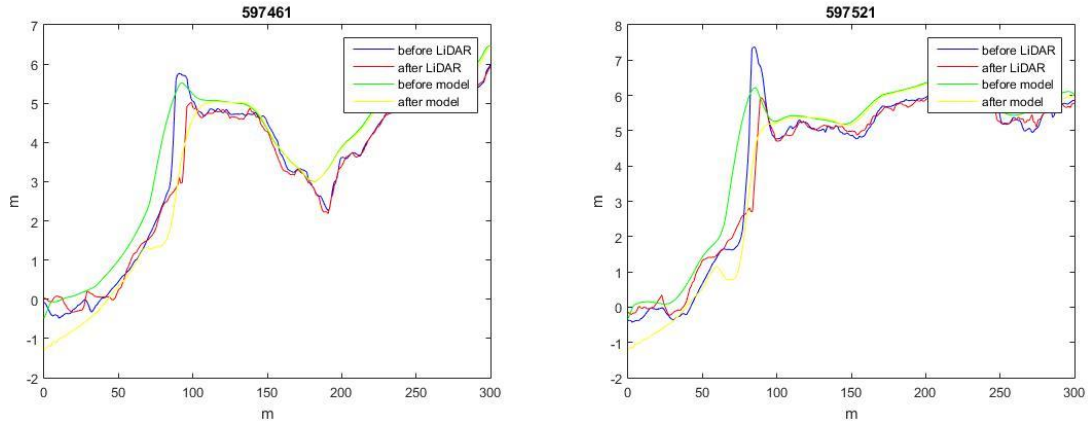

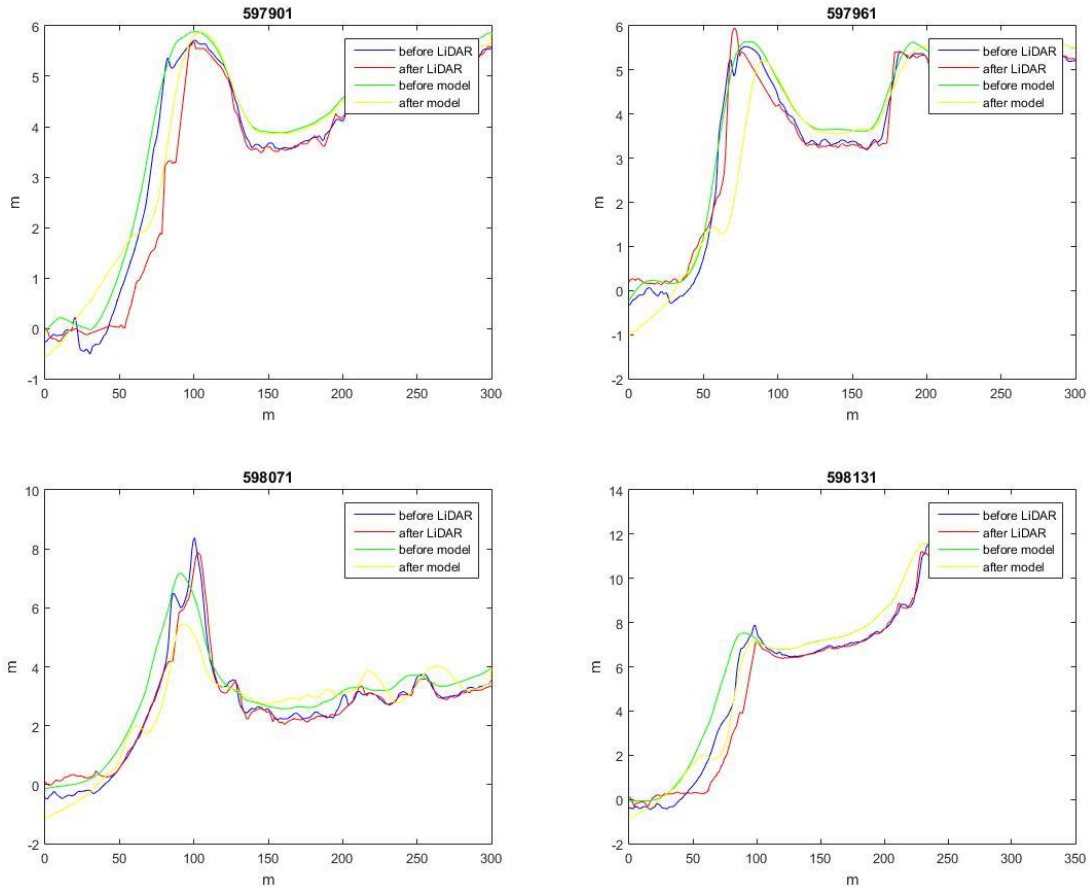

A23. The rest trials of sand lost comparison in dune on top of bluff NPFs continue 2, model results are green and yellow line before and after Sandy, LiDAR data are blue and red line before and after Sandy.

Appendix B. Tables

Time	Comments
Fall 1995	the color is too bright to draw the HWL
Fall 1996	check, 03_269, 271, 273, 275,277 big waves
Fall 1997	the color is strange, someplace is too bright
Fall 1998	the color is strange, do have some cusps
Fall 1999	check, fewer cusps compare to spring.
Fall 2000	check, near Montauk point, fewer land
Fall 2001	check
Fall 2003	too close to 2004
Spring 1995	check
Spring 1996	check, some is too bright
Spring 1997	check, strange color
Spring 1998	the color is strange, some are too bright
Spring 1999	check, many cusps
Spring 2000	check
Spring 2001	check, cusp
Spring 2002	too close to 2004
Spring 2003	too close to 2004
Spring 2005	too close to 2004

B1. New aerial photo checklist.

Number	Image ID	1st Order Polynomial	2nd Order Polynomial	3rd Order Polynomial
1	08-001	31.55	14.78	2.69
2	08-002	15.15	7.11	0.73
3	08-004	21.83	7.55	1.67
4	08-006	11.59	9.06	1.91
5	08-008	24.48	8.02	1.18
6	08-009	15.00	5.72	1.44
7	08-010	22.28	10.84	1.86
8	08-013	17.61	9.41	1.37
9	08-015	12.90	7.14	2.44
10	08-017	8.96	3.27	1.58
11	08-019	11.50	4.04	2.54
12	08-021	5.56	2.07	0.83
13	08-023	13.58	8.60	1.13
14	08-025	6.45	4.19	0.84
15	08-027	4.89	2.72	1.85
16	08-028	12.04	4.53	3.76
17	08-029	4.63	3.63	1.10
18	08-030	5.88	3.50	1.05
19	08-031	9.17	3.90	1.93
20	08-034	11.90	2.42	1.19
21	08-036	9.26	3.37	1.54
22	08-038	22.27	2.21	0.67
23	09-007	11.65	10.78	4.06
24	09-008	11.31	7.86	1.14
25	09-010	12.02	7.84	2.27
Average		13.34	6.18	1.71

B2. Georeferencing error for 25 sets of comparison between historical pictures from 1999 and modern image from 2010, units are in meters.

	1		2		3		4		5		6		7		8		9		10	
1983	0	SE	1	SE	1	SE	1	SE	1	SE	1	SE	0	SE	0	SE	0	SE	0	SE
1995 spring	0	SE	0	SE	2	SE	0	SE	1	SE	1	SE	1	SE	0	SE	0	SE	0	SE
1995 fall	0	SW	0	SW	2	SW	1	SW	1	SW	1	SW	1	SW	0	SW	0	SW	0	SW
1996 spring	0	SE	1	SE	0	SE	0	SE	1	SE	1	SE	1	SE	0	SE	0	SE	0	SE
1996 fall	0	SE	0	SE	0	SE	1	SE	1	SW	1	SW	1	SW	1	SW	0	SW	0	SW
1997 spring	0	SE	1	SE	1	SE	1	SE	1	SE	1	SE	1	SE	0	SE	0	SE	0	SE
1997 fall	0	SE	1	SE	1	SE	1	SE	1	SE	1	SE	1	SE	1	SE	0	SE	0	SE
1998 spring	0	SE	0	SE	1	SE	1	SE	1	SE	1	SE	1	SE	0	SE	0	SE	0	SE
1998 fall	2	SE	1	SE	1	SE	2	SE	1	SE	0	SE	1	SE	0	SE	0	SE	0	SE
1999 spring	1	SW	1	SW	1	SW	1	SW	1	SW	1	SW	0	SW	0	SW	0	SW	0	SW
1999 fall	0	SE	1	SE	0	SE	0	SE	1	SE	0	SE	0	SE	0	SE	0	SE	0	SE
2000 spring	2	SW	1	SW	1	SW	1	SW	1	SW	1	SW	0	SW	1	SW	0	SW	0	SW
2000 fall	0	SE	0	SE	0	SE	1	SE	1	SE	0	SE	0	SE	2	SE	0	SE	0	SE
2001 spring	0	SE	0	SE	0	SE	0	SE	2	SE	0	SE	0	SE	0	SW	0	SW	0	SW
2001 fall	0	SE	2	SE	1	SE	1	SE	1	SE	0	SE	0	SE	1	SE	0	SE	0	SE
2002 spring	1	SE	1	SE	1	SE	1	SE	1	SE	1	SE	0	SE	0	SE	0	SE	0	SE
2003 spring	0	SW	0	SW	0	SW	0	SW	2	SW	0	SW	0	SW	1	SW	0	SW	0	SW
2003 fall	0	SE	0	SE	0	SE	0	SE	2	SE	0	SE	1	SE	1	SE	2	SE	0	SE
2005 spring	0	SE	1	SE	0	SE	0	SE	1	SE	1	SE	1	SE	1	SE	0	SE	0	SE
2004	1	SW	1	SW	0	SW	0	SW	0	SW	1	SW	1	SW	1	SW	0	SW	0	SW
2010	1	SE	0	SE	0	SE	0	SE	1	SE	1	SE	1	SE	0	SE	0	SW	0	SW
2013	1	SW	1	SW	1	SW	1	SW	1	SW	1	SW	1	SW	0	SW	0	SW	0	SW

B3. Sandwave statistics, SE stands for wave comes from the south-east, SW stands for wave comes from the south-west; 0 means no sandwave appeared, 1 means sandwave appeared.

Dune on top		Dune in front	
LiDAR station	ACNYMP station	LiDAR station	ACNYMP station
597031	M39	598161	M32
597431	M36	598221	M31
597871	M34	599011	M26
597971	M33	599121	M25
598051	M32	620121	M7
598121	M32	620351	M5
Multiple dunes		Single dune	
LiDAR station	ACNYMP station	LiDAR station	ACNYMP station
599351	M23	599251	M24
599871	M19	600151	M17
601741	M8	600351	M16
599311	M23	620521	M3
600051	M18	621341	P39
621331	P39	602091	P36

B 4. Corresponding LiDAR station and ACNYMP for model trials during October 20th, 2012 to October 31th, 2012.

Dune on top		Dune in front	
LiDAR station	ACNYMP station	LiDAR station	ACNYMP station
596891	M39	597701	M35
596971	M39	597831	M34
597081	M38	598181	M31
597101	M38	598331	M30
597221	M37	599171	M24
597361	M37	599091	M25
597461	M36	620091	M7
597521	M36	620181	M6
597901	M34	620241	M6
597961	M33	620291	M5
598071	M32	620321	M5
598131	M32	620381	M4
Multiple dunes		Single dune	
599301	M23	597501	M36
599421	M22	599201	M24
599481	M22	600181	M17
599541	M22	600301	M16
599601	M21	600371	M15
599671	M21	600531	M15
599801	M20	600671	M14
599921	M19	601011	M12
600111	M17	601121	M11
601721	M8	601341	M10
620051	M7	601711	M8
601961	P38	601881	M7

B 5. Corresponding LiDAR station and ACNYMP for model trials during October 25th, 2012 to November 5th, 2012.